UNIVERSITA' DEGLI STUDI DI NAPOLI "FEDERICO II"
FACOLTA' DI SCIENZE MATEMATICHE, FISICHE E NATURALI

DOTTORATO IN SCIENZE CHIMICHE XX CICLO
2004-2007

STUDIES OF NEW MOLECULAR SYSTEMS BASED ON NUCLEIC ACIDS AND THEIR ANALOGUES FOR BIOTECHNOLOGICAL APPLICATIONS.

Tutore: *Ch.mo Prof. Carlo Pedone* **Dottoranda**: *Maria Moccia*

Coordinatore: *Ch.mo Prof. Aldo Vitagliano*

INDEX

ABBREVIATIONS

A	Adenine
Ac_2O	Acetic anhydride
ACN	Acetonitrile
Aeg	N-(2-aminoethyl) glycine
AMS	Amino methyl styrene resin
Bhoc	Benzhydryloxycarbonyl
Boc	tert-Butyloxycarbonyl
C	Cytosine
Cbz	Benzyloxycarbonyl
CD	Circular dichroism
CPG	Controlled pore glasses support
DABA	2,4-diaminobutyric acid
DCM	Dichloromethane
DIC	Diiso-propyl carbodiimide
DMAP	4-(Dimethylamino) pyridine
DIPEA	Diisopropylethylamine
DMF	N,N-dimethylformamide
DMSO	Dimethyl sulfoxide
Fmoc	9-fluorenylmethoxycarbonyl
G	Guanine
HATU	*O*-(7-azabenzotriazol-1-yl)-1,1,3,3-tetramethyluronium hexafluorophosphate
HOBt	N-hydroxybenzotriazole
LC/MS	Liquid chromatography/mass spectroscopy
LNA	Locked nucleic acid
MALDI-TOF MS	Matrix-assisted laser desorption/ionization time of flight mass spectroscopy
NMP	1-Methyl-2-pyrrolidinone
NMR	Nuclear magnetic resonance
PEG-PS	polyethylene glycol-polystyrene solid support
PNA	Peptide (polyamide) nucleic acid
PyBop	benzotriazol-1-yl-oxytripyrrolidinophosphonium hexafluorophosphate
RP-HPLC	Reverse phase-high performance liquid chromatography
T	Thymine

TCH_2COOH	Thymin-1-yl acetic acid
TFA	Trifluoroacetic acid
TMP	2,4,6, trimethylpiridine
TOF-SIMS	Time-of-flight secondary ion mass spectrometry

INTRODUCTION

The base pairing of nucleic acids is one of the fundamental processes in biological systems, it guarantees the storage, transfer and expression of genetic information in living systems.
Self-recognition by nucleic acid is based on the Watson-Crick[1] hydrogen bonds between the complementary nucleobases A-T and G-C (Figure 1).

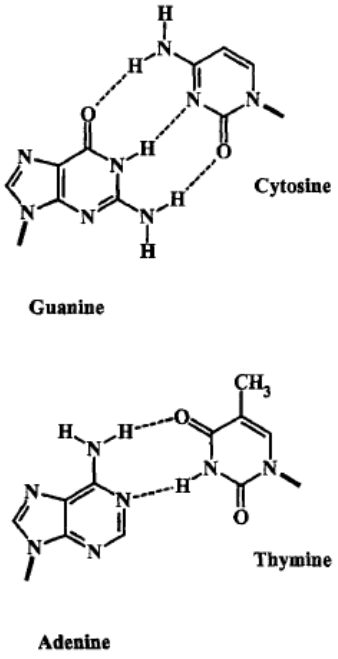

Figure 1 Watson-Crick hydrogen bonding.

This simple four base recognition has inspired chemists to develop self organizing systems based on DNA for therapeutic applications,[2] in the form of antisense and antigene oligonucleotides, as well as for diagnostic purposes, or for the development of new nanomaterials.

DNA as therapeutic agents

Different cellular processes could be inhibited depending on the site at which the oligonucleotide hybridizes to the target nucleic acid. The oligonucleotides that interact with single stranded RNA are called “antisense” whereas those interacting with double stranded DNA are called “antigene”.

The principle of action of the antisense oligonucleotides[3] (Figure 2 b) is the binding via Watson-Crick base pairing to a complementary region on target *m*RNA and the formation of a duplex (RNA-DNA hybrid).

In this way the RNA strand is blocked in a duplex, so to prevent the translation and subsequently the expression of the corresponding protein. When target proteins are disease related, this will have therapeutic value. Nature itself utilizes the antisense principle for the regulation of a variety of gene products and antisense RNA molecules have been found to be expressed intracellularly.

For an "antisense" oligonucleotide to be able to inhibit translation, it must reach the interior of the cell unaltered, so it has to be stable towards extra and intra cellular enzymes as well as able to traverse the cell membrane.

Once within the cytoplasm it must bind the target *m*RNA with sufficient affinity and high specificity.

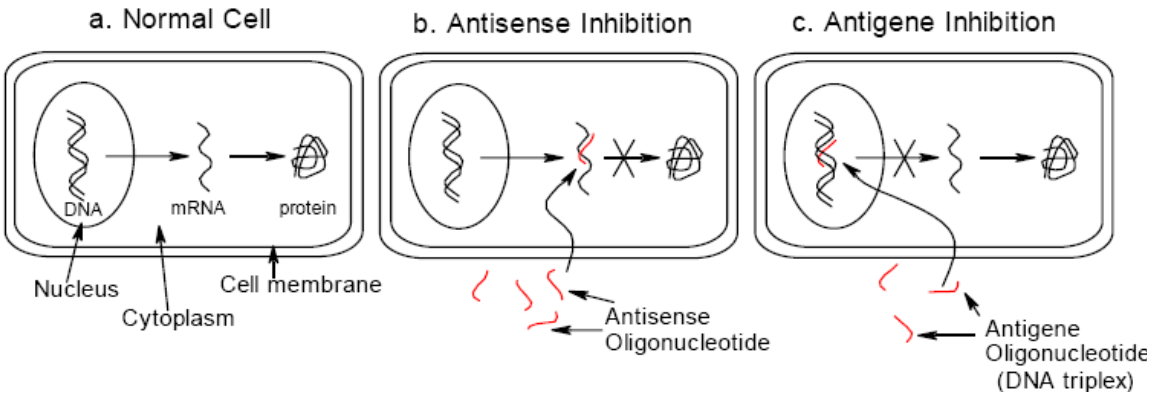

Figure 2 Schematic illustration of (a) Normal gene expression. DNA is transcribed into *m*RNA to give multiple copies of the protein gene product; (b) Antisense inhibition. An antisense oligonucleotide binds specifically to *m*RNA via Watson-Crick hydrogen bonding whereby it inhibits translation of *m*RNA into protein; (c) Antigene inhibition. Transcription is inhibited by the binding of an antigene oligonucleotide to DNA.

In another approach, the 'antigene strategy',[4] (Figure 2c) the transcription can be inhibited by the binding of an ODN to a duplex DNA *via* formation of triple helix through Hoogsteen (*) hydrogen bonds[5] (Figure 3). However, many factors, including instability of triple helical complexes in cells, limit the efficacy of this approach.

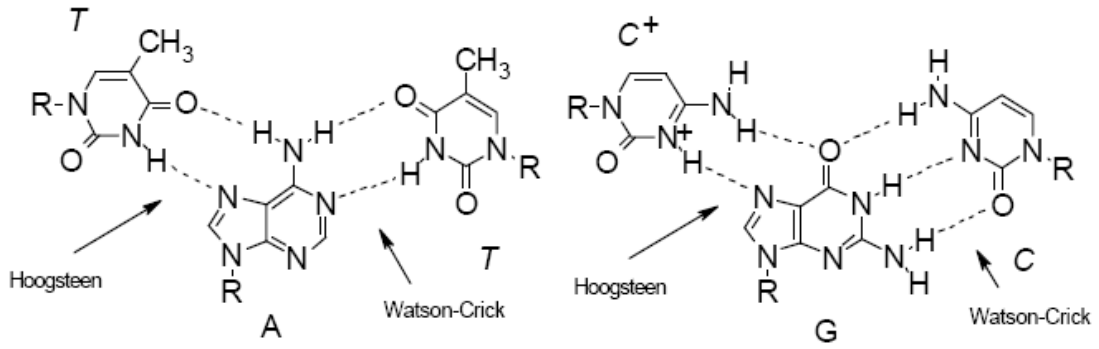

Figure 3 T* A-T and C^{+}* G-C triplets involving Hoogsteen and Watson-Crick base pairing.

DNA as diagnostics tools

Due to their relative simplicity, rapidity, workability and remarkable sensitivity, DNA diagnostics hold the distinct position in the area of molecular *in vitro* diagnostics. Various aspects of DNA diagnostics range from PCR-based techniques, DNA microarrays, microfluidics to fluorescent *in situ* hybridization (FISH), SNP detection, DNA nanotechnology, molecular beacons, and many others.[6]

DNA is particularly used in diagnostic as molecular beacon[7] that's a single-stranded oligonucleotide probe that form a stem-and-loop structure. The loop contains a sequence that is complementary to a target sequence, and the stem is formed by two complementary tracts flanking the loop sequence. A fluorophore and a quencher are covalently linked to the ends of the probe. The molecular beacons do not fluoresce when the probe is in its stem-and-loop form, with the quencher spatially near to the fluorofore, while they fluoresce brightly when the probe hybridize to the target sequence (Figure 4). Obviously the length of the loop and the stem has to be designed in a way to realize a probe-target complex more stable than the stem hybrid, consequently, the molecular beacons spontaneously form fluorescent probe-target hybrids.

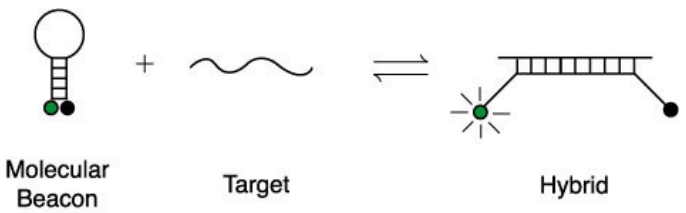

Figure 4 Molecular beacon.

Molecular beacons can be added to the assay mixture without carrying out gene amplification and fluorescence is measured in real time. The use of different molecular beacons with differently coloured fluorophores enable to detect different targets simultaneously in the same assay. Molecular beacons are extraordinarily specific, they easily discriminate target sequences that differ from one another by a single nucleotide substitution.

DNA as nanomaterials

Recently, physicists and chemists have become increasingly interested in the electronic properties of the DNA to be used as nanomaterial using its ability to self–assembly, a requirement essential for the construction of nanoscale devices. The construction of three dimensional cubes, simple switches and motors from DNA building blocks has already been reported.[8] However, the usefulness of DNA in nanotechnology would enhanced considerably if it were a good electronic conductor.

Y-shaped DNA template[9] incorporating a central biotin moiety may be used to assemble nanoscale architectures (Figure 5), as potential to the fabrication of next-generation electronic devices. There are potential applications of the above and related DNA templates in the emerging field of nanoelectronics.

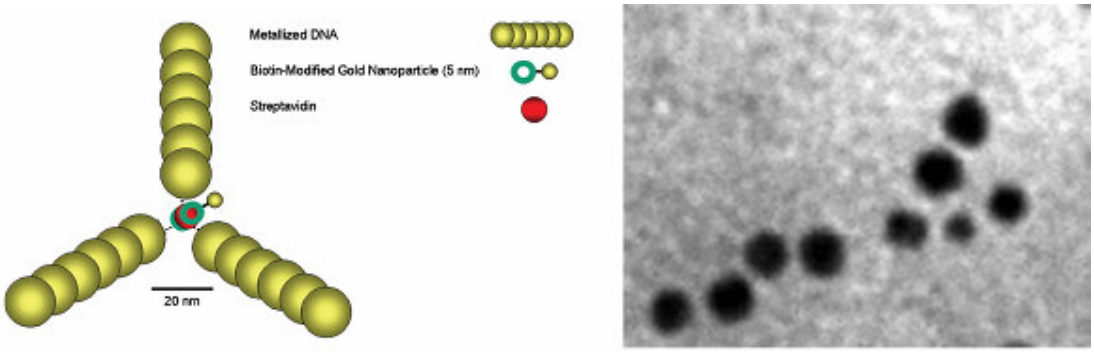

Figure 5 Y-shaped DNA template with a central biotin moiety.

DNA limits

In diagnostic the use of synthetic ODN is limited by the inaccessibility of the nucleic acid target site under the conditions required for the probes to bind. Therefore, many nucleic acids (dsDNA and *m*RNA) cannot be easily analyzed using conventional DNA and RNA probes. Furthermore, the

general applicability, for example of PCR approach, is limited by the fact that the majority of primer-template mismatches have no significant effect on the amplification process.[10]

In addition, the practical application of ODN as useful therapeutic agents have two severe limits: the enzymatic degradation of ODN by cellular nucleases, and the poor cellular uptake. To address the issue of poor cellular uptake, a number of delivery systems have been proposed, including cationic liposomes,[11] cationic lipids,[12] and cationic polymers.[13] The problem of enzymatic susceptibility of ODN has been partially solved by chemical modifications of ODN, like in the case of phosphorothioate,[14] or by employing new ODN analogous, such as peptide nucleic acids (PNA)[15] or LNA.

DNA modifications

In order to confer resistance to cellular enzymes but still allowing the formation of stable duplexes/triplexes with target nucleic acids, several chemical modifications[16] have been introduced in the oligonucleotide structure.

The various possible sites of modification in a nucleotide are shown in Figure 6 and could involve the sugar-phosphate backbone and/or the nucleobases. The modifications are commonly grouped into three 'generations': 1) analogues with altered phosphate backbones, 2) modified sugars (especially at the 2′ position of the ribose) or unnatural bases, and 3) modified phosphate linkages or riboses as well as nucleotides with a completely different chemical moiety replacing the furanose ring. However, the modified ODNs should have resistance to nuclease digestion, good cellular uptake, satisfactory hybridization affinity to the target nucleic acids, binding specificity and low toxicity.

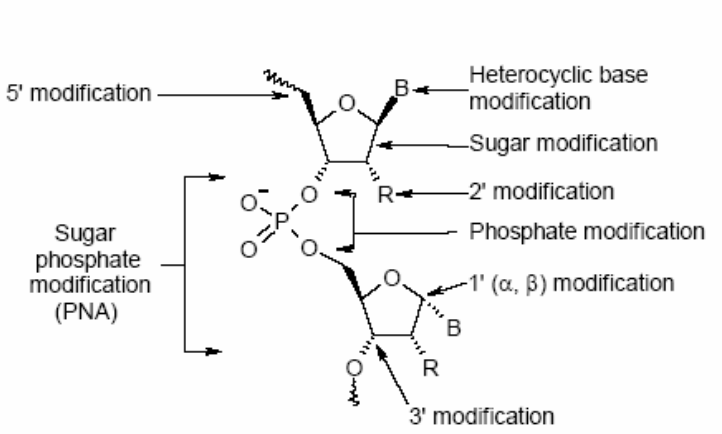

Figure 6 DNA's modification sites.

The first generation modifications, designed to make the internucleotide linkages more resistant to nuclease attack, regarded the phosphodiester backbone and have led to a large variety of new ODN analogous, like as phosphorothioates (1a), phosphorodithioates[17] (1b), methyl phosphonates (1c), hydroxymethyl phosphonates (2), phosphotriesters (3), phosphoramidates[18] (4) (Figure 7). The phosphorothioate ODN, in which a sulphur atom substitutes a non-bridging oxygen in the phosphate backbone, resulted to be the most promising analogs in the antisense approach. Vitravene**,** [19] a phosphorothioate ODN with potent and specific anticytomegalovirus (CMV) activity, is the first antisense oligonucleotide based drug approved by FDA.

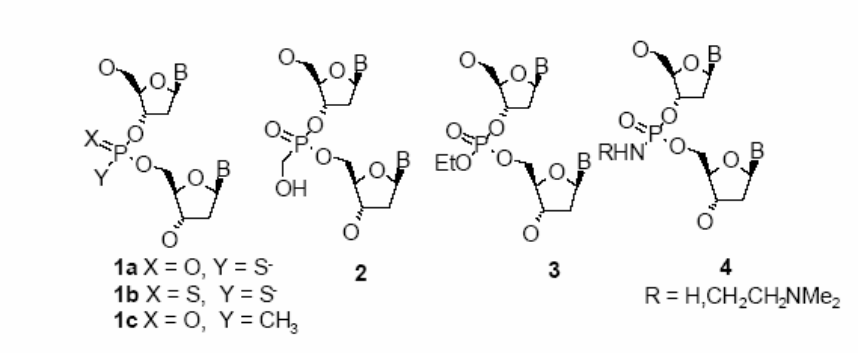

Figura 7. Phosphate modification: first generation antisense oligonucleotides.

Nucleotides with alkyl modification at the 2′ position of the ribose belong to the second generation modifications, among which 2'-*O*-methyl and 2'-*O*-methoxy-ethyl are the most important representatives (Figure 8). The significant improvements are: a reduction in general of toxicity, increased hybrid stability, and increased nuclease resistance. However, these desirable properties are counterbalanced by the fact that 2'-*O*-methyl RNA cannot induce RNase H cleavage of the target mRNA.

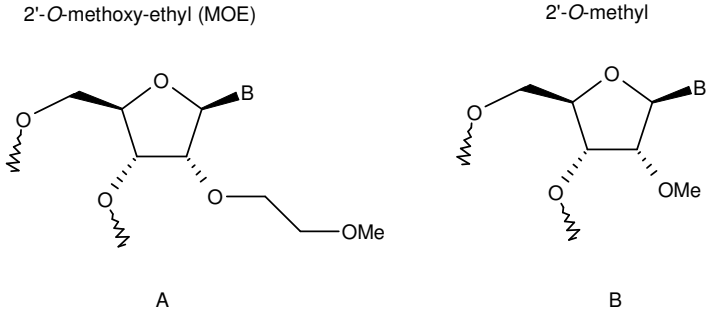

Figure 8. Second generation antisense oligonucleotide A) 2-O-methoxyethyl (MOE) B) 2-O-methyl.

In the class of third generation ODN modifications, morpholino phosphoroamidates (MF), peptide nucleic acids (PNA) and locked nucleic acids (LNA) are three interesting RNA/DNA analogues that attract much attention (Figure 9). These compounds are essentially nuclease resistant while maintaining good hybridization affinity with their complementary mRNA.

Effective gene knock-down by antisense MFs *in vivo* has been shown, and therapeutic compounds are being developed. One of this morpholino phosphoroamidates targets the c-*myc* oncogene[20] and is currently being tested in phase I and II clinical trials by AVI BioPharma (Portland, OR, USA).

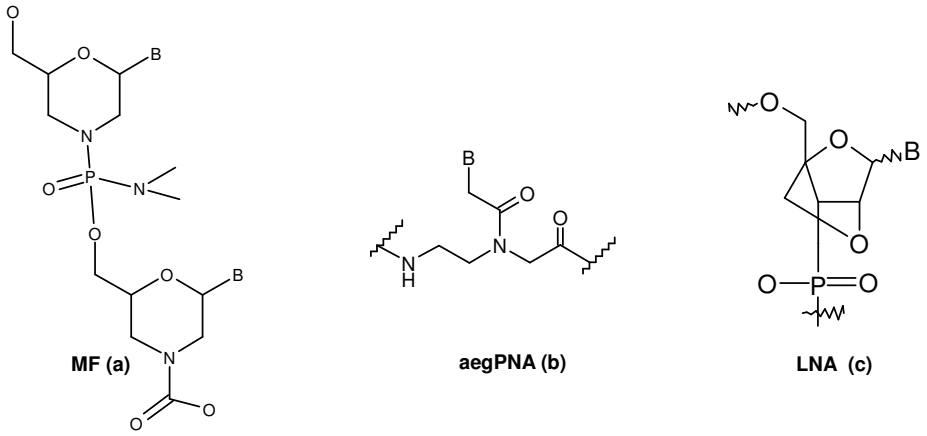

Figure 9. Class of third generation ODN modifications. a) morpholino phosphoroamidates (MF), b) PNA (peptide nucleic acid), c) LNA (β-D-ribo).

In LNA nucleoside monomer (Figure 9c) the furanose ring being part of dioxabicyclo[2,2,1]heptane skeleton is locked in an N-type conformation (C3' endo or 3E conformation). Such a conformational or structural pre organization of the furanose ring is an important factor for the high binding affinity for natural nucleic acids of these analogues. Full LNA ONs have been successfully used *in vivo* to block the translation of an RNA polymerase.[21] These ONs inhibited tumor growth in a xenograft model with an effective concentration that was five times lower than was found previously for the corresponding PS-ODN.

The most important success of the ODN chemical modifications has probably been the PNA (Peptide Nucleic Acids), firstly described by Nielsen et al. in 1991.[22] PNAs are homomorphous DNA analogues in which the entire sugar phosphate backbone of DNA is replaced by a neutral and achiral polyamide backbone consisting of N-(2-aminoethyl) glycine (*aeg*) moieties (Figure 10). Each of the four nucleobases, adenine, cytosine, guanine, thymine (A, C, G, T), are attached to the backbone through a methylene carbonyl linkers.

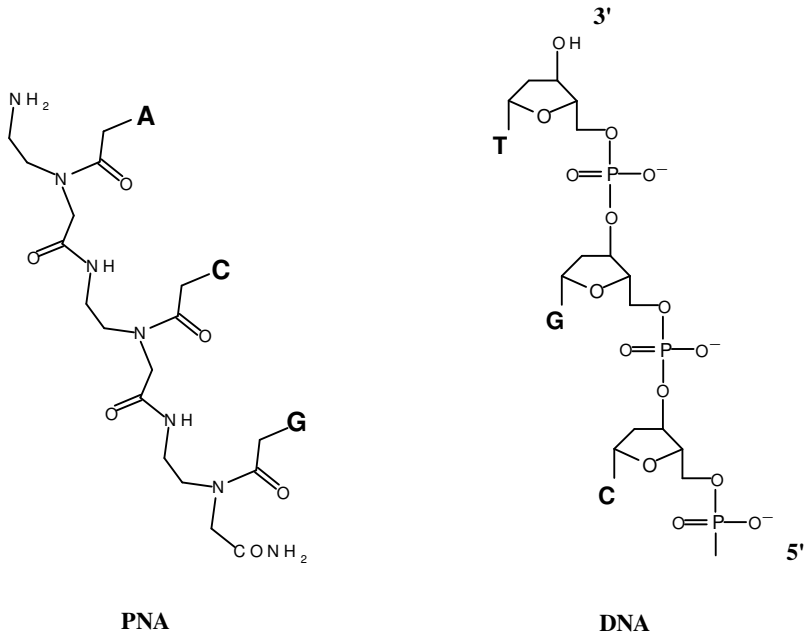

Figure 10 Comparison of PNA and DNA oligomer.

The particular arrangement of atoms in PNA is the same of the '6 + 3' number of bonds arrangement found for DNA. Considering the geometry of the DNA backbone this reveals that six bonds separate each nucleobase unit, while the distance between the backbone and the nucleobase is three bonds. Since the first reports on PNA, a large number of approaches to the synthesis of PNA monomers have been reported.[23] In the majority of the synthetic strategies the monomer was disconnected about the central amide bond, a protected nucleobase acetic acid and a protected N-(2-aminoethyl) glycine were used.

PNAs are resistant to nucleases and proteases,[24] they bind with high affinity and specificity to complementary RNA and DNA.

By convention, PNAs are depicted like peptides with N-terminus at the left and C-terminus at the right. Being achiral, PNAs bind DNA/RNA in either parallel or antiparallel modes, the antiparallel mode is slightly preferred over the parallel one.[25]

The orientation in which the amino terminus of PNA binds to the 5' end of DNA is designated as *parallel*, while the orientation resulting from the amino terminus of PNA binding to the 3' end of the target DNA is termed *antiparallel* (Figure 11).

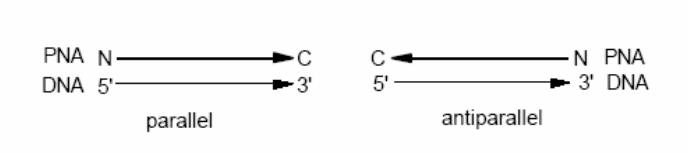

Figure 11 PNA-DNA binding mode

PNA synthesis

PNA synthesis uses Fmoc or *t*Boc based chemistry as peptide synthesis.[26] The four PNA monomers (a, t, g, c) are commercially available with either Fmoc or tBoc protecting groups on the primary amine and a Bhoc or Cbz protecting groups on the nucleobase. For manual PNA synthesis, Boc/Cbz-PNA monomers are used due to the less stringent requirement for anhydrous conditions during coupling reactions. For automated synthesis, Fmoc/Bhoc PNA monomers (Figure 12) are routinely used because the conditions for Fmoc removal are less caustic to the instrumentation respect to the Boc deprotection.

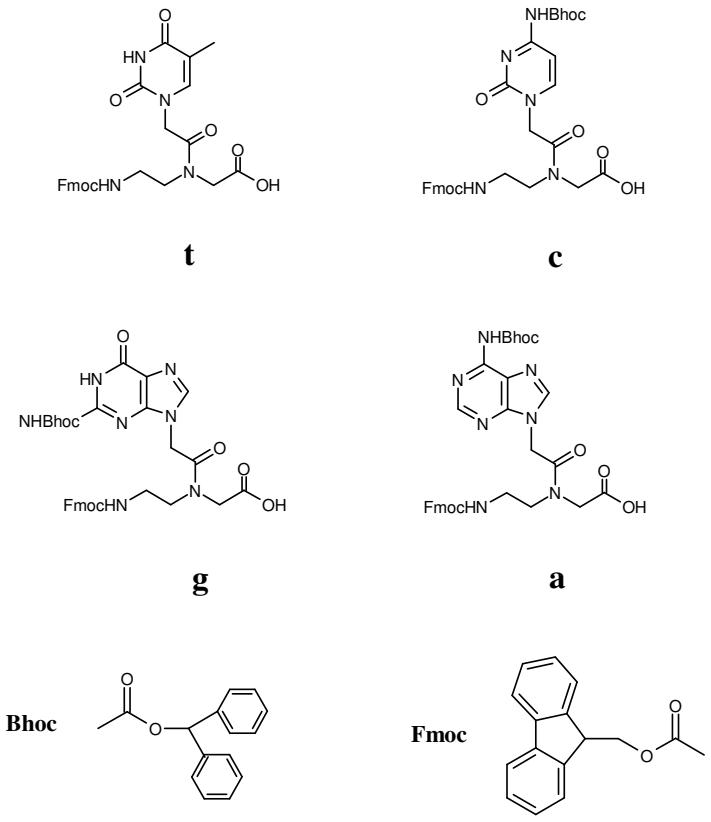

Figure 12 Fmoc/Bhoc PNA monomers.

The PNA automated synthesis is performed on the Perceptive Expedite 8909 from Applied Biosystem (Figure 13).

Figure 13 Perceptive Expedite 8909.

Starting from a solid support resin, PNA synthesis occurs from C-terminus to N-terminus repeating the base cycle depicted in Figure 14. The cycle starts with the removal of the Fmoc groups from the solid support with a solution of piperidine (20%) in DMF. Successively, the protected monomer is coupled to the growing chain. In coupling step the carboxyl group of the Fmoc (Bhoc)-protected PNA monomer is activated by HATU in presence of DIPEA/Lutidine as base. This activated carboxyl group is coupled to an exposed reactive primary amine group (uncharged under basic conditions) at the end of the resin-bound PNA. A capping step with acetic anhydride is included at the end of the cycle to prevent chain elongation of PNA oligomers with missing bases that leads to truncated PNA products.

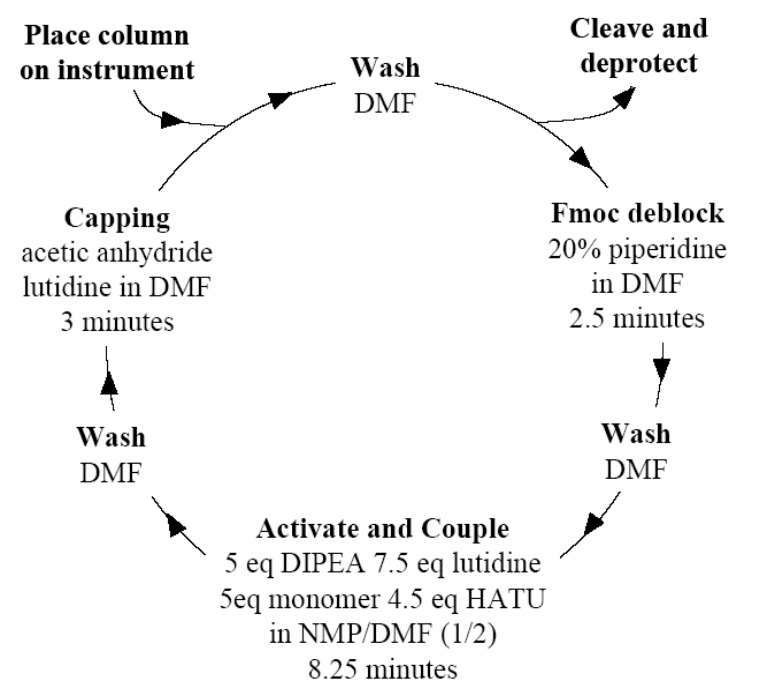

Figure 14 Automated PNA synthesis on the Expedite 8909 (Cycles).

Upon completion of the synthesis, the PNA is cleaved from the solid-support resin with TFA and simultaneously the Bhoc protecting groups are removed from the nucleobases. Also included with TFA in the cleavage step is m-cresol that acts as a scavenger for the released protecting groups, preventing undesired side reactions with the free amino groups present on the PNA oligomer.
The PNA is then precipitated in cold diethyl ether, dried to a solid, and resuspended in water. Being neutral compounds, pure PNAs have a tendency for self aggregation and a low water solubility. The introduction of charged groups at N/C terminus, or of positive charges by modification of PNA backbone greatly improves their properties.[27]Alternatively, negative charges can be introduced, such as in the PNA-DNA chimeras, which show enhanced water solubility. [28]

PNA complex stability

PNAs are able to form stable duplexes with complementary DNA and RNA. Duplexes between PNA and DNA or RNA are in general thermally more stable than the corresponding DNA-DNA or DNA-RNA duplexes.[29] Very importantly, the stability of PNA-DNA duplexes are not influenced by the ionic strength of the medium.[30] This is in contrast to the behavior of DNA-DNA (or RNA) duplexes, in which the stability decreases dramatically at low ionic strength because of the lack of counterion shielding of the phosphate backbone.[30]

Biophysical structures of PNA complexes

When annealed the PNA oligomer conforms to its nucleic acid partner. The backbone of the PNA oligomer is flexible enough to adopt the preferred duplex conformation of its bound nucleic acid complement, but not so flexible to destabilize hydrogen bond formation.

The PNA-RNA[31] and PNA-DNA[32] duplex structures were determined by NMR methods, while the structures of a PNA_2:DNA triplex[33] and a PNA:PNA duplex[34] were solved by X-ray crystallography (Figure 15). In the PNA-RNA and PNA-DNA duplexes the oligonucleotide adopts close to its natural A-conformation and B-conformation in terms of sugar puckering, while the helix parameters have both A- and B-form characteristics. From these two cases it seems that the PNA is an excellent DNA/RNA mimic. Anyway the PNA prefer a unique, different helix form, the P-form, which is taking over already in the PNA_2:DNA triplex and is of course fully developed in the PNA-PNA duplex. This helix is very wide (28 Å diameter) and has a very large pitch (18 base pairs) unlike the "A" form of PNA:RNA duplex or the "B" form of PNA:DNA duplex.

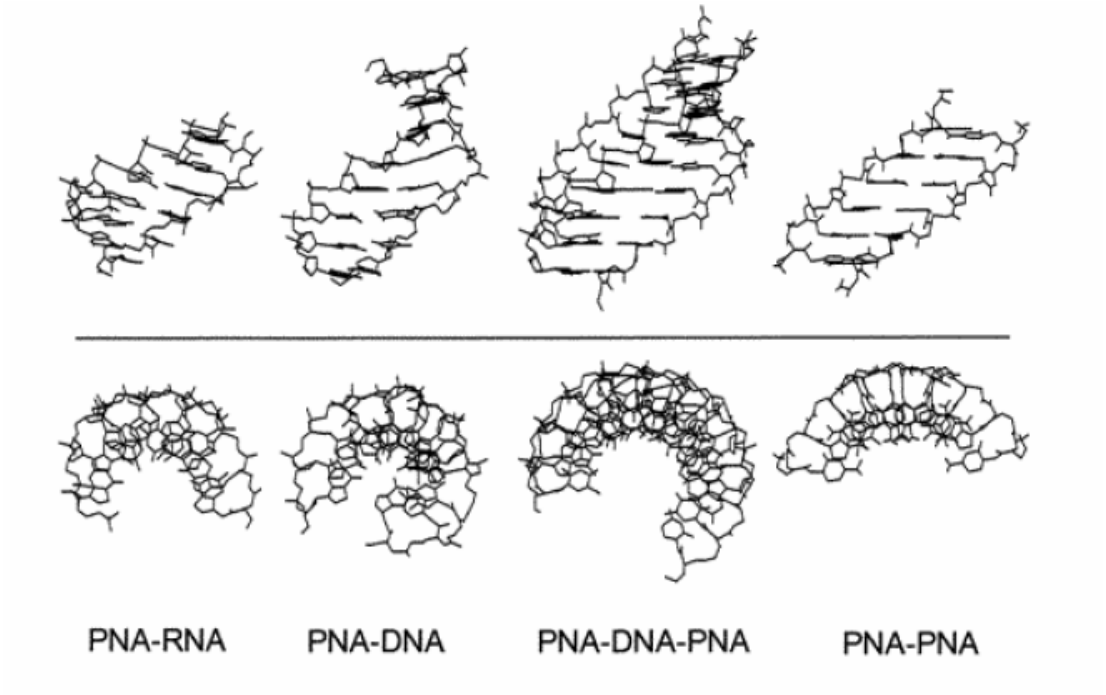

Figure 15 Structural features of PNA:RNA, PNA:DNA, PNA_2:DNA triplex, PNA:PNA. The double helix formed by PNA:RNA and PNA:DNA resembles the form of RNA:RNA and DNA:DNA double helices. PNA_2:DNA triplex and PNA:PNA takes on a new form called the P-form (neither A- nor B-form).

PNA applications

Since its introduction, an increasing number of applications of PNA technology have been described, confirming the high potential of PNAs in biotechnological applications.

Applications of PNA can be divided into four main categories, namely PNA for antigene and antisense therapy, PNA as a tool for molecular biology and functional genomics, PNA as a probe for diagnosis and detection and PNA as biosensors.[35] PNAs can be used in many of the applications where traditional synthetic DNA or RNA have been used, but with the added benefits of tighter binding, greater specificity and stability.

PNA as therapeutic agent: antigene and antisense strategies

Antisense properties of PNA

In antisense strategy the nucleic acid analogues can be designed to recognise and hybridise to complementary sequences in mRNA and thereby inhibit its translation. Normally, the PNA antisense effect is based on the steric blocking of either RNA processing, transport into cytoplasm, or translation. It has been found by *in vitro* translation experiments that mixed purine-pyrimidine PNA sequence that form PNA-RNA duplexes with the target, did not arrest translation elongation, indicating that the PNA was displaced by the moving ribosome. However, when homopurine targets are present in the translated region of the RNA, these can be targeted by homopyrimidine (*bis*)[36] PNAs, which form very stable PNA_2-DNA triplexes that are able to arrest the ribosome during elongation. Triplex-forming PNAs can inhibit translation at initiation codon targets and ribosome elongation at codon region targets.

Antigene properties of PNA

Originally conceived as agents for double-stranded DNA binding, the unique properties of PNAs as DNA mimics were first exploited for gene therapy drug design.

PNAs should be capable of arresting transcriptional process for their ability to form a stable triple helix by strand-invasion or strand displacement of a DNA duplex (Figure 16). Such complexes can create a structural hindrance to block the function of RNA polymerase and thus are capable of working as antigene agent[37] causing the distortion of the DNA helix. Therefore PNA gene targeting at the DNA level should be very efficient. The main obstacle appears to be the access of PNA to the DNA under physiological conditions, which includes the presence of cations that stabilize the DNA double helix but reduce the rate of helix invasion by the PNA.[38]

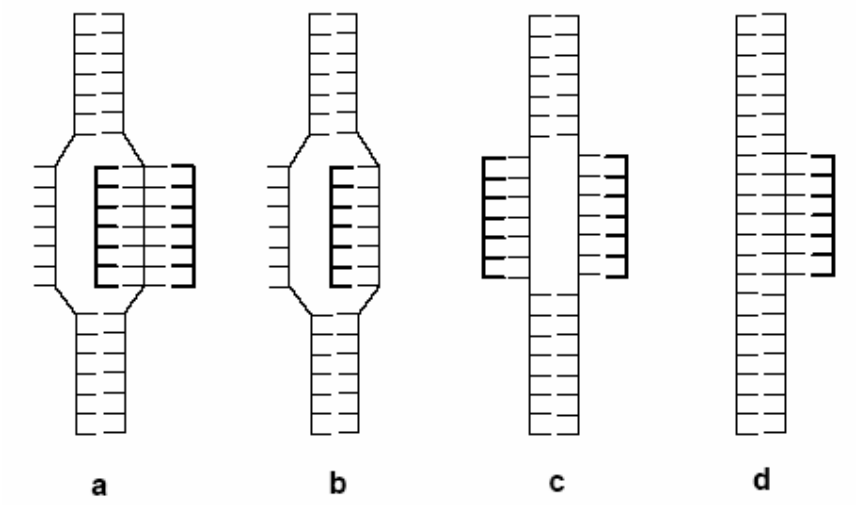

Figure 16 Schematic drawing of the mode by which PNA binds to duplex DNA targets. PNA oligomers are in bold. **a)** Strand displacement *via* PNA-DNA*PNA triplex formation, **b)** strand displacement *via* PNA-DNA duplex formation, **c)** strand invasion *via* PNA-DNA double duplex formation, **d)** PNA*DNA-DNA triplex formation.

PNA for diagnosis and detection

SNP detection using PNA-directed PCR clamping

The high affinity and specificity of PNA binding to DNA, and the inefficiency of PNA to act as a primer for DNA polymerases, make PNAs suitable to use in PCR techniques to reveal single-base-pair mutation or single-nucleotide polymorphism (SNP). Basically, in the PCR clamping technique, at the annealing step the PNA is targeted to one of the PCR primer sites.[39] The PNA, which binds to the primer binding site instead of the primer, effectively blocks the formation of a PCR product. PNA is able to discriminate between fully complementary and single-mismatch targets (mutations) in a mixed target PCR, because in the case of mismatches the PNA/DNA hybrid has a melting temperature much lower than the corresponding fully complementary one. Hence the binding of primer will be favoured to out-compete PNA annealing. Consequently, mutated sequences will be preferentially amplified (Figure 17).

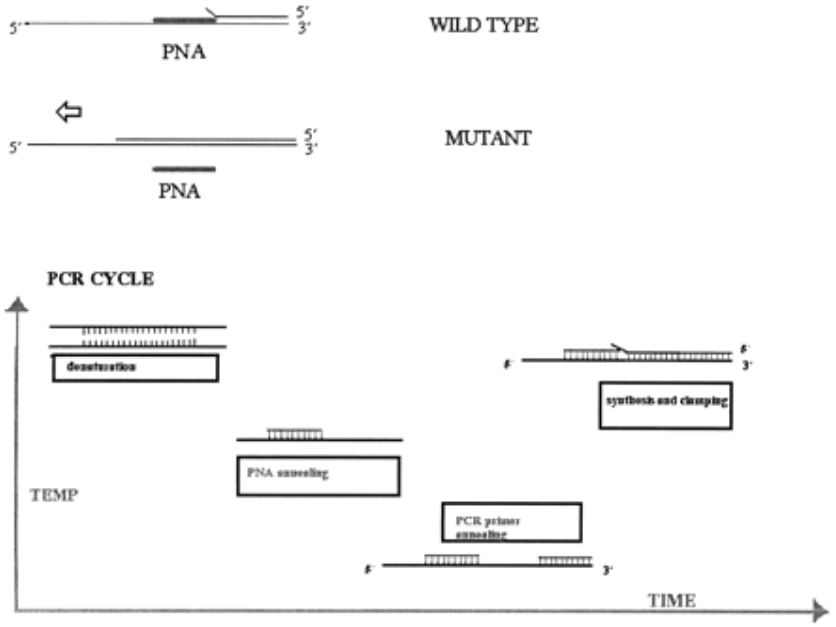

Figure 17 Mutation analysis using PNA-directed PCR clamping: schematic representation of the strategy for the PCR cycle involving PNA-directed clamping. In the case of the normal (wild-type) DNA, the bound PNA will sterically hinder annealing of a partially overlapping primer sequence, thus preventing the normal sequence from appropriate PCR amplification. In the case of mutant alleles, the melting temperature of the PNA/DNA is reduced and the primer can out-compete PNA annealing to carry on preferential amplification of mutant sequences.

PNA as molecular beacon

PNA molecular beacon (MB) were successfully used to detect rRNA in solution and in whole cells[40] rRNA molecules have been used widely as target molecules for rapid monitoring of changes in microbial population abundance. In the case of the detection in whole cells fluorescence in situ hybridization (FISH) experiments were perfomed. FISH results with the PNA molecular beacons were superior to those with the DNA one: the hybridization kinetics were much faster, the signal-to-noise ratio was much higher, and the specificity was much better.

In addition, a real-time PCR assay using PNA molecular beacons to discriminate between the *A*-allele and *C*-allele of a SNP in exon 6 of the *XPD* gene[41] has been developed.

PNA probe for microarray

The analysis of biomolecules using microarrays and other biosensors has a significant role in molecular biotechnology. By combining peptide nucleic acid (PNA) microarray chips[42] as probes for hybridization of DNA sequences with time-of-flight secondary ion mass spectrometry (TOF-

SIMS) for detecting complementary hybridization with high sensitivity, label-free and PCR-free DNA diagnostics should become possible (Figure 18). TOF-SIMS is a technique that can identify the presence of phosphates in a molecular surface layer with high sensitivity in the attomole range. The detection of hybridization with unmodified genomic DNA becomes possible without any amplification or labeling step needed.

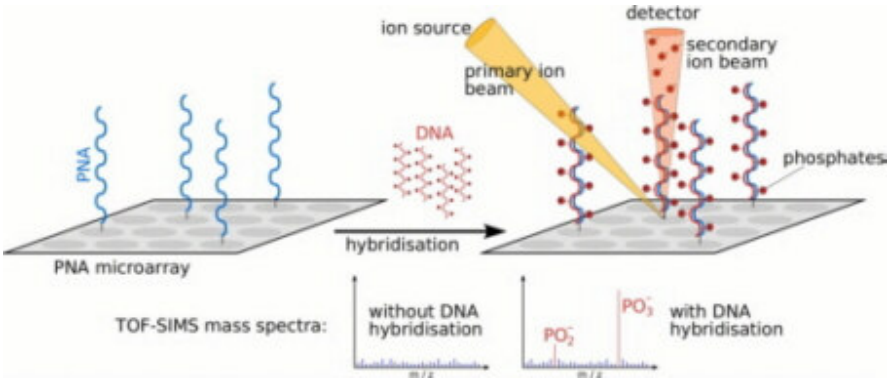

Figure 18 Label-free detection by TOF-SIMS analysis. A primary ion beam hits the surface, from which secondary ions, including phosphate fragments, are released. PNA does not contain phosphates. Therefore, phosphate ions are visible in the mass spectrum of a PNA-microarray only upon hybridisation of nucleic acids.

PART 1: Dendrimeric system based on ODN and analogues

Dendrimers based on poly-amidoamine (PAMAM) were the first and most extensively studied family of dendrimers which provided a large variety of biomedical applications (i.e., the delivery of active pharmaceuticals, imaging agents, or gene transfection).[43] Using the four base recognition of the DNA many researchers were interested in dendrimeric systems based on DNA in order to develop new drug delivery system or new nanomaterials.

The huge interest in nanomaterials is driven by their many desirable properties. In particular, the ability to tailor the size and structure and hence the properties of nanomaterials offers excellent prospects for designing novel sensing systems, enhancing the performance of bioanalytical assays. Thanks to the specificity of assembly of nucleic acid strands, oligonucleotides can be used as generic instead of genetic material.[44] The possibility to form extended oligonucleotidic systems with well-defined sizes, shapes, branching length/density and their surface functionality[45] could be of eminent interest in certain medical applications such as drug delivery, gene transfection, and imaging.

In order to develop ODN dendrimers, with enhanced thermal stability and good nuclease resistance, to be used for drug delivery or diagnostic applications, we realised two dendrimeric systems: a monomolecular system based on PNA (**A**, Figure 19) and a bimolecular one based on PNA and DNA building blocks (**B**, Figure 19).

Both systems have the ability to form a three-dimensional network by means of specific W-C base pairing.

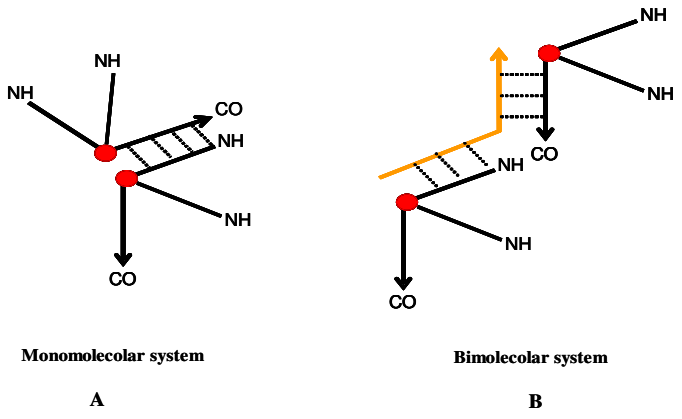

Figure 19 Schematic view of the dendrimeric systems.

1.1 Monomolecular PNA dendrimer

The first dendrimeric system realized is a PNA-based monomolecular *tridendron* formed by an autoassembling PNA (a, Figure 20) with the following sequence: $(Ac\text{-}t\text{-}t\text{-}t\text{-}t\text{-}t)_2\text{-}K\text{-}a\text{-}a\text{-}a\text{-}a\text{-}a\text{-}KNH_2$ (**1**). The dendrimeric system realized, that can self-assembly in the way showed in Figure 20 (b), should have the ability to form a three-dimensional network by specific W-C base pairing, to obtain a gel for encapsulating drugs.

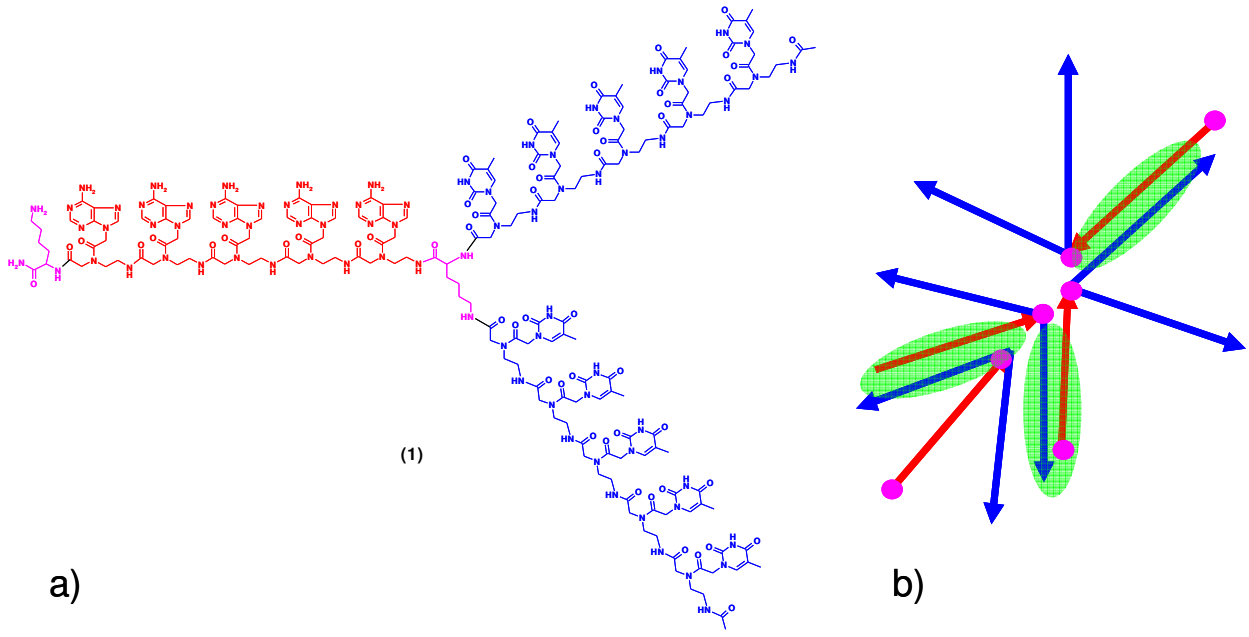

Figure 20 a) Chemical structure of PNA-based monomolecular *tridendron,* b) Schematic view of the self-assembly system (red: poly-adenine tract; blue: poly-thymine tracts; magenta: lysines; green shadowing: PNA-PNA double helices).

The PNA *tridendron* (**1**) has been assembled on an automatic synthesizer (Figure 14) using standard 2 µmol-scale protocol and Fmoc chemistry, following the synthetic procedure described in Scheme 1.

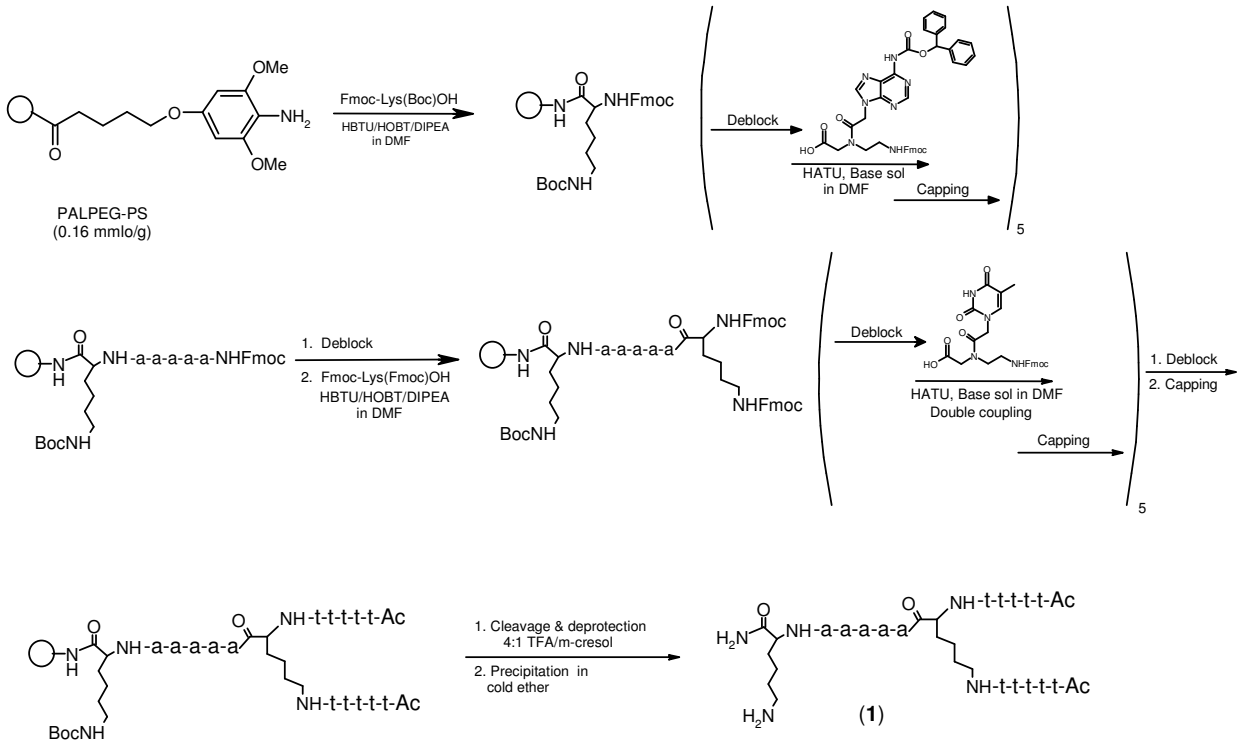

Scheme 1 PNA **1** *tridendron* synthesis.

Starting from the C-terminus, PNA *tridendron* is constituted by a Lysine residue, a poly-adenine branch (a_5), another Lysine in the middle of the sequence and two poly-thymine branches (t_5), assembled simultaneously on both amino groups of the central Lysine which was doubly Fmoc-protected. The C-terminal Lysine was useful to improve the final product solubility.

After removal and quantification of the final Fmoc groups both N-terminal thymine NH_2 were acetylated; the oligomer was cleaved and deprotected by acidic treatment (TFA:m-cresol, 4:1, v/v). The PNA *tridendron* was purified on RP-HPLC and characterized by LC-ESIMS (Figure 21).

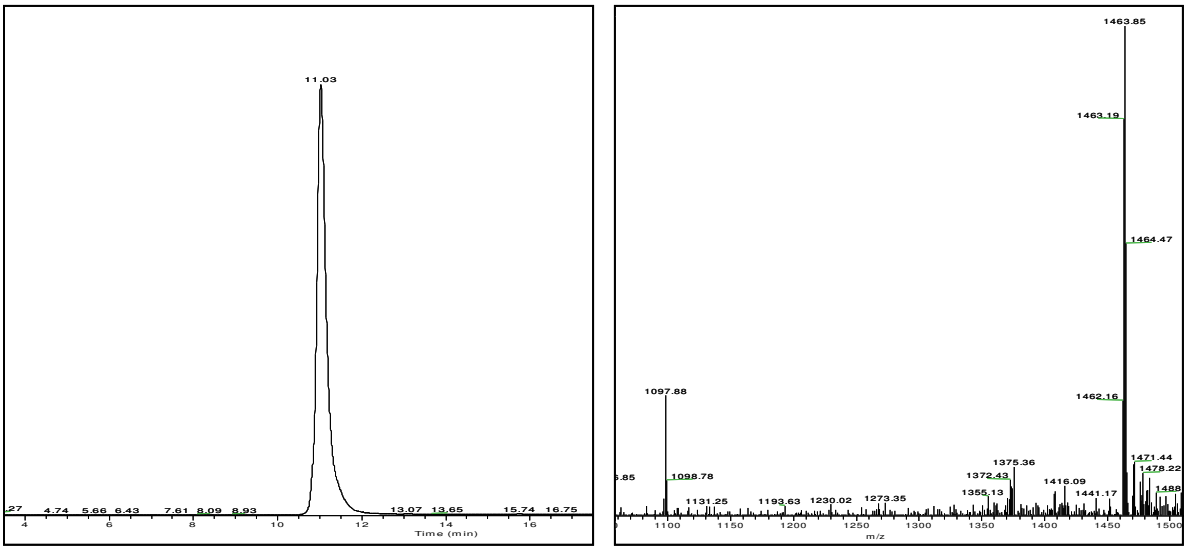

Figure 21 LC-ESI MS monomolecular PNA tridendron.

The PNA was lyophilised, dissolved in a known amount of milliQ water and quantified by UV measurements (T= 85 °C, absorbance value at λ=260 nm). The epsilon used for the quantification of the oligo is ε_{260}=154500 M^{-1} and was calculated using the molar extinction coefficients as follows: a, 15.4; t, 8.8. UV quantification of the PNA provided the following value: 15 mer = 395 nmol (1.7 mg, 24 % yield).

A detailed spectroscopic study was performed on the annealed PNA to verify the stability of the system as well as the formation of the three-dimensional network, allowing to elucidate its thermodynamic and structural properties. Circular dichroism (CD) spectum of the annealed PNA is shown in Figure 22. Even if single strand PNA, being achiral, doesn't show CD signal, when it forms duplex or triplex structures exhibits a significant signal. In our case a positive band centred at 275 nm is indicative of a duplex formation.

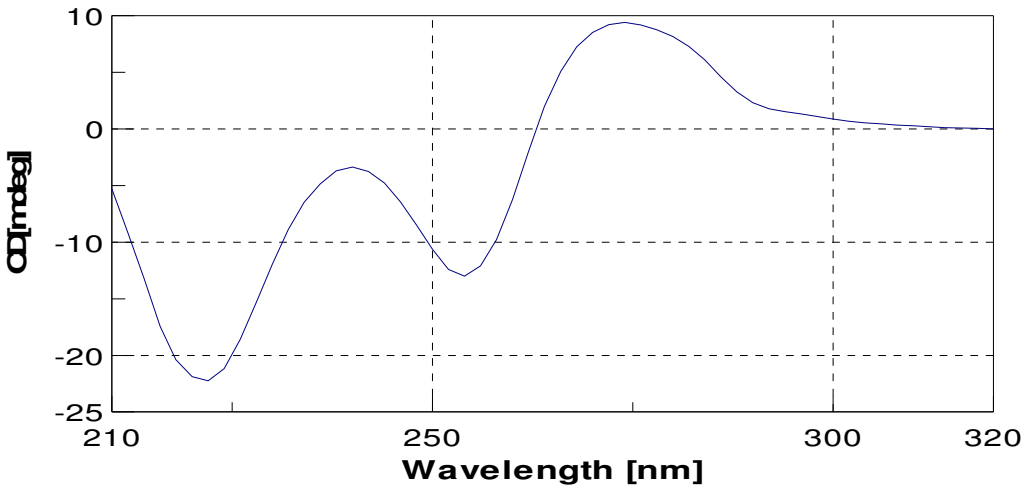

Figure 22 CD spectrum of PNA *tridendron* **1**, 8 µM in H_2O, 20 °C.

After the annealing of the system **A** (Figure 19), performed by dissolving the oligomer in milliQ water, heating the solution at 90 °C (5 min) and then allowing to cool slowly to room temperature, we proceeded to determine its thermal stability by UV melting experiments. The T_m of the self-assembly PNA system was 58 °C at 4 µM concentration (Figure 23).

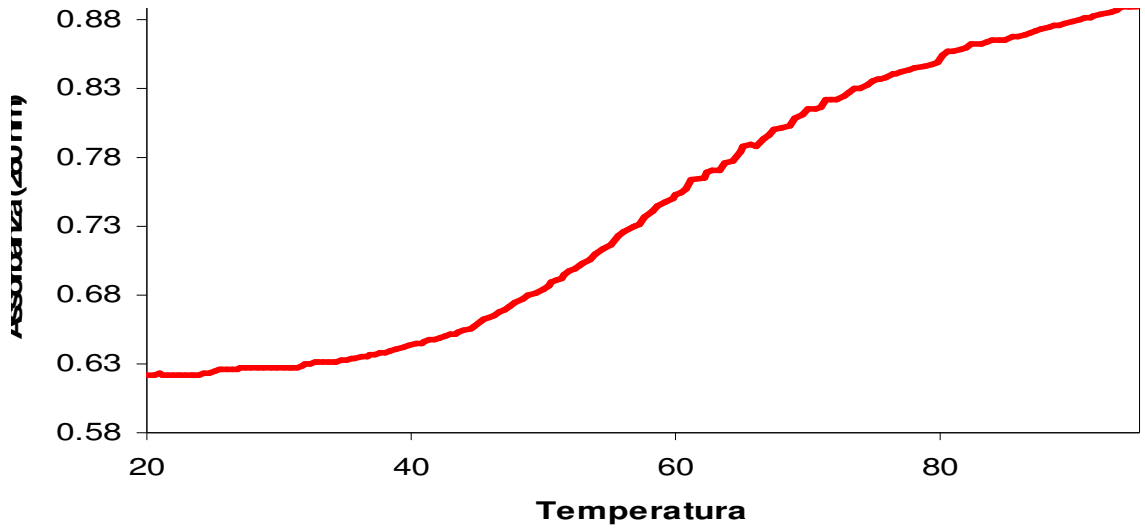

Figure 23 UV melting of monomolecular PNA system.

By recording UV melting curves at different PNA concentrations, we observed a logarithmic dependence of the melting temperature from concentration (Figure 24), with an increasing of the T_m value from 54.9 °C to 59.5 °C, going from 1 to 17 µM.

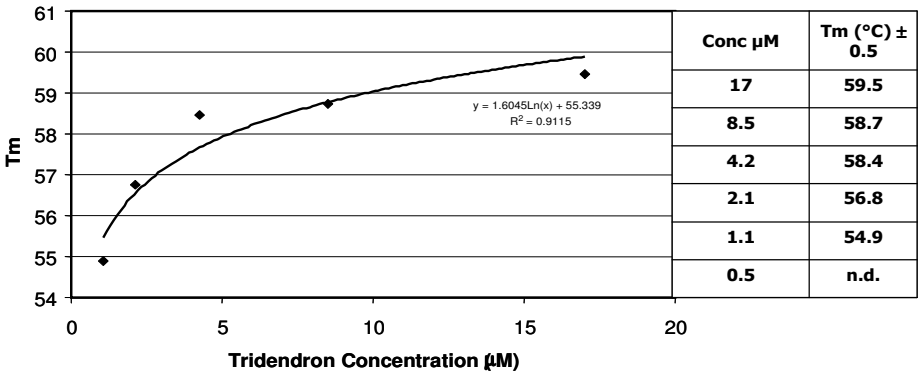

Conc µM	Tm (°C) ± 0.5
17	59.5
8.5	58.7
4.2	58.4
2.1	56.8
1.1	54.9
0.5	n.d.

Figure 24 Dependence of T_m from concentration of PNA *tridendron*.

Furthermore, a linear self-complementary PNA, Ac-t_5-K-a_5-KNH_2 (**2**), was realized as control. It has been synthesised in analogy to PNA *tridendron* **1** (2 µmol scale, Fmoc chemistry), purified on RP-HPLC and characterized by LC-ESIMS (Figure 25). The UV quantification of the PNA **2** provided a 30 % overall yield (600 nmol, 1.9 mg), using the ε_{260} of 111500 M^{-1} for the a_5t_5 sequence of this oligomer. In Figure 26 is reported the UV melting profile of a 5 µM solution of PNA **2** (T_m=54 °C). Contrarily to PNA *tridendron* **1**, in this case no significant changes in the T_m of oligomer **2** was revealed, by varying its concentration from 1 to 30 µM. All these findings support the formation of a three-dimensional network for system **A**.

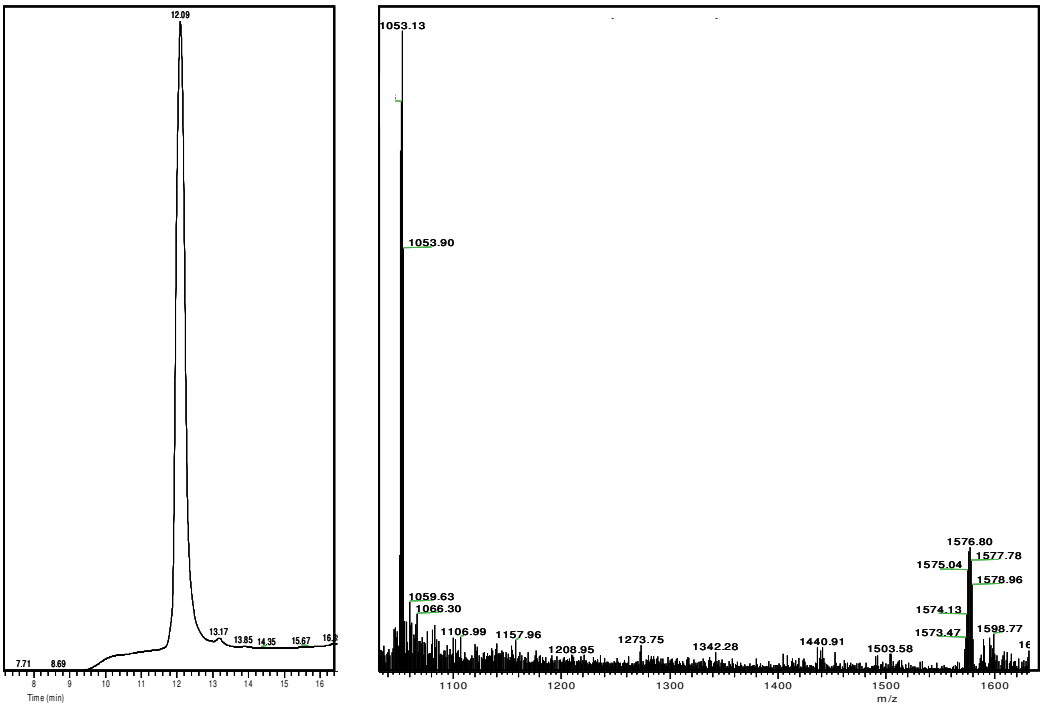

Figure 25 LC-ESIMS profile of Ac-t_5-K-a_5-KNH_2

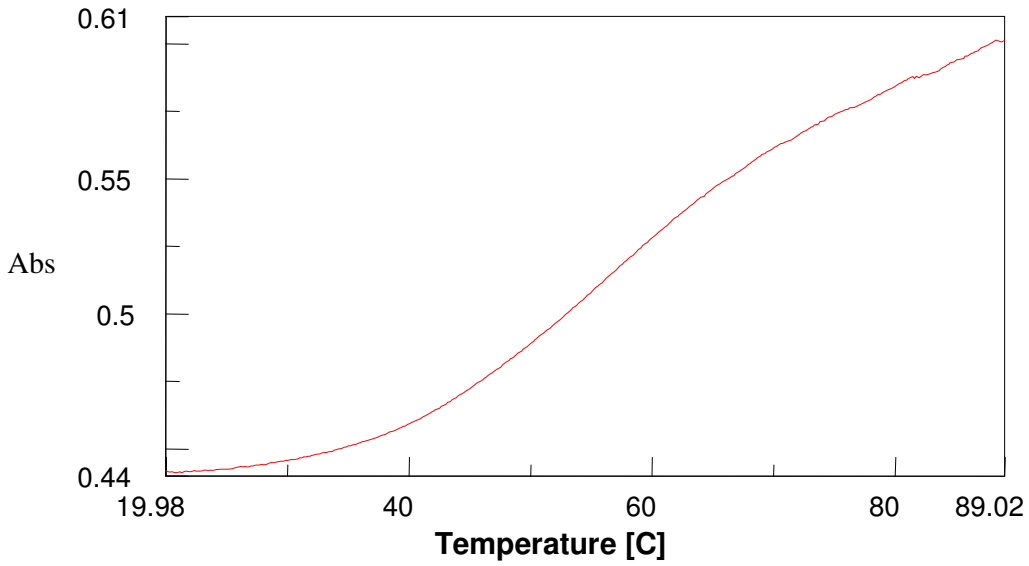

Figure 26 UV melting curve of Ac-t_5-K-a_5-KNH_2 (**2**).

To exclude the possibility that the central lysine in system **A** could interrupt the cooperativity of the duplexes formed by the *tridendron* arms, leading to the formation of a less stable three-dimensional network, we synthesized, as controls, two linear PNA strands having the sequences of the PNA *tridendron* arms: H-G-a_5-KNH_2 **(3)** and H-G-t_5-$KKNH_2$ (**4**). Oligomers **3** and **4** were synthesized on solid phase using standard 2 μmol-scale protocol, purified on RP-HPLC and characterized by LC-ESIMS (Figures 27 and 28).

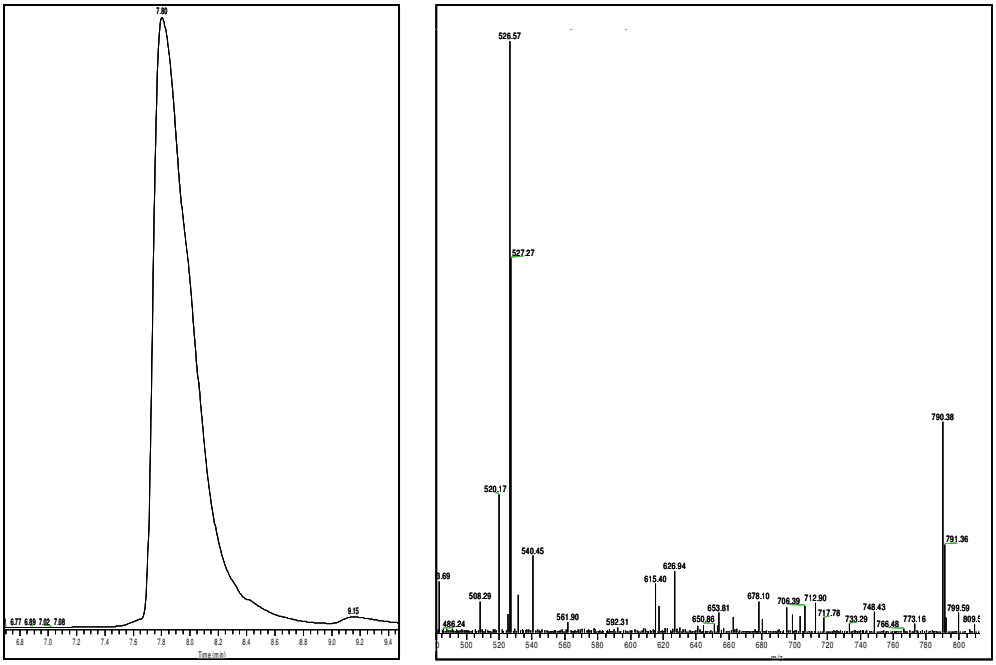

Figure 27 LC-ESIMS of H-G-a_5-KNH_2 (**3**).

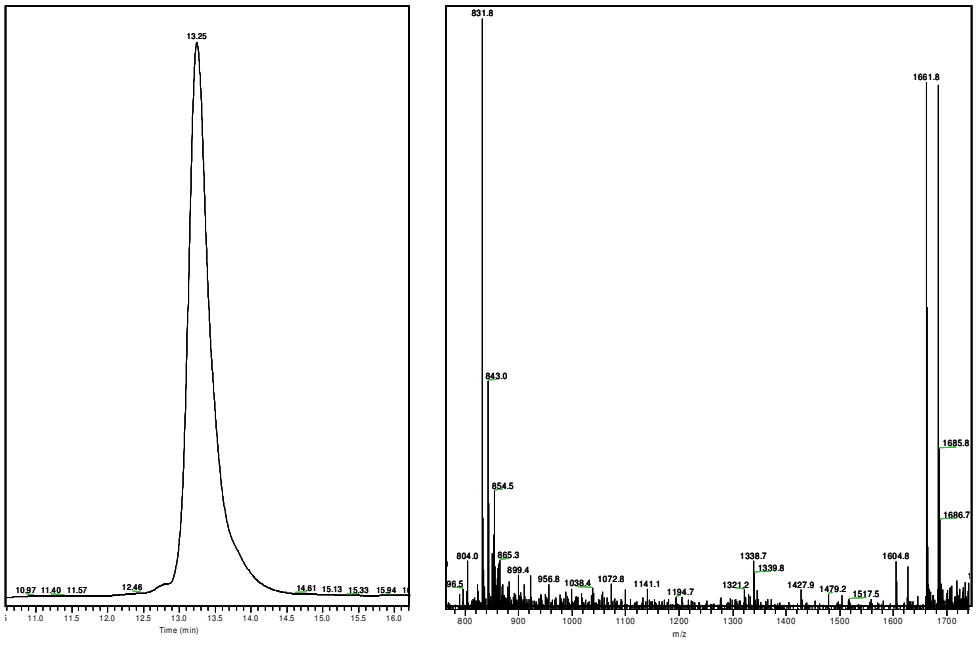

Figure 28 LC-ESI MS of H-G-t_5-$KKNH_2$ (**4**).

The UV quantification of the PNA **3** and **4** provided the following value: 750 nmol, 1.2 mg, 37 % overall yield for **3** (ε_{260}=68500 M^{-1}); 650 nmol, 1.0 mg, 33 % overall yield for **4** (ε_{260}=43000 M^{-1}).

The UV melting curve of the 1:1 complex of **3** and **4** showed a T_m value of only 19 °C at 4 uM (Figure 29) respect to 58 °C for *tridendron* **1** at the same concentration, demonstrating that the lysine core in system **A** doesn't create a great issue for the cooperativity of the duplexes formation.

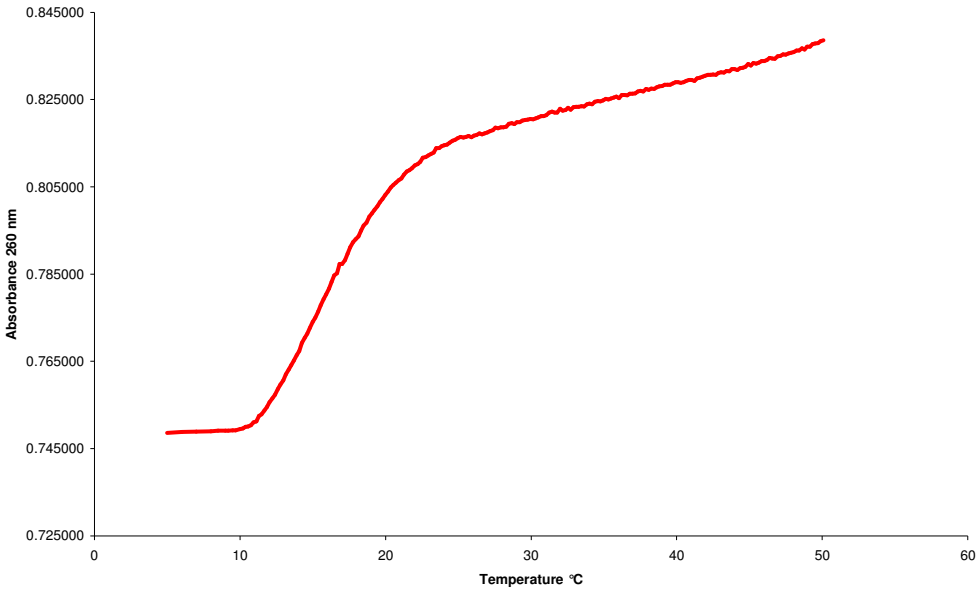

Figure 29 UV melting curves of 1:1 a_5/t_5 complex.

Since the dimension of the monomolecular self-assembly dendrimeric system is not easily controllable, if not acting on the concentration of the component (**1**), we also designed and realized a bimolecular system (**B**, Figure 19) constituted of PNA and DNA *building blocks*.
A two component system should give the possibility to perform a fine control of the shape and the dimension of the three-dimensional dendrimeric network.

1.2 Bimolecular PNA/DNA dendrimer

The bimolecular dendrimeric system **B** (Figure 19), made up of a PNA *tridendron* with a not self-assembly sequence and a DNA crosslinker, has the ability to form a three-dimensional network exploiting the formation of PNA/DNA duplexes. In Figure 30 is shown a schematic view of the bimolecular system realized.

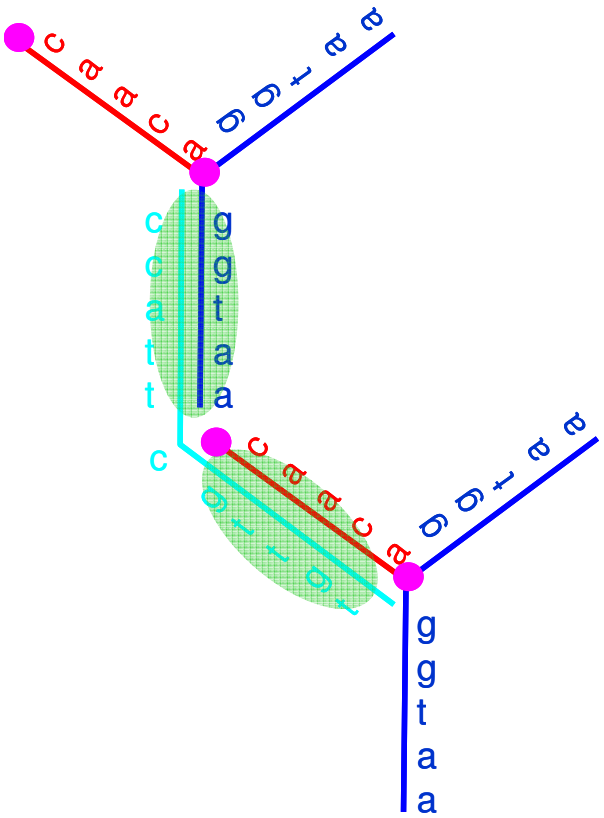

Figure 30 PNA/DNA dendrimeric system **B**. Red: PNA arm at C-terminus; blue: 2 arms of PNA having the same sequence; magenta: lysines; light blue: DNA crosslinker; green shadowing: PNA-DNA double helix.

The PNA *tridendron* sequence is (Ac-a-a-t-g-g)$_2$- K-a-c-a-a-c-KNH$_2$ (**5**), while the DNA crosslinker one is $^{5'}$C C A T T C G T T C T$^{3'}$ (**6**). The DNA was complementary to two of the PNA *tridendron* branches.

PNA **5** was synthesized on solid phase synthesis by using Fmoc chemistry and 2 μmol-scale standard protocol. The crude PNA was purified on RP-HPLC and characterized by ESI-MS (Figure 31).

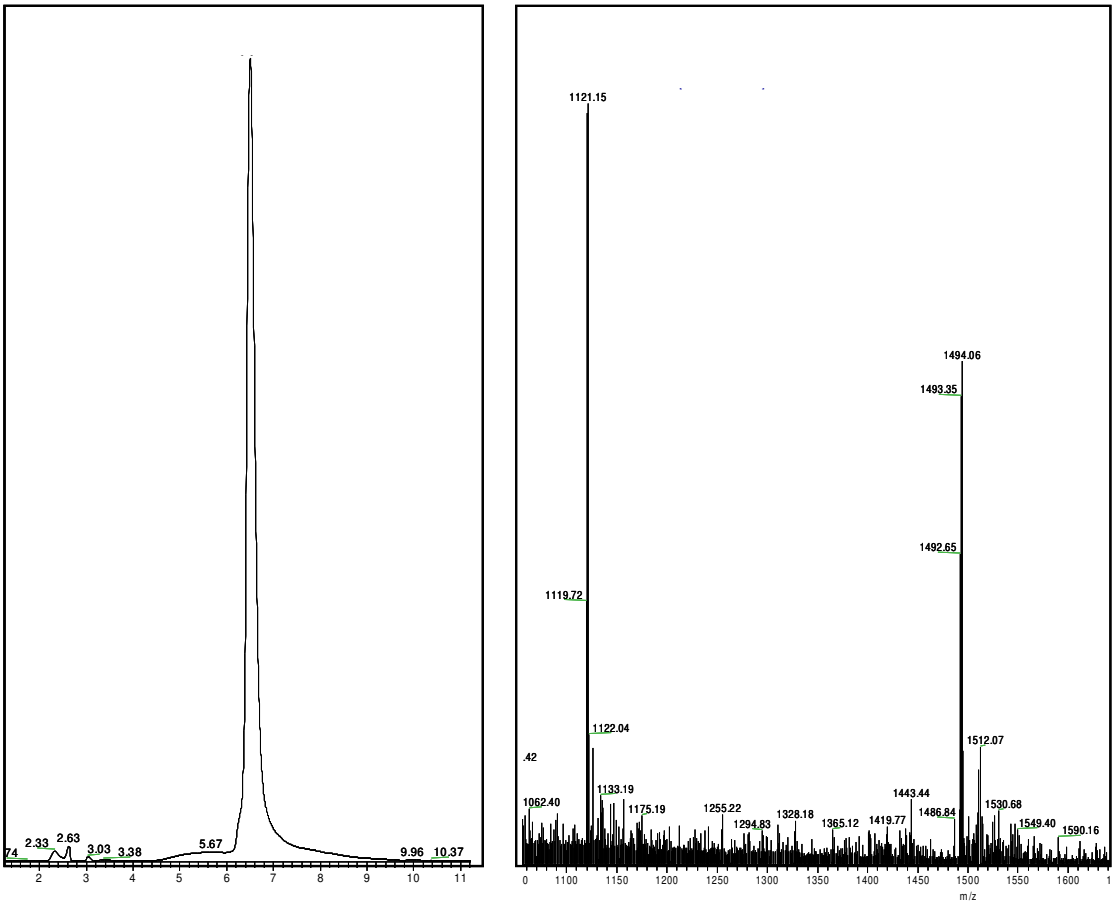

Figure 31 LC-ESIMS profile of the PNA *tridendron* **5**.

Crosslinker **6** was assembled on automatic synthesizer using standard 1 μmol-scale protocol and phosphoroamidite chemistry. After cleavage and deprotection, the DNA oligo was purified by HPLC using an anionic exchange column, desalted by gel filtration, and characterized by MALDI-TOF spectrometry (data not shown).

The oligomers **5** and **6** were lyophilised, dissolved in a known amount of milliQ water and quantified by UV measurements (T= 85 °C, absorbance value at λ=260 nm). UV quantification of **5** ($c_2a_7t_2g_4$) provided 500 nmol of the PNA (2.1 mg, 25 % yield), using ε_{260}=173100 M^{-1}. UV quantification of DNA **6** was performed using the ε_{260}=104700 M^{-1}, calculated considering as extinction coefficients for the single base the following values: A, 15.4; T, 8.8; G, 11.7; C, 7.3 mM^{-1}. In this way 586 nmol (1.9 mg, 58.6 % yield) of purified product was estimated.

We realized the bimolecular system **B** with the aim to investigate: 1) the PNA/DNA duplex formation; 2) the optimal crosslinker/*tridendron* ratio to obtain the most extensive network formation; 3) the gelation process.

We verified PNA/DNA duplex formation by CD experiments using a *tandem cell* (Figure 32) which minimize errors relative to the obtainment of the exact concentration of both PNA and DNA before and after the complex formation.

Figure 32 Hellma *tandem cell*.

Figure 33 shows the sum CD spectrum (red line) of the two separated strands (PNA *tridendron* in one compartment and DNA in the other one before mixing) and the complex spectrum (blue line) obtained after mixing the two samples; both spectra were recorded at T=20 °C in H_2O and using a 1:2.5 *tridendron*/crosslinker ratio. As shown in Figure 33, there is a significant difference between the two spectra with an increase of intensity and shift to lower wavelength of the band at 280 nm, a clear evidence of duplex formation.

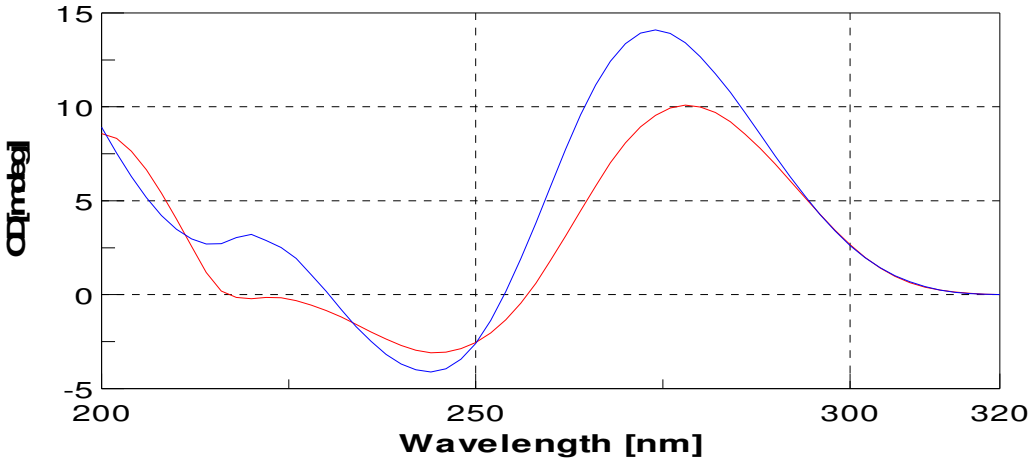

Figure 33 Sum (red line) and Mix (blue line) CD spectra of *Tridendron* **5**/Crosslinker **6**, 1:2.5, 20 °C in H_2O.

A kinetic study of the complex formation for the bimolecular system **B** was performed by CD experiments, recording CD spectra at different times, after mixing the two strands. In Figure 34 the CD signal variation at 240 nm and 275 nm was reported in function of time: after 100 min the recorded CD signal presented more or less the same value for the two wavelengths, suggesting the complete formation of the bimolecular system and hence of the three-dimensional network.

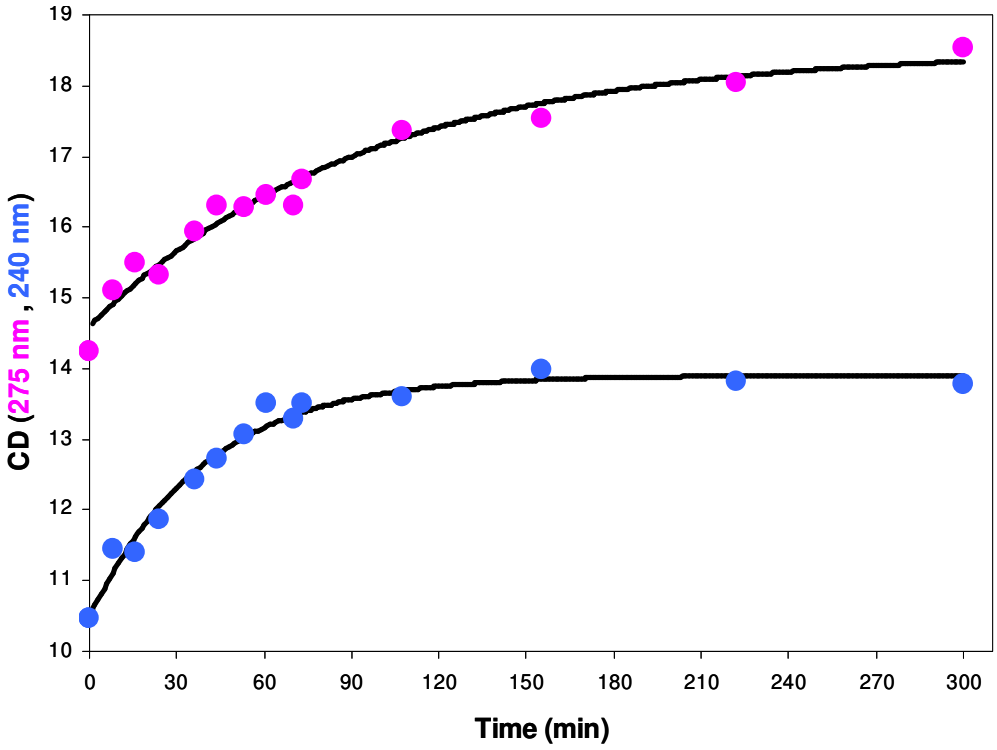

Figure 34 CD kinetic studies on bimolecular system **B**.

Being the bimolecular system formed by two components, it would be fundamental to find the optimal ratio of the two parts to obtain the most extensive and stable network. The hypothesis about the equilibrium of the network formation is reported in Figure 35: at low concentration of crosslinker there will be a certain amount of duplex formed and some free *tridendron*. In excess of DNA crosslinker, all the *tridendron* sites will be saturated and there will be some free crosslinker ends. In these two extreme cases we would expect for the system **B** a lower stability than in the case of the optimal crosslinker/*tridendron* ratio, in which there will be the maximum amount of duplex formed and consequently of the network formation.

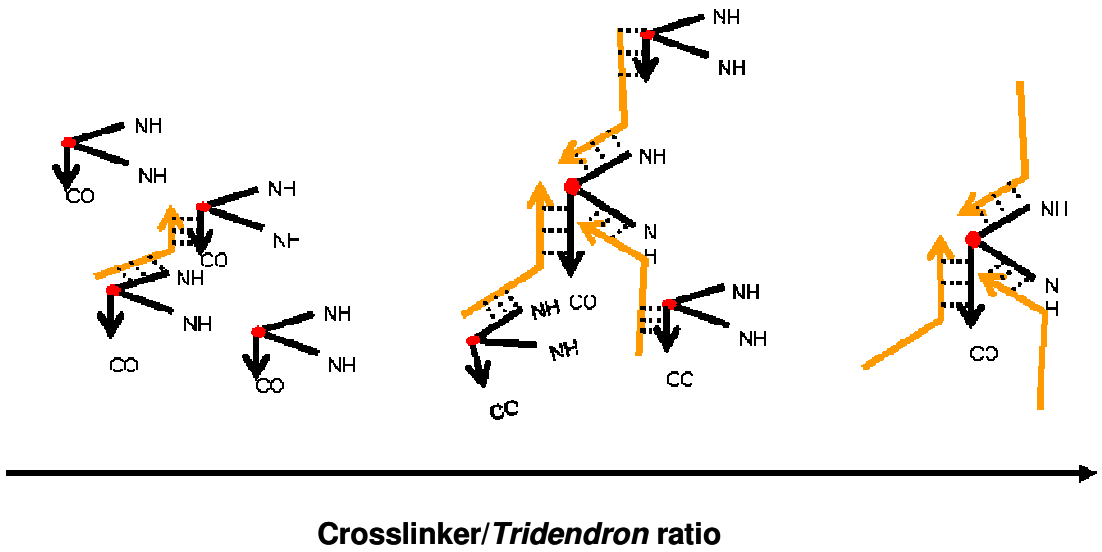

Figure 35 Equilibrium network formation.

In order to find the optimal crosslinker/*tridendron* ratio for obtaining the most extensive network formation, we performed UV melting studies on the annealed strands in H_2O with experiments in which the *tridendron* concentration was fixed and the crosslinker one was gradually increased.

The table contained in Figure 36 summarizes T_m values, calculated with the first derivatives method, at the corresponding crosslinker/*tridendron* ratios. By reporting T_m values *vs* crosslinker/*tridendron* ratios, we obtained a bell curve (Figure 36) showing a maximum at 2:1 ratio, which is thus the best one leading to the most extensive formation of the three-dimensional net. These data are in agreement with the aforementioned hypothesis on the equilibrium network formation.

Crosslinker (3)/ Tridendron (2)	$T_m \pm 0.5$ (°C)
1	38.8
1.5	41.6
2	42.8
2.5	40.3
3	37.0

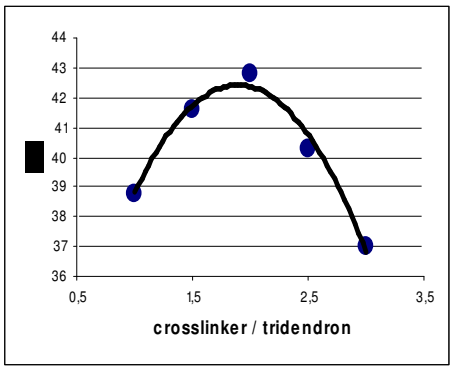

Figure 36 Table and bell curve of T_m *vs* crosslinker/*tridendron* ratio.

In Figure 37 the UV melting profile of a solution contained the PNA *tridendron* **5** and the DNA crosslinker **6** at the best ratio (1:2) is reported.

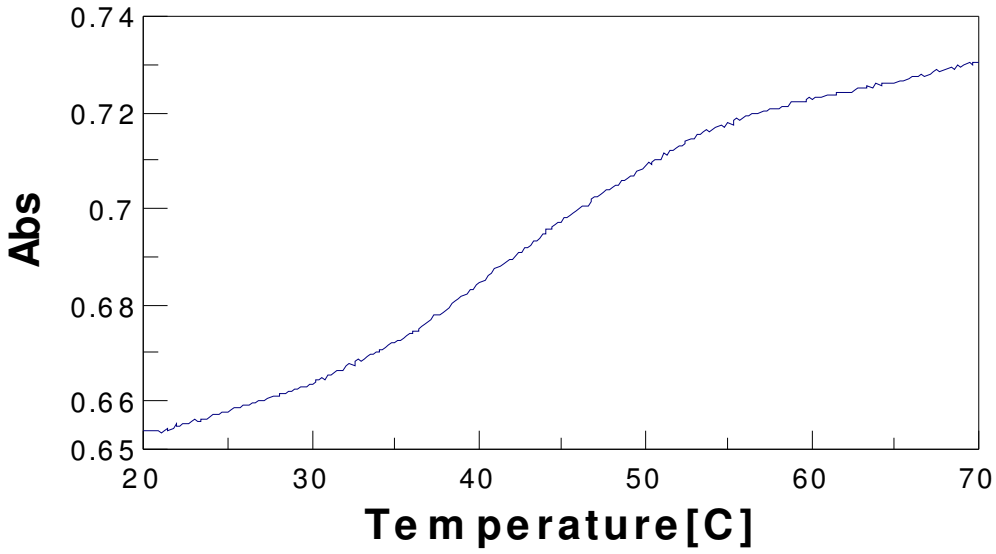

Figure 37 UV melting curve of *tridendron*/crosslinker, 1:2.

1.3 Preliminary gelation test.

We continued our studies testing the ability of the two new dendrimeric systems to realize hydro gels, exploiting the formation of a three-dimensional network obtained by specific W-C base pairing, to be used in various applications, like as for encapsulating drugs. Preliminary gelation tests were performed on both the systems **A** and **B** by dissolving the lyophilized oligomers in 200 µL water, heating at 90 °C for 5 minutes, slowly cooling at room temperature and finally storing at 4 °C for 12 hours. For system **A**, the tests were performed using 50µM and 200µM concentrations at 20 °C. For system **B**, we used the optimal ratio *tridendron*/crosslinker, of 1:2, 50 µM and 200 µM overall concentrations at 20 °C, 400 µM and 600 µM concentrations at 4°C.

In the case of system **B**, we observed the formation of a labile layer on the bottom of the glass tube as showed in the picture below (Figure 38).

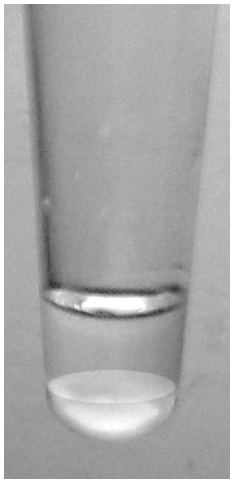

Figure 38 Preliminary gelation test on system **B**.

1.4 Microrheology experiments on systems A and B.

In general, the aim of microrheology, performed by using the Multiple Particle Tracking (MPT) technique, is to study the viscoelastic properties of materials, exploiting the Brownian motion of micron-sized particles embedded in samples.[46] A typical experimental setup employs videomicroscopy to track the Brownian motion of micron-sized, inert, fluorescent particles.[47] Information about the local mechanical properties of the sample is then obtained by performing statistical analysis of the tracer particle motion.

For both the systems **A** and **B**, a solution of fluorescent polystyrene beads (diameter, 0.55 μm) was added to the sample solutions, obtained as described for the gelation tests. 80µL of the resulting mixture were fixed on a glass slides and stored 10 minutes at 4°C to perform microrheology experiments.

We performed and processed the motion of these fluorescent particles in our dendrimeric systems to obtain information on the rheological behaviour of the systems, as well as of sterical and chemical interactions between the particles and the network.

The experiments on the dendrimeric systems were performed as follows: for 15 different zones on the glass slides, a stack of 250 images of the beads were recorded on a digital microscope Olimpus 1X51 (Schematic view Figure 39). For each of the 250 images the computer calculates the number of beads, their position in the recorded image by using a 2-D particle tracking algoritm.

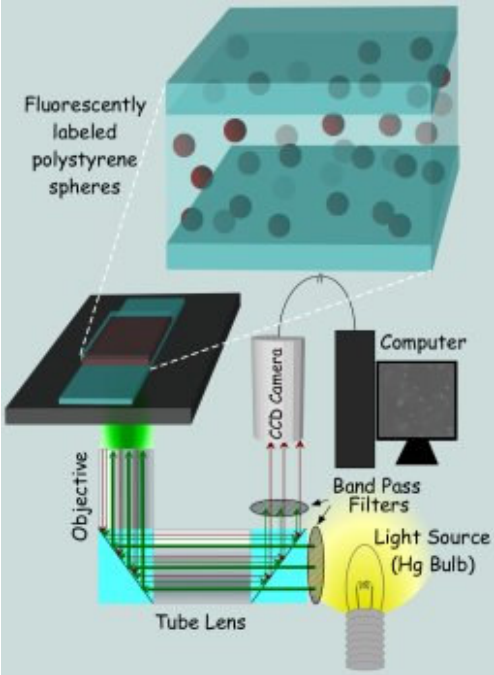

Figure 39 Microrheology apparatus

The results obtained were processed by an home made Matlab program, allowing us to obtain, by the generalized Stokes-Einstein equation, the dynamic parameters G ' (elastic modulus) and G" (viscosity modulus), which, reported in graph *vs* frequency, showed us the behaviour of the medium (G'<G''=sol, G'>G''= gel, G'= G'' sol-gel equilibrium.).

From the data analysis the behaviour of the dendrimeric systems realized are typical of a polymer solution. Indeed, in the case of bimolecular system, shown in Figure 40 G''>G' in all the investigated frequency range, and, furthermore, both the dynamic moduli show a dependence upon the frequency as typical of a polymer solution.

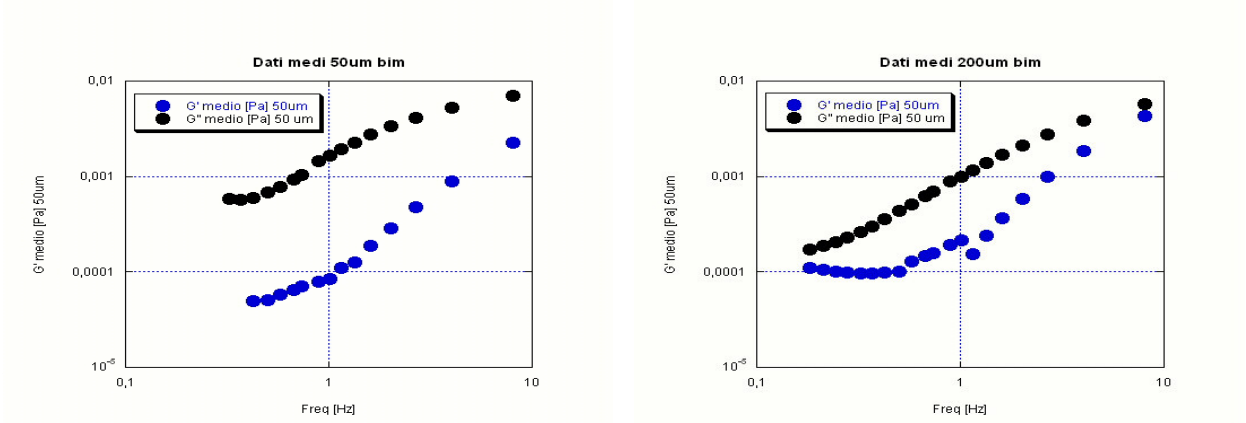

Figure 40 Bimolecular system microrheology test .

1.5 Conclusion

This part of thesis describes kinetic and thermodynamic study relative to the formation of PNA and PNA/DNA dendrimers. We realized two kind of systems: a PNA-based monomolecular system (**A**, Figure 19) and a PNA/DNA bimolecular one (**B**, Figure 19). The system **A** is formed exclusively of a three branched PNA (PNA *tridendron*), while the bimolecular system **B** is made of a PNA *tridendron* with a mixed sequence, and a DNA crosslinker. Both systems have the ability to form a three-dimensional network by means of specific W-C hybridization.

The components of the two systems were realized in solid phase by using Fmoc chemistry for the PNA, and phosphoroamidite chemistry in the case of the DNA. All the oligomers, deprotected and detached from the solid support, were purified by HPLC and characterized by MALDI-TOF and ESI-MS. A detailed spectroscopic study was performed on both systems to verify the formation of the oligonucleotidic network allowing us to elucidate its thermodynamic and kinetic properties. Finally, we proceeded with microrheology experiments to test the ability of the systems to realize hydro gels for encapsulating drugs.

Unfortunately our system was not able to form stable hydro gels , probably due to the not so high concentration realized. Thus, other gelation experiments, using greater concentrations of the components, will be under investigation and as a consequence it will require large scale synthesis of PNA and DNA components.

Furthermore, we will explore other dendrimeric systems, using for example *tridendron* with arms more than 5 base in length, to verify if in the previous analyzed cases (**A** and **B** systems Figure 19) the sol behaviour was due to the concentration used or to the inability to form extended three-dimensional network with short arms.

1.6 Materials and methods

Chemicals

Fmoc-Gly-OH, HATU, Fmoc-Lys(Boc)-OH, Fmoc-Lys(Fmoc)-OH, and PyBOP were purchased from Novabiochem. Anhydroscan DMF and NMP were from LabScan. Piperidine was from Biosolve. Solvents for HPLC chromatography and acetic anhydride were from Reidel-de Haën. TFA, Rink-amide resin, were Fluka. Perspective Biosystem PAL-Peg resin, PNA kit (Fmoc/Bhoc monomers, HATU activator, Base solution, Wash B, DIEA, Cap Solution, Deblock solution) was purchased from PRIMM (Milan, Italy). TFA (for HPLC) were from Romil.

Apparatus

aegPNA oligomers were assembled on solid-phase with an Applied Biosystems Expedite 8909 oligosynthesizer.

Crude samples containing PNA oligomers were centrifuged for 4 min at 4000 rpm (Z 200 A, Hermle).

Products were analysed by LC-MS, performed on an MSQ mass spectrometer (ThermoElectron, Milan, Italy) equipped with an ESI source operating at 3 kV needle voltage and 320 °C, and with a complete Surveyor HPLC system, comprising an MS pump, an autosampler, and a PDA detector, by using a Phenomenex Jupiter C18 300 Å (5 µm, 4.6×150 mm) column. Gradient elution was performed at 40 °C (monitoring at 260 nm) by building up a gradient starting with buffer A (0.05% TFA in water) and applying buffer B (0.05% TFA in acetonitrile) with a flow rate of 0.8 ml/min.

Semi-preparative purifications were performed by RP-HPLC on a Shimadzu LC-8A, equipped with an SPD-10A VP UV/Vis detector, and on a Hewlett Packard/Agilent 1100 series, equipped with a diode array detector, by using a Phenomenex Juppiter C18 300 Å (10 µm, 10×250 mm) column. Gradient elution was performed at 45 °C (monitoring at 260 nm) by building up a gradient starting with buffer A (0.1% TFA in water) and applying buffer B (0.1% TFA in acetonitrile) with a flow rate of 4 ml/min.

Samples containing PNAs (crude or purified), were lyophilized in a FD4 Freeze Dryer (Heto Lab Equipment) for 16 hours.

Circular dichroism (CD) spectra were obtained at 20 °C on a Jasco J-810 spectropolarimeter using 1-cm cuvette and tandem cuvette quartz (Hellma).
Tandem cell, containing two compartments separated by a quartz window (2 × 4.375 mm, Suprasil quartz, Hellma). CD spectra parameters were: spectral window 320-200 nm, data pitch 2 nm, band width 2 nm, response 4 sec, scanning speed 50 nm/min, 3 accumulations.

Ultraviolet (UV) spectra and UV melting experiments were recorded on a UV-Vis Jasco model V-550 spectrophotometer equipped with a Peltier ETC-505T temperature controller using 1-cm quartz cuvette (Hellma).

Microrheology experiments were performed on an Olympus 1x51 microscope (10x, 60x, 100x lenses) equipped with a Hg lamp and a camera Princeton Instrumentation Micromax 5MHz (model vt-133).

Solid phase synthesis of oligomers 1-5

Solid support functionalization and manual solid-phase oligomerizations were carried out in short PP columns (4 ml) equipped with a PTFE filter, a stopcock and a cap. Solid support used were PalPegPs (0.16 NH_2/g) resin and Rink-amide one (0.48 mmol NH_2/g, 128 mg), both functionalized with a lysine residue. The Rink-amide resin was functionalized with a lysine (Fmoc-Lys(Boc)-OH), (0.5 eq, 14.8 mg, 32 µmol) using PyBOP (0.5 eq, 16.8 mg, 32 µmol) as activating agent and DIEA (1 eq, 12 µL, 64 µmol) as base for 30 min at room temperature. Capping of the unreacted amino groups was performed with Ac_2O (20%)/ DIEA (5%) in DMF. Loading of the resin was checked by measuring the absorbance of the released Fmoc group (ε_{301}=7800, quantitative yield) after treatment with a solution of piperidine (30%) in DMF (UV Fmoc test) and resulted reduced to 0.25 mmol/g respect to the initial functionalization. Automatic solid-phase assembly of the *aeg*PNAs was performed on an Expedite 8909 Nucleic Acid Synthesis System using a standard 2 µmol-scale protocol and Fmoc chemistry leaving the final Fmoc on in order to evaluate SPS yields by UV Fmoc test. A glycine residue (3 eq) was attached to the N-terminus of the oligomers (3,4) by using PyBOP (3 eq)/DIEA (6 eq) as activating system in DMF. After removal and quantification of the Fmoc group, all oligomers were cleaved from the resin and deprotected under acidic conditions (TFA/m-cresol 4:1 v/v). The oligomers were isolated by precipitation with cold diethyl ether, centrifugation and lyophilization. Purified oligomers (semipreparative HPLC) were quantified and characterised by LC-ESIMS.

Ac-$(t_5)_2$-K-a_5-K-NH_2 (**1**) Standard *aeg*PNA was assembled on PAL-PegPS-K-NH_2 resin (0.16 mmol/g, 2µmol, 12.5 mg) on the automatic synthesizer. The synthesis proceeded till the first poly adenine tract on the synthesizer then manually was added Fmoc-Lys(Fmoc)-OH (8 eq) HATU (7.2 eq)/DIEA (8 eq), performing a double coupling. Capping of the unreacted amino groups with (5% Ac_2O, 6% lutidine in DMF) and then the deblock (25% piperidine in DMF) to remove both the Fmoc groups, were performed. The synthesis continued on the automatic synthesizer till the end. After the synthesis was complete the final Fmoc was left on and removed manually to perform Fmoc UV test, at the end the free amino group were acetylated. The cleaved and deprotected oligomer was purified by semipreparative RP-HPLC using a linear gradient of 10% (for 5 min) to 20% B in A over 35 min: t_R=27.7 min. The purified yield of Ac-$(t_5)_2$-K-a_5-K-NH_2 was of 24%. ESI-MS (Figure 21) *m/z*: 1463.85 (found), 1466.33 (expected for $[M+3H]^{3+}$), *m/z*: 1097.88 (found), 1099.75 (expected for $[M+4H]^{4+}$).

Ac-t_5-K-a_5-KKNH_2 (**2**) was assembled on automatic synthetizer on Rink-amide-K-NH_2 resin (0.25 mmol/g, 2µmol, 8 mg) using the standard Fmoc protocol used for sequence **1**. After cleavage and deprotection, the oligomer **2** was purified by semipreparative RP-HPLC using a linear gradient of 7% (for 5 min) to 22% B in A over 20 min: t_R=18.0 min; ESI-MS (Figure 25) *m/z*: 1053.13 (found), 1051.01 (expected for $[M+3H]^{3+}$), *m/z*: 1576.80 (found), 1575.90 (expected for $[M+2H]^{2+}$).

H-G-a_5-KNH_2 (**3**) was assembled manually on Rink-amide-K-NH_2 resin (0.25 mmol/g, 2µmol, 8 mg) using the following protocol: 0.1 M Fmoc-a(Bhoc)-OH monomer in NMP (40 µl, 8 µmol, 4 eq), 0.18 M HATU in DMF (40 µl, 8 µmol, 4 eq) and base solution [0.2 M Dipea, 0.3 M Lutidine] (40 µl, 8 µmol, 4 eq) in DMF. Preactivation (2 minutes) of the monomer, HATU and base solution was performed, then the mixture was added to the resin, and the coupling was left for 15 min with shaking at room temperature.

Successively, unreacted amino groups were capped with PNA Cap solution for 5 min. Fmoc removal was accomplished with PNA Deblock solution (5 min) and was monitored for every step by UV measurements: average yield for the five steps was 90% . After last coupling with the glycine, oligomer was cleaved from the resin and deprotected under acidic conditions (TFA/m-cresol 4:1 v/v) and isolated by precipitation with cold diethyl ether, centrifugation and lyophilization. The oligomer was purified by semipreparative RP-HPLC using a linear gradient of 1% (for 5 min) to 18% B in A over 30 min: t_R=20.2 min; and characterised by LC-ESIMS (Figure

27) *m/z*: 526.57 (found), 526.72(expected for $[M+3H]^{3+}$ *m/z*: 790.38 (found), 789.58 (expected for $[M+2H]^{2+}$).

G-t_5-KKNH$_2$ (**4**) was obtained analogously to sequence **3**, purified by RP-HPLC using 5% (for 5 min) to 22% B in A over 30 min: t_R=26.8 min; characterized by ESI-MS (Figure 28) *m/z*: 1661.8 (found), 1661.64 (expected for $[M+H]^+$). *m/z*: 831.8 (found), 831.76 (expected for $[M+2H]^{2+}$).

(Ac-a-a-t-g-g)$_2$-K-a-c-a-a-c-KNH$_2$ (**5**) was obtained analogously to sequence **1**, purified by semipreparative RP-HPLC using a linear gradient of 8% (for 5 min) to 18% B in A over 35 min: t_R=24.4 min, characterized by LC-ESI MS (Figure 31); *m/z*: 1021.15 (found), 1122.2 (expected for $[M+4H]^{4+}$), *m/z*: 1494.06 (found), 1492.97 (expected for $[M+3H]^{3+}$).

The synthesis of **$^{5'}$C-C-A-T-T-C-G-T-T-C-T$^{3'}$**(**6**) was performed on an Expedite 8909 synthesizer (ABI/Perceptive Biosystems), using standard phosphoramidite chemistry and 1 µmole scale protocol. DNA synthesis was carried out in 3' to 5' direction using, as solid support, CPG 500 Å resin (40 umol/g, 1 umol), functionalized with the first 3'-hydroxyl-5'-Dimethoxytrityl-nucleoside. After deprotection and cleavage from the solid support with ammonia solution (55 °C, 15h), the crude chimeric oligomer was purified by HPLC on a Nucleogel SAX column (Machery Nagel SAX 4.6x50 mm) eluted with linear gradients of KCl (0-100%) in 20 mM K_2HPO_4, pH 7.0, 20 % CH_3CN. The major peak collected was liophylized, dissolved in 2.5 ml of milliQ water and desalted by gel filtration on a NAP-25 column. Desalted oligo was quantified by UV measurerements and characterized by MALDI-TOF *m/z* : 3294 (found), 3299 expected for MH^+.

UV and CD studies

Purified oligomers were dissolved in a known amount of milliQ water and quantified by UV measurements (T=85 °C, absorbance value at λ=260 nm). The epsilon used for the quantification of the oligomers was calculated using the molar extinction coefficient of *aeg*PNA monomers and of DNA one in the case of the crosslinker.

Annealing of all PNA oligomers with complementary part was performed by mixing amounts of the two strands to achieve duplex of the desiderated concentration. The solution was heated at 85 °C (5 min) and then allowed to cool slowly to room temperature.

Thermal melting curves were obtained by recording the UV absorbance at 260 nm while the temperature was ramped from 20 to 90 °C at a rate of 0.5°C/min. T_m values, calculated by the first derivative method, were reported .

CD spectra were recorded from 320 to 200 nm at 20°C: scan speed 50 nm/min, data pitch 2 nm, band width 2 nm, response 4 sec, 3 accumulations.

Michrorheology experiments.

The samples for michrorheology experiments for both systems **A** and **B** were obtained by dissolving the lyophilized oligomers in 200 µL water, heating at 90 °C for 5 minutes, slowly cooling at room temperature and finally storing at 4 °C for 12 hours.

The mixtures were embedded with 3 µL of diluted solution of fluorescent polystyrene beads (0.55 µm). The beads are molecular probe with 0.2% of the solid part in solution. 80 µL of each sample were fixed in a chamber on a glass slides to perform microrheology experiments at microscope.

For system **A**, the tests were performed using 50µM and 200µM concentrations at 20 °C. For system **B**, we used the optimal ratio *tridendron*/crosslinker, of 1:2, 50 µM and 200 µM overall concentrations at 20 °C, 400 µM and 600 µM concentrations at 4°C.

PART 2: Synthesis and hybridization studies of new oligonucleotidic analogous.

Aminoethylglycyl peptide nucleic acids (*aeg*PNAs 1, Figure 41) emerged more than a decade ago as strong and specific DNA/RNA binding agents, triggering much research interest into the development of PNA based antisense/antigene therapeutics or diagnostics[48] thanks to their remarkable properties. Many efforts have mainly been directed towards the refinement of *aeg*PNA properties such as binding affinity to DNA/RNA, water solubility, cellular uptake and discrimination between parallel and antiparallel binding modes. Different PNA modifications are widely described in the scientific literature,[49-56] having met in some cases with success.

The most explored PNA modifications regarded the aminoethylglycine backbone and the methylene carbonyl linker (1st generation modifications). In the 1st generation modifications the only tolerated substitution regards the α-position of the glycine. For example, substitution of the glycine with an alanine (D or L) resulted in a slightly lower binding affinity towards DNA.[50]Introduction of a D-lysine resulted in a slight increase of T_m in the binding to DNA, while the L-isomer had the opposite effect. [53]

In addition, much work has been devoted to investigate various cyclic backbone-based PNAs[49,52-54, 56] (2nd generation modifications) with the goal of increasing the selectivity or strength of interaction with natural nucleic acids. This class of modifications, by connecting different parts of the PNA backbone, introduces conformational restrictions and stereocenters into the polymer which can present remarkable hybridization properties. Among these kind of modifications aminoprolyl PNA containing oligomers are very interesting.[51-54] *aeg*PNAs with a single aminoprolyl PNA unit at *N*-terminus showed discrimination of antiparallel vs parallel binding to DNA. Another class of interesting PNA analogues is based on a diaminoacid backbone carrying the nucleobase by means of an amidic bond to one amino group. In particular, it was recently reported that an oligo thymine PNA analogue based on D- or L-ornithine (**3**, Figure 41) binds to RNA by forming triple helices.[55]

In this context we report our investigation about novel chiral PNA analogues, focusing the attention not only to the synthetic strategies but also to the binding studies towards natural and non-natural targets.

In our research for the development of new ODN-like drugs or diagnostics, we designed and realized a chiral nucleo-γ-peptide, *dab*PNA (**2**, Figure 41), isomer of the *aeg*PNA unit (**1**, Figure 41) and characterized by a 2,4-diaminobutyric acid (DABA)-based backbone carrying the carboxymethylated nucleobase on its α amino group.

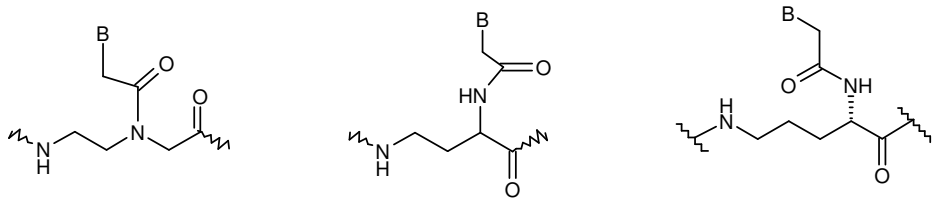

*aeg*PNA **1** *dab*PNA **2** *orn*PNA 3

Figure 41 Chemical structure of *aeg*PNA (**1**), *dab*PNA (**2**), *orn*PNA (**3**).

Differently from *aeg*PNA monomers, *dab*PNA (**2** Figure 41) presents a shorter backbone (3C between the nitrogen atom and the carbonyl) and an enhanced distance between the nucleobase and the backbone, i.e. 3 atoms (1N+2C) instead of 2C in *aeg*PNAs. Furthermore, in comparison with *orn*PNA (3) that binds to RNA forming a stable triplex, DABA-based PNA has a methylene group less in the backbone.

Our interest to the presented *dab*PNA arises from the possibility to obtain new molecules able to bind DNA and RNA for therapeutical or diagnostic applications. Furthermore, this research was supported by the known stability of γ-peptides to enzymatic degradation and also by the proposal formulated by Meierhenrich et al.[57]DABA-based PNAs as prebiotic material in a primordial "PNA world" that would have preceded our present-day "two-polymer world". This hypothesis followed the recovery of DABA and other diaminoacids[57] in the extraterrestrial soil of the Murchison meteorite together with the DNA purine and pyrimidine bases.[58]

2.1 Synthesis and oligomerization of $t_{L\text{-}dab}$ monomer, and binding studies on $(t_{L\text{-}dab})_{12}$ oligomer

The L-enantiomer of the natural diaminobutyric acid, was chosen, as starting material for the synthesis of the new monomer, in analogy to the L-ornithine-based PNAs, proposed by Petersen *et al.*[59] The thymine containing monomer was synthesised starting from the commercially available Boc-(L)-DAB(Fmoc)-OH diaminoacid (**1**, Scheme 2). In the first synthetic step the Boc group was selectively removed with trifluoroacetic acid (TFA) to give the free amino group in α-position. The obtained product **2**, characterized by ^{1}H NMR and LC-ESIMS, was coupled with the thymine-1-acetic acid using HATU/DIEA/TMP as activating system in DMF leading to the compound **4** (Scheme 2) in 72 % yield.

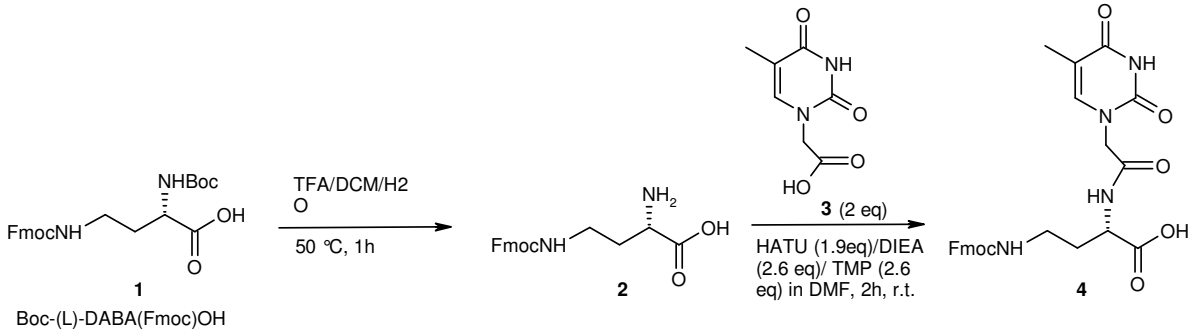

Scheme 2 Synthesis of $t_{L\text{-}dab}$ monomer.

The Fmoc-protected monomer **4** was purified by precipitations and characterized by $^{1}H/^{13}C$ NMR and LC-ESIMS, shown in Figure 42.

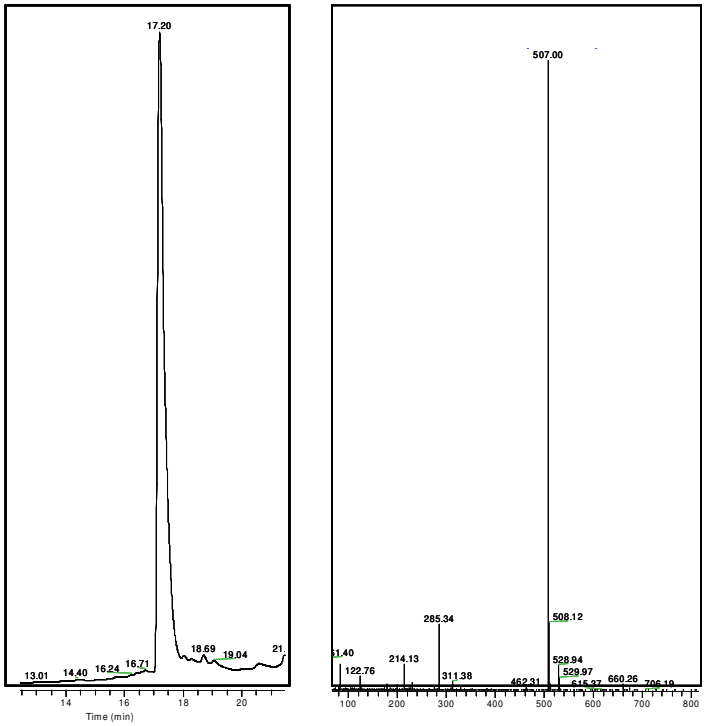

Figure 42 LC-ESIMS of $t_{L\text{-}dab}$ monomer.

The new monomer **4** was oligomerized manually on solid phase to the corresponding *dab*PNA dodecamer (**5**, Table 1) as showed in scheme 3. Since the base-mediated deprotonation of the carboxylic group and the time for its preactivation in basic conditions are critical points to avoid

racemization during the amidation of carboxylic acids with a chiral carbon in α-position,[60,61] the coupling conditions we chose made use of a mild base (TMP) and HATU as an activator, without preactivation, following the procedure introduced by Sforza et al.[61]

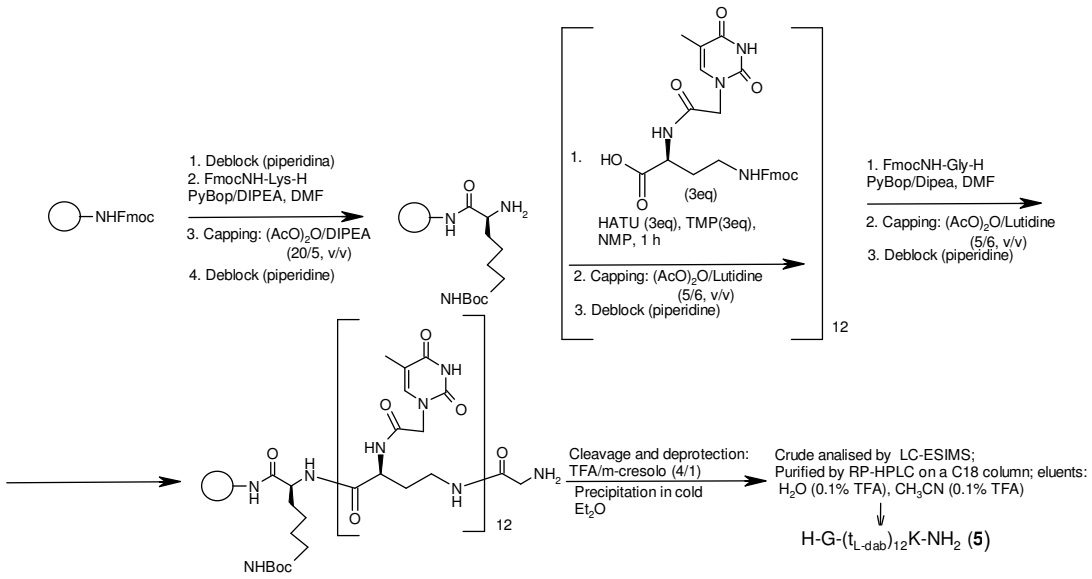

Scheme 3 Synthesis of H-G-$(t_{L\text{-}dab})_{12}$K-NH_2 oligomer.

The manual synthesis of the oligomer **5** allowed us to check, by UV Fmoc test, the coupling efficiency which was high in the first six steps (about 96%) and decreased gradually from 96% to 70% in the last six steps, probably because of the enhanced aggregation tendency of the increasing homo thymine chain. L-lysine and glycine residues were incorporated in the strand at C and N termini, respectively, to improve the solubility of the homo thymine polymer (overall yield: 24%). After cleavage and deprotection, the oligomer **5** was purified by semipreparative RP-HPLC, and successively characterized by LC-ESIMS (Figure 43).

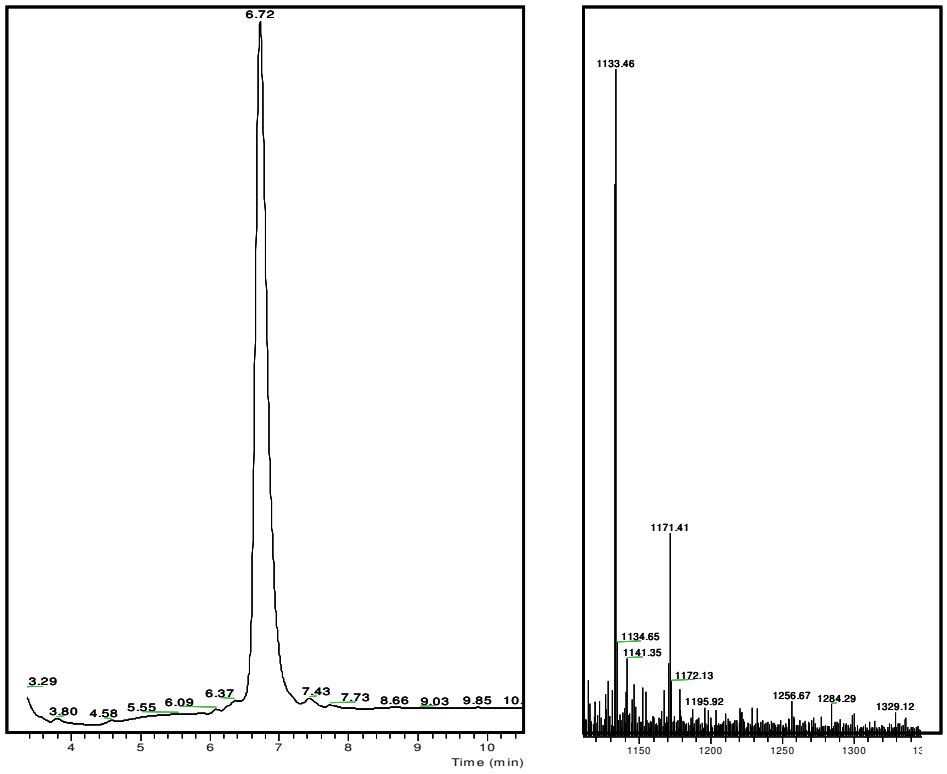

Figure 43 LC-ESI MS of H-G-$(t_{L\text{-}dab})_{12}$K-NH_2 oligomer.

A t_{12} *aeg*PNA (**6**, Table 1) was synthesised as reference oligomer for the binding studies. The synthesis of **6** was realized on the automatic synthesizer showed in Figure 13 using standard 2 μmol scale protocol and the commercial PNA monomers (Figure 14). Overall yield of **6** was only of 18 % probably for aggregation problems concerning the homothymine sequence and enhanced by the automatic *flow through* synthesis. Furthermore, other two dodecamer (7 and 8, Table 1), both carrying a single $t_{L\text{-}dab}$ unit at N-terminal and central position of the *aeg*PNA chain, respectively, were synthesized in order to explore the influence of the new DABA-based monomer on the *aeg*PNA binding ability. These oligomers were assembled on automatic synthesizer using a standard 2 μmol-scale protocol for the *aeg*PNA part and with manual single insertion of $t_{L\text{-}dab}$ monomer using the protocol described for **5**. The overall yields of **7** and **8** were 18% and 19%, respectively. After deprotection and detachment from the solid support with TFA, oligomer **6-8** were purified by RP-HPLC and characterized by LC-ESIMS.

All the dodecamers, **5-8**, were quantified by UV spectroscopy, measuring the 260 nm absorbance at 85 °C, due to the tendency of PNA to aggregate at room temperature, and calculating the overall extinction coefficient (ε_{260}) as the sum of the ε_{260} of the PNA thymine monomer.

For each oligomer the CD spectrum was registered. As expected, a solution of the aegPNA **6** didn't show a significant CD spectrum. In contrast, CD spectrum of the oligomer H-G-$(t_{L\text{-}dab})_{12}$K-NH_2, due to its chiral nature, showed CD signal. In particular, a negative band in the 260-290 nm region was detected (Figure 44a) analogously to the spectrum reported in literature for the PNA analogue based on the L-ornithine, H-$(t_{L\text{-}orn})_{10}$K-NH_2, that presents a negative band in the same region (Figure 44b). The chiral $t_{L\text{-}dab}$ unit in **7** and **8** seemed to be not sufficient to these oligomers to show a significant CD signal.

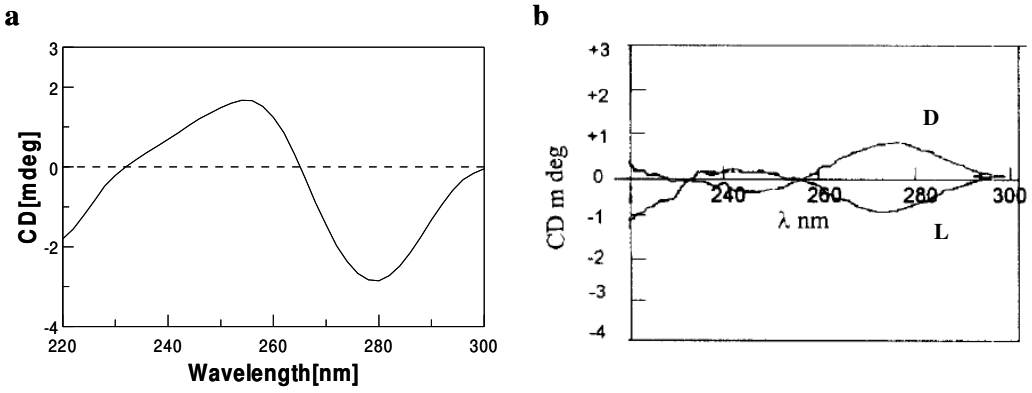

Figura 44: (a) CD spectrum of oligomer 5 H-G-$(t_{L\text{-}dab})_{12}$K-NH_2 (4 μM) in 10 mM, phosphate buffer pH 7.5; (b) CD spectra of oligomers H-$(t_{L\text{-}orn})_{10}$K-NH_2 (L, 10 μM) e H-$(t_{D\text{-}orn})_{10}$K-NH_2 (D, 10 μM) in 10 mM phosphate buffer, 100 mM NaCl, 0.1M EDTA, pH 7.

Successively, the ability of the new oligomer $(t_{L\text{-}dab})_{12}$ to bind natural nucleic acids was evaluated by CD experiments, using a *tandem cell*, constituted from two separated reservoir communicating just by the upper part of the cell, in which two solutions, initially separated, come in contact only after mixing by turning upside down the cell (Figura 45).

Light Path:	2 x 4.375 mm
Height:	46 mm
Width:	12.5 mm
Depth:	12.5 mm
Width:	9.5 mm
Base Thickness:	1.5 mm

Figure 45 Hellma *tandem cell*.

Initially, we considered a DNA strand complementary to the PNA dodecamers (dA_{12}): a solution of dA_{12} in phosphate buffer was kept in one of the *tandem cell* reservoir (1 mL), while oligomer **5**, in the same buffer conditions, was in the other one. CD spectrum from 200 to 320 nm, corresponding to the "sum" spectrum of the separated strands, was registered. Successively the cell was turned upside down to allow the mixing of the two samples and again a CD spectrum was recorded. As shown in Figure 46a, since the "sum" and "mix" CD spectra were almost the same, no binding evidence was revealed, even recording CD spectra of the "mix" sample at different time (10 min, 30 min, 1 h, 2 h, 3 h, 24 h), performing a kinetic experiment. Furthermore, also adding one equivalent more of oligomer **5**, in a 2:1 total ratio of $(t_{L\text{-}dab})_{12}/dA_{12}$, in order to verify the possibility to form a triple helix complex, the binding was not detected.

As positive reference, the aforementioned CD experiment was also performed between the *aeg*PNA **6** and dA_{12}, obtaining the spectra reported in Figure 46b: in this case a clear evidence of the binding was detected.

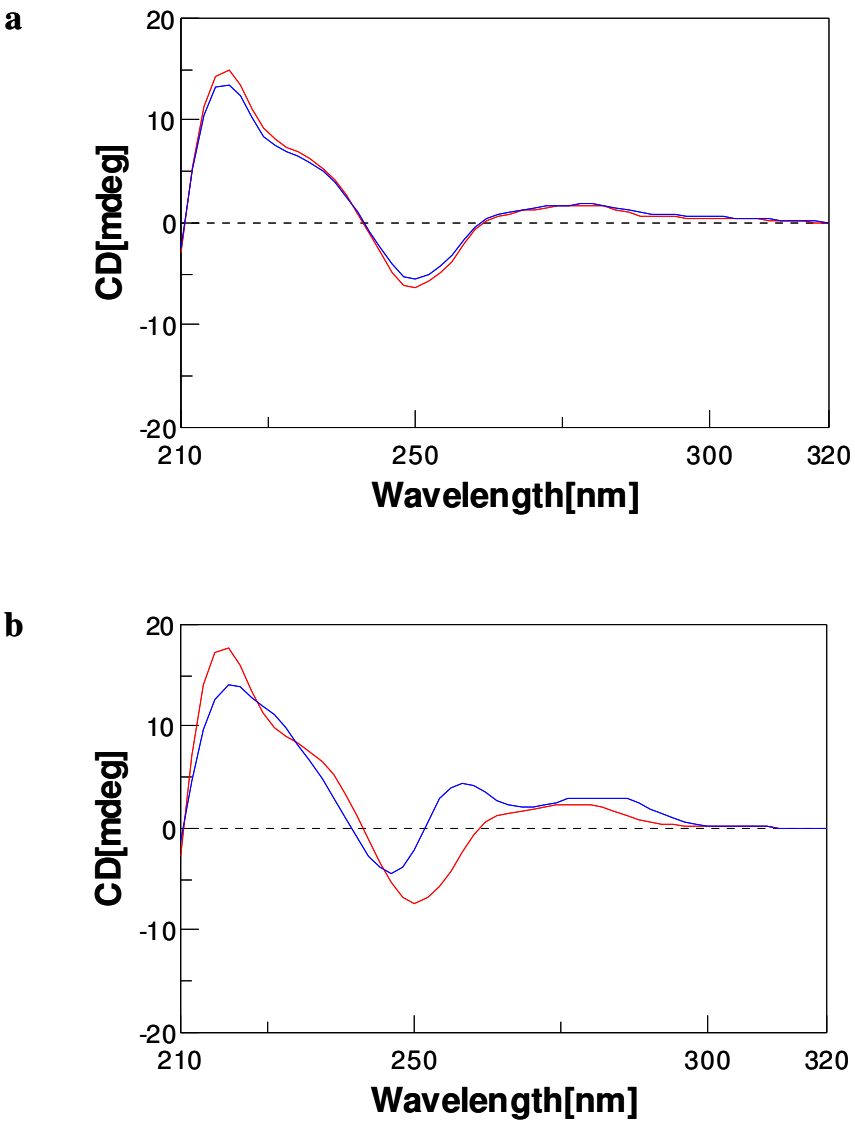

Figura 46: Sum (red) and Mix (blue) CD spectra of (a) $(t_{L\text{-}Dab})_{12}$ **6**/dA_{12} H-G-$(t_{L\text{-}dab})_{12}$K-NH_2 4 µM and dA_{12} 4µM in 10 mM phosphate buffer of (b) t_{12} PNA **7**/dA_{12}.

Furthermore, also from UV melting experiment on the solution of **5** and dA_{12}, correctly annealed, no binding was revealed, as shown in Figure 47: the melting curve of H-G-$(t_{L\text{-}dab})_{12}$-K-NH_2/dA_{12} was a drift (red line).

In order to study the effect of the single *dab*PNA insertion on the ability of *aeg*PNA strands to bind complementary DNA, UV melting experiments on annealed samples containing dA_{12} and, respectively, oligomers **6**, **7** and **8**, were performed. Overlapped melting curves are shown in Figure 47 and the corresponding T_m values are summarized in Table 1. From the melting data it was clear

that the insertion of $t_{L\text{-}dab}$ monomer in the middle (oligomer **8**) or at N terminus (oligomer **7**) of the homothymine *aeg*PNA chain leads to a decreased binding efficiency to the target DNA in comparison to *aeg*PNA **6**.

Sequences		T_m (°C) ± 0.5
H-G-$(t_{L\text{-}dab})_{12}$-K-NH_2/dA_{12}	**(5)**	-
H-G-t_{12}-K-NH_2/dA_{12}	(6)	86.2
H-G-$t_{L\text{-}dab}t_{11}$-K-NH_2/dA_{12}	(7)	84.8
H-G-$t_6t_{L\text{-}dab}t_5$-K-NH_2/dA_{12}	**(8)**	72.0

Table 1 Homo thymine sequences synthetized.

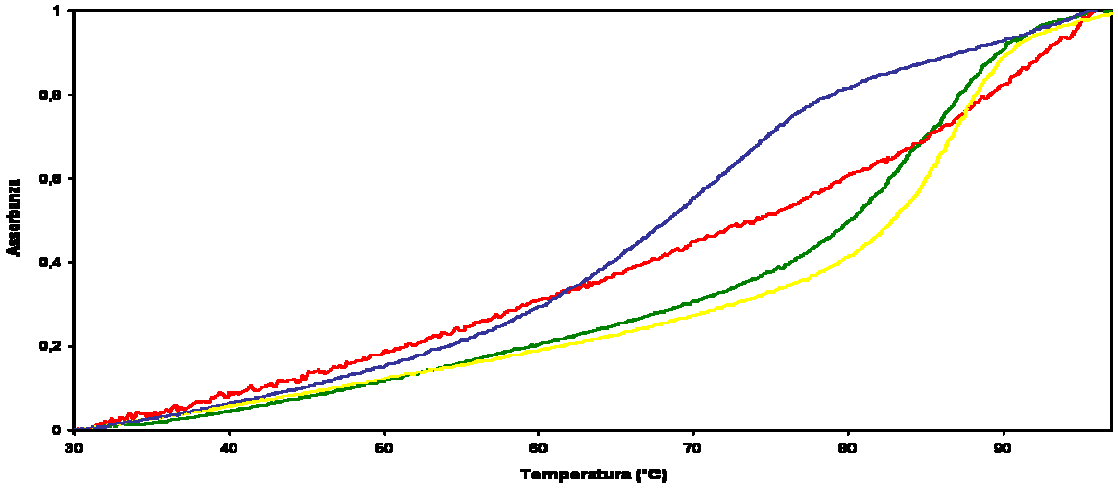

Figure 47 Melting curves of **(5)** H-G-$(t_{L\text{-}dab})_{12}$-K-NH_2/dA_{12}, (6) H-G-t_{12}-K-NH_2/dA_{12}, (7) H-G-$t_{L\text{-}dab}t_{11}$-K-NH_2/dA_{12}, **(8)** H-G-$t_6t_{L\text{-}dab}t_5$-K-NH_2/dA_{12}

In addition, the ability of the H-G-$(t_{L\text{-}dab})_{12}$K-NH_2 oligomer to hybridise a complementary strand of RNA (A_{12}) was explored. Even in this case, from the binding experiment with the *tandem cell* (Figura 48a), as well as from the kinetic CD experiment, no binding evidence was revealed.

As reference, the same experiment on the RNA A_{12} was performed with the *aeg*PNA strand (**6**) and, as expected, in this case the "sum" and "mix CD spectra resulted different, clear evidence of binding (Figura 48 b).

On the basis of these findings we concluded that L-*dab*PNAs based oligomers were not able to bind natural nucleic acids.

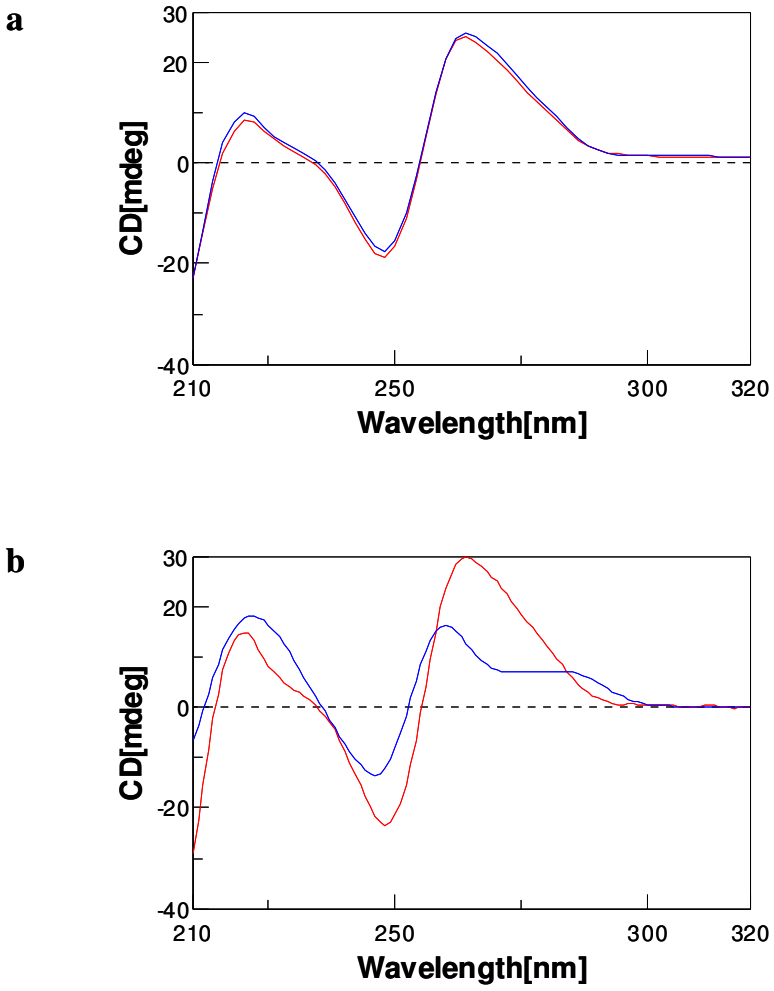

Figure 48 sum (red) and Mix (blue) CD spectra of (a) H-G-$(t_{L\text{-}dab})_{12}$K-NH_2 4 μM and A_{12} RNA 4μM in 10 mM phosphate buffer and (b) t_{12} **7**/A_{12}.

2.2 Synthesis and oligomerization of $t_{D\text{-}dab}$ monomer, and binding studies on $(t_{D\text{-}dab})_6$ oligomer

Since the PNA oligomer based on L-DABA don't bind natural nucleic acids and considering that different stereoisomers have different ability to adopt the conformation required to bind DNA or RNA, we thus explore the hybridization of the D-DABA-based nucleopeptides to nucleic acid targets. Nevertheless, in this way we continue our investigation on the hypothized prebiotic role of *dab*PNAs, after the recovery of both L and D-DABA enantiomers in meteoritic soil.[57] Our interest was successively devoted to the realization of the enantiomeric $t_{D\text{-}dab}$ monomer, starting from the commercial Boc-(D)-DAB(Fmoc)-OH (Scheme 4).

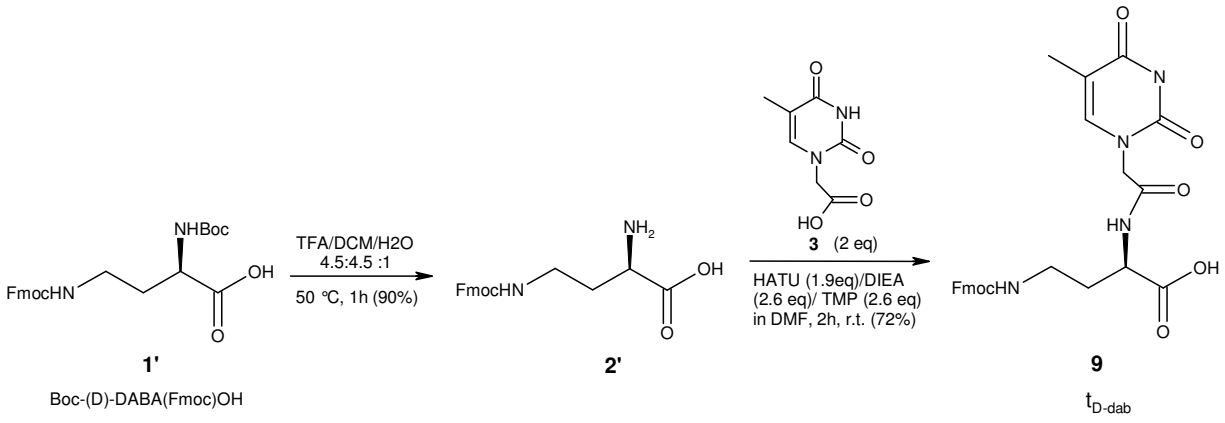

Scheme 4 Synthesis of $t_{D\text{-}dab}$ monomer.

The $t_{D\text{-}dab}$ monomer **9**, purified by RP-HPLC and characterized by NMR and LC-ESI MS, was oligomerized manually on solid phase (Scheme 5) to the corresponding H-G-$(t_{D\text{-}dab})_6$K-NH_2 (**10**) following the same synthetic procedure used for the obtainment of oligomer **5**.

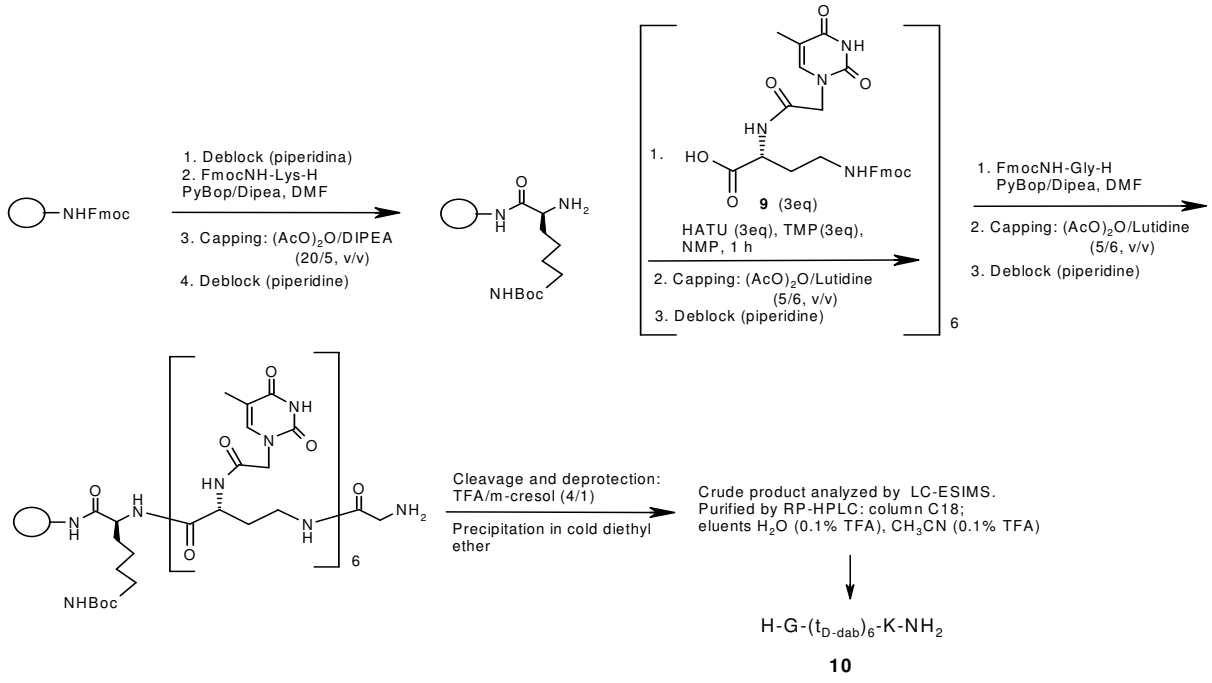

Scheme 5 Synthesis of H-G-$(t_{D\text{-}dab})_6$K-NH_2 oligomer.

After cleavage and deprotection, homopolymer **10** was purified by semipreparative RP-HPLC on a C18 column, and successively characterized by LC-ESIMS (Figure 49).

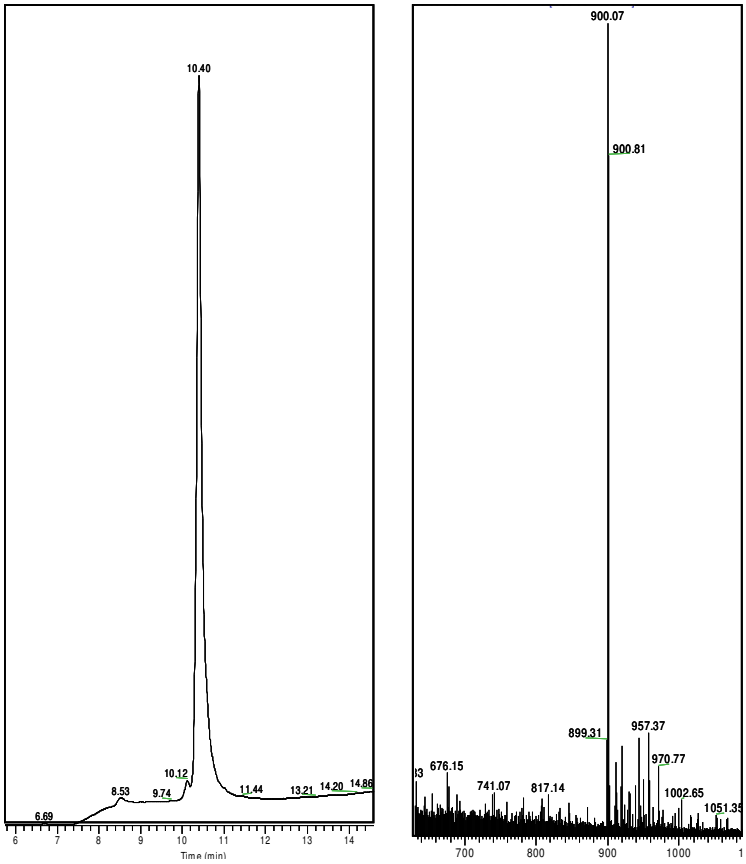

Figure 49 LC-ESIMS of H-G-$(t_{D\text{-}dab})_6$K-NH_2 homopolymer .

CD spectrum of single strand H-G-$(t_{D\text{-}dab})_6$K-NH_2 (**10**), depicted in Figure 50a (blu line), showed a mirror image relationship relative to the enantiomer H-G-$(t_{L\text{-}dab})_{12}$K-NH_2 **5** (red line, Figure 50a), in analogy to the CD spectra reported in literature by Sforza et al.[61] for the L- and D-*orn*PNAs H-$(t_{orn})_{10}$K-NH_2, showed in Figure 50b.

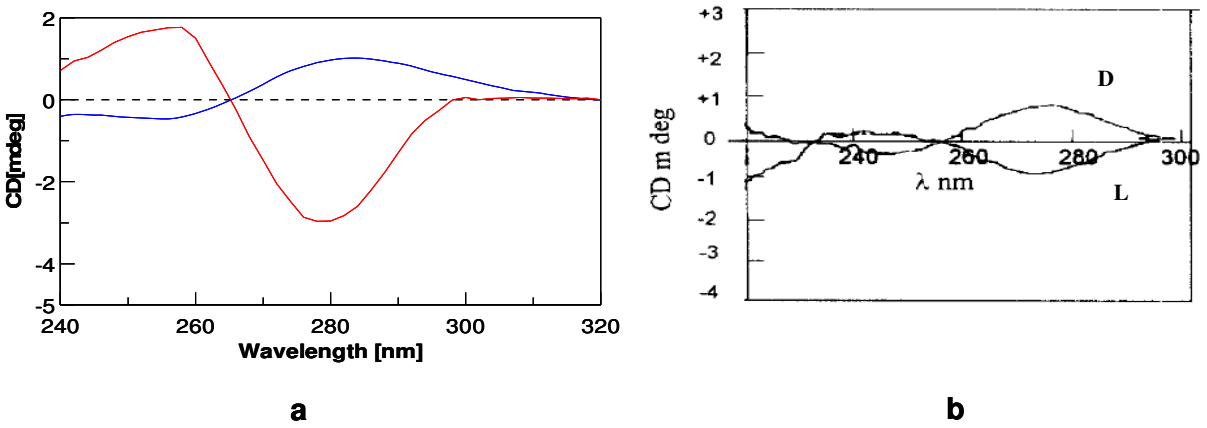

Figure 50 a) Mirror-image relationship between H-G-$(t_{L\text{-}dab})_{12}$-K-NH_2 (red line) and H-G-$(t_{D\text{-}dab})_6$K-NH_2 (blu line), 4 uM, 10 mM Pi, 10 °C; b) H-$(t_{L\text{-}orn})_{10}$K-NH_2 (**L**, 10 µM) e H-$(t_{D\text{-}orn})_{10}$K-NH_2 (**D**, 10 µM) in 10 mM phosphate, 100 mM NaCl, 0.1M EDTA, pH 7.

Furthermore, we performed CD experiments to verify the ability of H-G-$(t_{D\text{-}dab})_6$K-NH_2 to bind DNA and RNA (dA_{12}/A_{12}) using the "*tandem cell*". No difference between the sum CD spectrum, obtained before mixing the two components, and the complex CD spectrum, recorded after the mixing, was revealed for oligomer **10** with both DNA and RNA. The CD spectra remained almost the same also at different times by performing kinetic CD studies, or adding another equivalent of H-G-$(t_{D\text{-}dab})_6$K-NH_2 to the solution obtaining a 2:1 final ratio of $(t_{D\text{-}dab})_6/dA_{12}$ to verify the possibility to form triple helix. In addition UV thermal experiments of the annealed mixture confirmed the absence of any significant H-G-$(t_{D\text{-}dab})_6$K-NH_2 /DNA(RNA) interaction, showing little drift curves.

2.3 Syntheses and oligomerization of $a_{L\text{-}dab}$ and $a_{D\text{-}dab}$ monomers, and binding studies

Since *dab*PNAs based on L- and D-DABA don't bind natural nucleic acids, we explored the possibility that complementary nucleopeptides based on D or L-DABA could bind between themselves. This property would be interesting in order to develop novel DABA-based dendrimeric systems, as new materials, and also to realize new diagnostic tools, as for example new molecular beacon probe. In particular, in the case of the molecular beacon, it would be very interesting if the stem portion of this kind of probe don't recognize natural targets (Figure 51), increasing the specificity of the system.

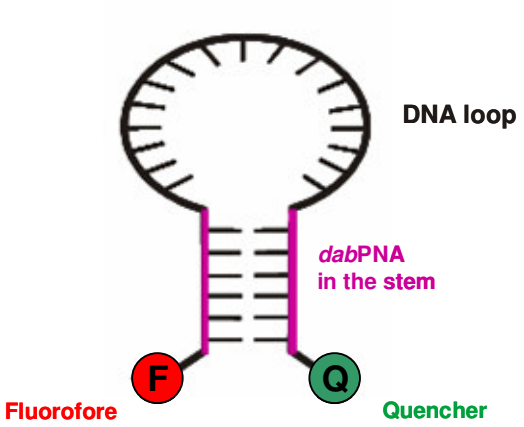

Figure 51 Molecular beacon with *dab*PNA-based stem.

To verify this interesting possibility, homoadenine and homothymine hexamers based on L- and D-DABA were realized in order to find, if possible, the correct combination of chirality suitable for obtaining the binding. In particular, we obtained and studied the following systems:

H-G-$(a_{L\text{-}dab})_6$K-NH_2 / H-G-$(t_{L\text{-}dab})_6$K-NH_2; H-G-$(a_{L\text{-}dab})_6$K-NH_2 / H-G-$(t_{D\text{-}dab})_6$K-NH_2;

H-G-$(a_{L\text{-}dab})_6$K-NH_2/H-G-$(t_{L\text{-}dab}\text{-}t_{D\text{-}dab})_3$K-$NH_2$; H-G-$(a_{L\text{-}dab}\text{-}a_{D\text{-}dab})_3$K-$NH_2$/H-G-$(t_{L\text{-}dab}\text{-}t_{D\text{-}dab})_3$K-$NH_2$.

With the previously synthesized $t_{L\text{-}dab}$ and $t_{D\text{-}dab}$ monomers, we initially realized the sequences H-G-$(t_{L\text{-}dab})_6$K-NH_2 (**11**) and H-G-$(t_{L\text{-}dab}\text{-}t_{D\text{-}dab})_3$K-$NH_2$ (**12**), following the same synthetic procedure for **5**.

In order to assemble the poliadenine sequences, the new $a_{L\text{-}dab}$ and $a_{D\text{-}dab}$ monomers were synthesized, by reacting L and D-Boc-DAB(Fmoc)-OH (**1** and **1'**), respectively, with Bhoc-protected carboxy methylated adenine. (Scheme 6).

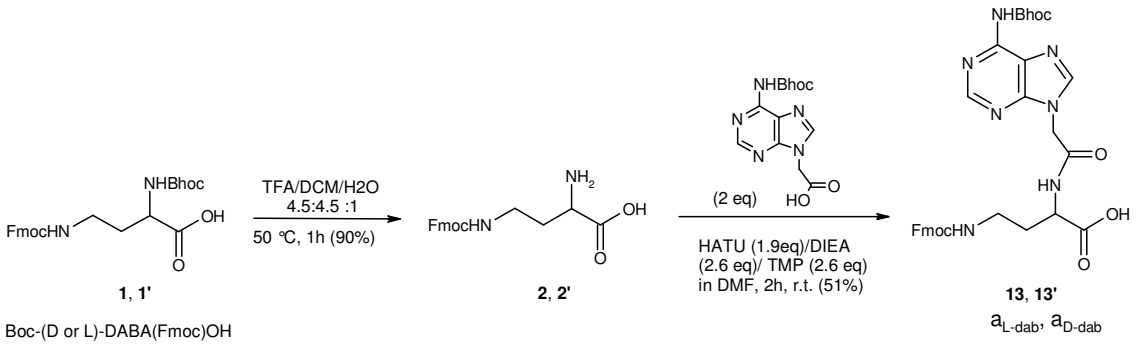

Scheme 6 Syntheses of $a_{L\text{-}dab}$ / $a_{D\text{-}dab}$ monomers.

The Fmoc-protected monomers (**13** and **13'**) synthesized, were purified by RP-HPLC without TFA in the eluents, to avoid the loss of the acid labile Bhoc protecting group. $a_{L\text{-}dab}$ and $a_{D\text{-}dab}$ were characterized by ^{1}H /^{13}C NMR and LC-ESI MS (Figure 52).

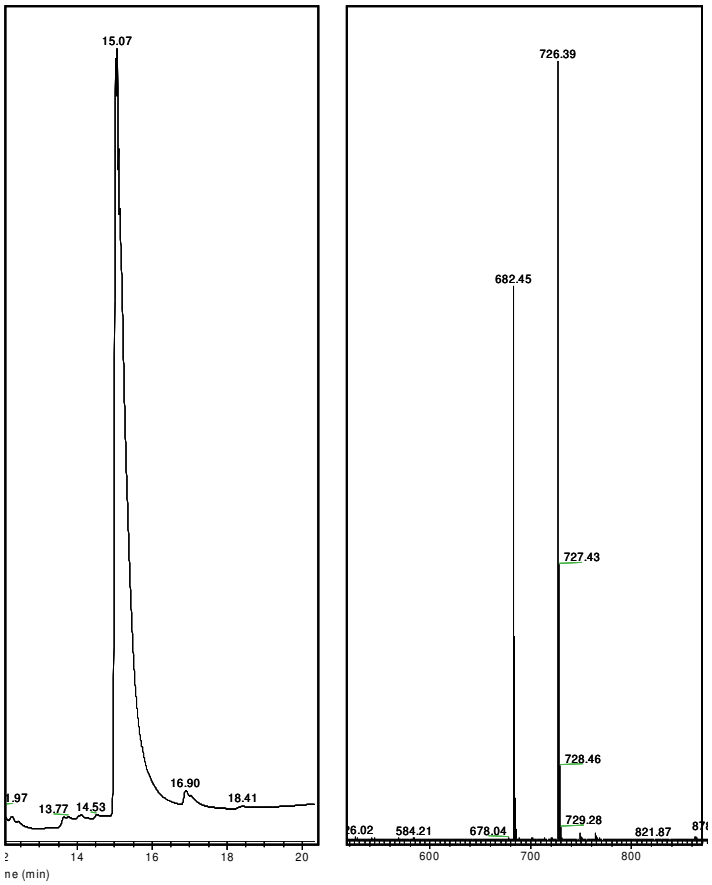

Figure 52 LC-ESI MS profile of $a_{L\text{-}dab}$ monomer.

The new chiral monomers $a_{L\text{-}dab}$ and $a_{D\text{-}dab}$ were used to synthetize H-G-$(a_{L\text{-}dab})_6$K-NH_2 **14**, and H-G-$(a_{L\text{-}dab}$-$a_{D\text{-}dab})_3$K-NH_2 **15**, with alternate chirality, following the same manual synthetic protocol used for all the previous syntheses to minimize racemization problems.

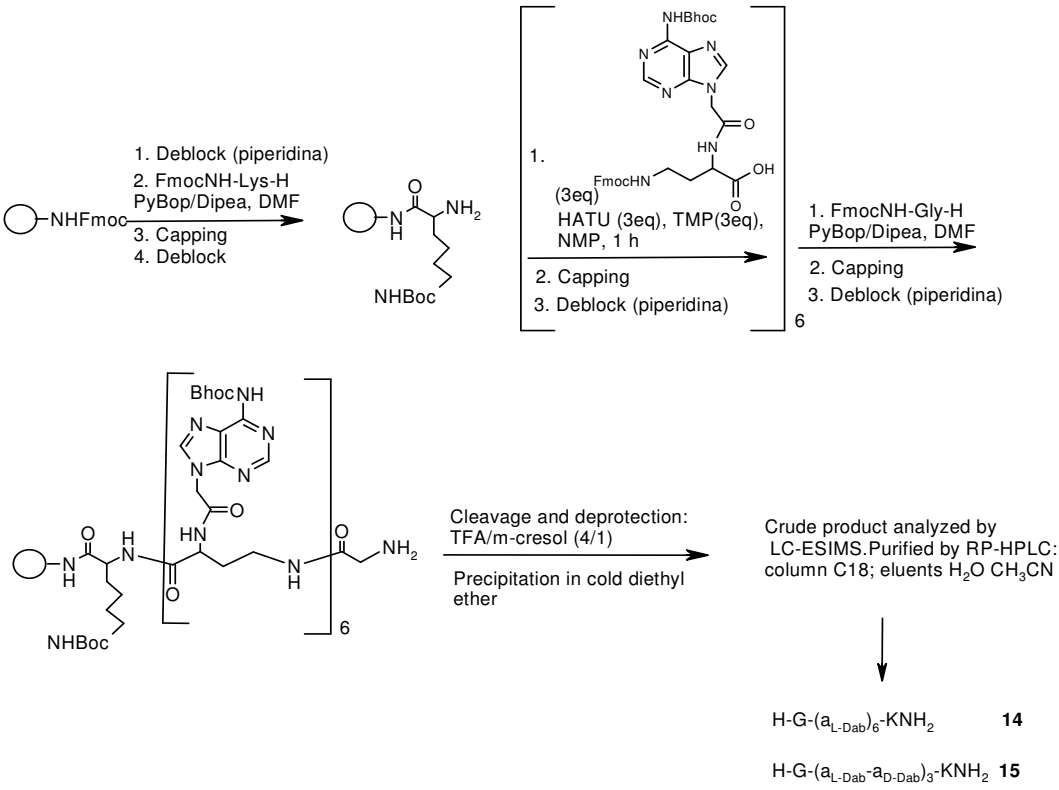

Scheme 7 Syntheses of polyadenine DABA-based oligomers.

The coupling efficiency for the synthesis of **14** and **15**, checked by UV Fmoc test, was on average around 70% in the first five synthetic steps and decreased rapidly in the last ones, giving an overall yields of 16% (**14**) and 18% (**15**).

After cleavage and deprotection, the oligomers were purified by semipreparative RP-HPLC, and successively characterized by LC-ESIMS, which confirmed the identity of the products. The LC-ESIMS profile of the new oligomer **14** is reported in Figure 53 as an example.

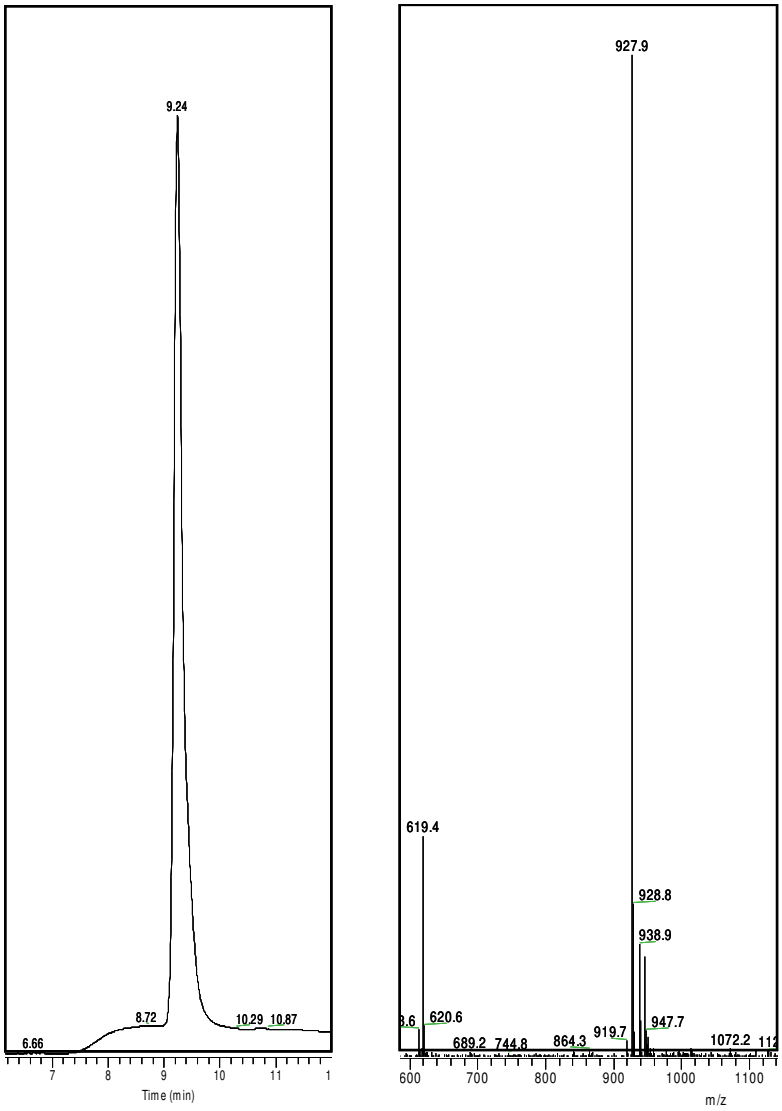

Figure 53 LC-ESI MS of H-G-$(a_{L\text{-}dab})_6$K-NH_2.

Oligomer **14**, due to its chiral nature, showed CD signal, as evidenced by its CD spectrum reported in Figure 54a (blue line). CD experiments revealed that the spectrum of $(a_{L\text{-}dab})_6$ showed the same trend as that of homo polymer having the same chirality $(t_{L\text{-}dab})_{12}$ (red line, Figure 54b), with a band shift of the minimum between 250-300 nm from 276 nm of $(t_{L\text{-}dab})_{12}$ to 266 nm.

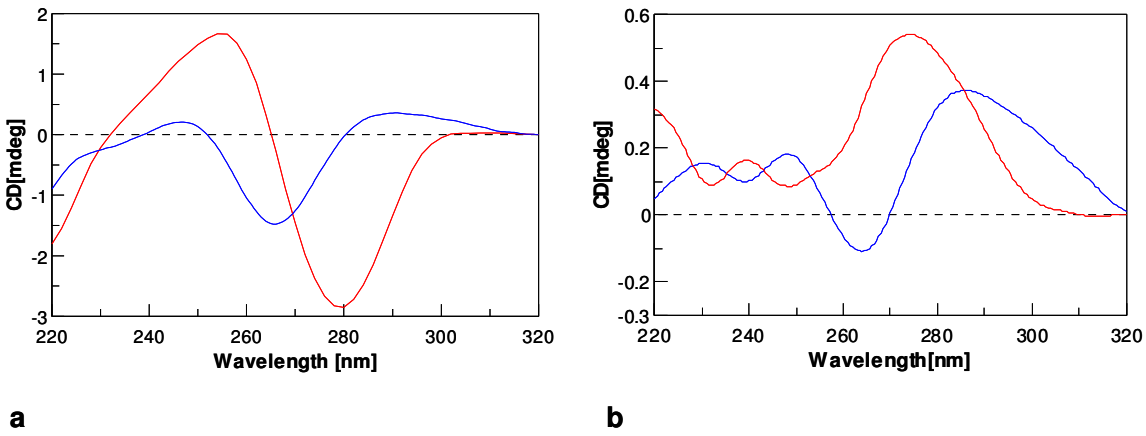

Figure 54 a) Overlapped CD spectra of $(a_{L\text{-}dab})_6$ (blue line)and $(t_{L\text{-}dab})_{12}$ (red line), 8 µM in 10 mM phosphate buffer, pH 7.5; b) Overlapped CD spectra of $(a_{L\text{-}dab}\text{-}a_{D\text{-}dab})_3$ (blue line) and $(t_{L\text{-}dab}\text{-}t_{D\text{-}dab})_3$ (red line), 4 µM in 10 mM phosphate buffer, pH 7.5.

In addition, by comparing the CD spectra of the alternate oligomers $(a_{L\text{-}dab}\text{-}\ a_{D\text{-}dab})_3$ and $(t_{L\text{-}dab}\text{-}\ t_{D\text{-}dab})_3$, a positive band between 260-320 nm was revealed, with the maxima centred at 274 nm, in the case of $(t_{L\text{-}dab}\text{-}\ t_{D\text{-}dab})_3$, and at 284 nm, in the case of $(a_{L\text{-}dab}\text{-}a_{D\text{-}dab})_3$ (Figure 54b).

CD hybridization studies were performed with *tandem cell* on H-G-$(a_{L\text{-}dab})_6$K-NH_2 /$(t_{L\text{-}dab})_6$: no significant binding evidence was revealed in this case. Indeed only little changes are recorded for the sum and mix spectra relative to this complex (Figure 55).

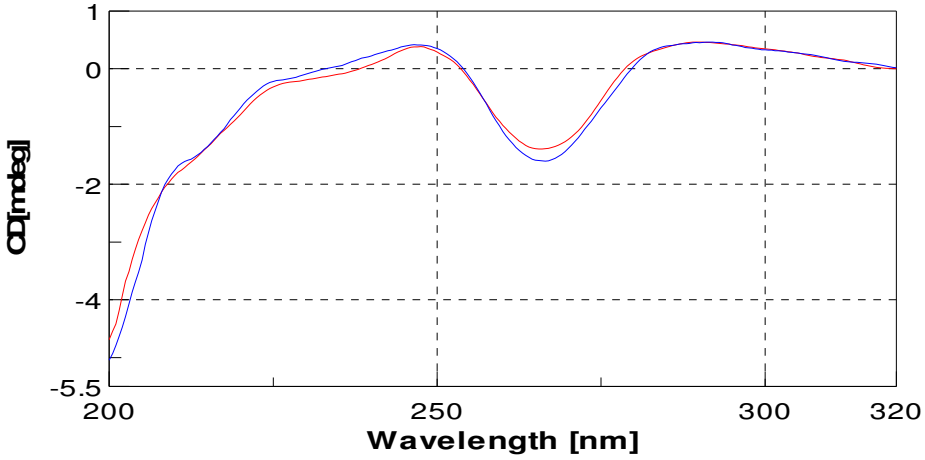

Figure 55 Red sum and blue mix of $(a_{L\text{-}dab})_6$/ $(t_{L\text{-}dab})_6$ (4 µM in 10 mM phosphate buffer, pH 7.5).

Other CD experiments were carried out on the following systems: $(a_{L\text{-}dab})_6$/ $(t_{D\text{-}dab})_6$, $(a_{L\text{-}dab})_6/(t_{L\text{-}dab}\text{-}t_{D\text{-}dab})_3$ and $(a_{L\text{-}dab}\text{-}\ a_{D\text{-}dab})_3/(t_{L\text{-}dab}\text{-}\ t_{D\text{-}dab})_3$. In the first case, no binding evidence was revealed, while in the second one, a little difference between the sum spectra (red line) and the mix (blue line) was observed (Figure 56), suggesting a possible hybridization between the strand with alternate chirality and homochiral oligomer. However, this finding was not supported by the UV melting experiment on the annealed strands: drift curve was recorded (data not shown).

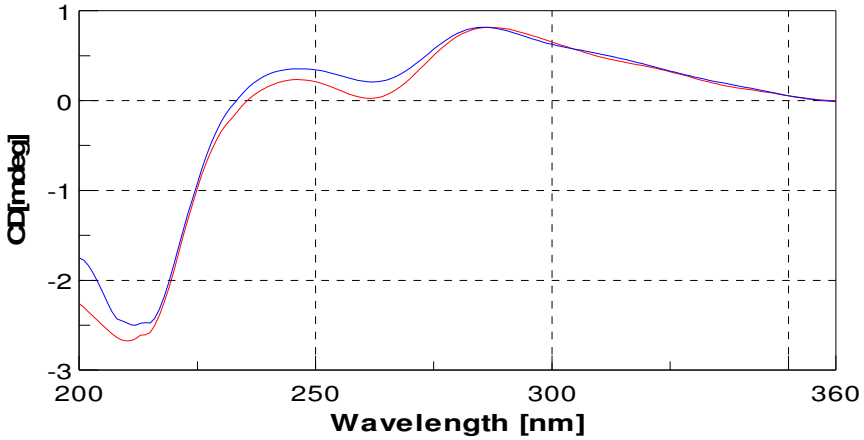

Figure 56 Red sum and blue mix of $(a_{L\text{-}dab})_6/(t_{L\text{-}dab}\text{-}t_{D\text{-}dab})_3$ (4 µM in 10 mM phosphate buffer, pH 7.5).

In the case of $(a_{L\text{-}dab}\text{-}\ a_{D\text{-}dab})_3/(t_{L\text{-}dab}\text{-}t_{D\text{-}dab})_3$, CD measurements with *tandem cell* revealed a difference between the sum and mix spectra (Figure 57), which, in this case, was confirmed also by the UV thermal denaturation curve (Figure 58): indeed, a transition phase at 11 °C was detected.

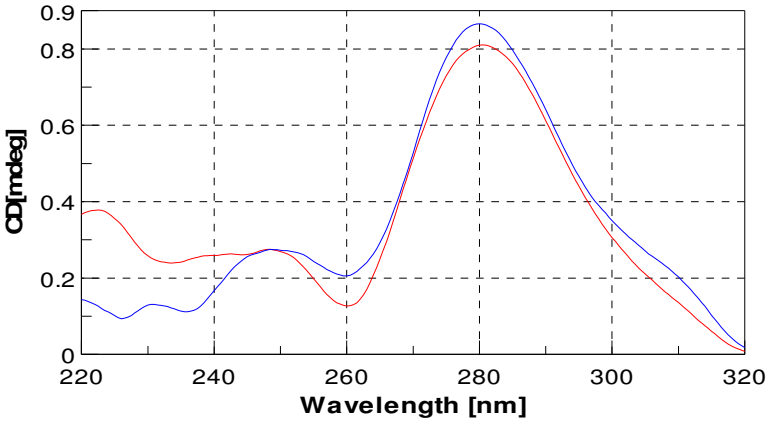

Figure 57 Red sum and blue mix of $(a_{L\text{-}dab}\text{-}\ a_{D\text{-}dab})_3/(t_{L\text{-}dab}\text{-}t_{D\text{-}dab})_3$

Nevertheless we plan to perform a large scale synthesis of the strands involved in this experiment, in order to evaluate the stability of the system in function of the concentration of the two strands and to obtain a CD titration curve, useful to establish the stoichiometry of the formed complex.

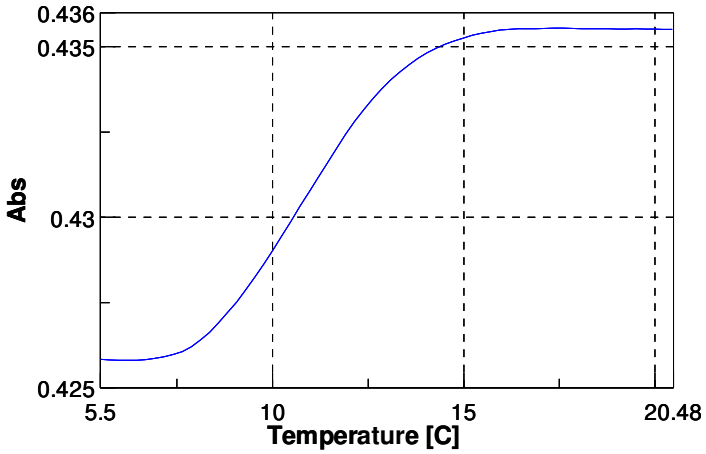

Figure 58 UV melting of $(a_{L\text{-}dab}- a_{D\text{-}dab})_3/(t_{L\text{-}dab}-t_{D\text{-}dab})_3$.

2.4 Conclusion

In our research for the development of new ODN-like drugs or diagnostics, we designed and realized chiral nucleo-γ-peptides, *dab*PNAs, isomer of the *aeg*PNAs and characterized by a 2,4-diaminobutyric acid (DABA)-based backbone carrying the carboxymethylated nucleobase on its α amino group. Our interest to *dab*PNAs arises, besides from the obtainment of new molecules for potential therapeutic and diagnostic applications, also from their involvement in the prebiotic world, as recently proposed by Meierhenrich et al. [57] This proposal followed the recovery of DABA in the extraterrestrial soil of the Murchison meteorite together with the molecular DNA constituent purine and pyrimidine bases, and other diaminoacids.[57,58] In order to realize the chiral dabPNA oligomers, the new monomers $t_{L\text{-}dab}$, $t_{D\text{-}dab}$, $a_{L\text{-}dab}$ and $a_{D\text{-}dab}$ were synthesized in good yield using suitable protected building blocks and characterized by NMR and ESI-MS techniques.

Initially, the homothymine oligomers $(t_{L\text{-}dab})_{12}$ and $(t_{D\text{-}dab})_6$ were synthesized using a synthetic strategy that ensured the maintenance of chirality during the coupling steps, and tested for hybridization towards natural nucleic acids. No binding evidence with both DNA (dA_{12}) and RNA (A_{12}) was revealed by CD and UV experiments.

Furthermore, the insertion of a single $t_{L\text{-}dab}$ unit in the middle or at N terminus of a homothymine *aeg*PNA chain leads to a decreased binding efficiency to the target DNA in comparison to full *aeg*PNA.

Since *dab*PNAs based on L- and D-DABA don't bind natural nucleic acids, we explored the possibility that complementary nucleopeptides based on D or L-DABA could bind between themselves. This property would be interesting in order to develop novel DABA-based dendrimeric systems, as new materials, and also to realize new diagnostic tools, as for example new molecular beacon probes. To verify this interesting possibility, $a_{L\text{-}dab}$ and $a_{D\text{-}dab}$ monomers were oligomerized to the homoadenine hexamers $(a_{L\text{-}dab})_6$ and $(a_{L\text{-}dab}\text{-}\ a_{D\text{-}dab})_3$. In order to find the correct combination of chirality suitable for obtaining the binding also the oligomer $(t_{L\text{-}dab}\text{-}t_{D\text{-}dab})_3$ was realized, to perform the hybridization studies. From CD and UV experiments, binding evidence was revealed in the case of the complementary oligomers with alternate chirality, $(a_{L\text{-}dab}\text{-}a_{D\text{-}dab})_3$ and $(t_{L\text{-}dab}\text{-}t_{D\text{-}dab})_3$ even if the stability of the complex formed was not so high (T_m=11°C). However further experiments to better establish the stability and stoichiometry of this hybrid are required.

2.5 Materials and methods

Chemicals

Fmoc-Gly-OH, HATU, Fmoc-Lys(Boc)-OH, PyBOP were purchased from Novabiochem. Anhydroscan DMF and NMP were from LabScan. Piperidine was from Biosolve. Solvents for HPLC chromatography and acetic anhydride were from Reidel-de Haën. TFA, Rink-amide resin, TCH_2COOH, acetic acid were Fluka. [N6-(benzhydryloxycarbonyl)-adenine-9-yl] was purchased from ASM Research Chemicals GmbH & Co. Perspective Biosystem PNA kit (Fmoc/Bhoc monomers, HATU activator, Base solution, Wash B, DIEA, Cap Solution, Deblock solution) was purchased from PRIMM (Milan, Italy). Boc-DAB(Fmoc)-OH is from Bachem. DCM and TFA (for HPLC) were from Romil. Deuterated solvents (DMSO, methanol) were from Aldrich. Thin-layer chromatography (TLC) analyses were performed on silica gel Macherey-Nagel G-25 UV_{254} plates (0.25 mm thick) visualised by UV light and by a ninhydrin staining solution. The reactions were monitored by TLC until all starting material had been consumed. Solvents for TLC analyses and diethyl ether were from Carlo Erba, dA_{12} was purchased from Biomers (Ulm, Germany).

Apparatus

^1H NMR and ^{13}C NMR spectra were recorded at 25 °C on Varian unity 300 MHz and Varian Inova 600 MHz spectrometers. Chemical shifts (δ) are given in parts per million (ppm) and all coupling constants (J) in Hz. Proton chemical shifts were referenced to residual CHD_2SOCD_3 (δ=2.49, quin) and CHD_2OD (δ=3.30, quin) signals. ^{13}C NMR chemical shifts were referenced to the solvent (CD_3SOCD_3: δ=39.5, sept; CD_3OD: δ=49.0, sept).

*aeg*PNA oligomers were assembled on solid-phase with an Applied Biosystems Expedite 8909 oligosynthesizer.

Crude samples containing PNA oligomers were centrifuged for 4 min at 4000 rpm (Z 200 A, Hermle).

Products were analysed by LC-MS, performed on an MSQ mass spectrometer (ThermoElectron, Milan, Italy) equipped with an ESI source operating at 3 kV needle voltage and 320 °C, and with a complete Surveyor HPLC system, comprising an MS pump, an autosampler, and a PDA detector, by using a Phenomenex Jupiter C18 300 Å (5 µm, 4.6×150 mm) column. Gradient elution was

performed at 40 °C (monitoring at 260 nm) by building up a gradient starting with buffer A (0.05% TFA in water) and applying buffer B (0.05% TFA in acetonitrile) with a flow rate of 0.8 ml/min.
Semi-preparative purifications were performed by RP-HPLC on a Shimadzu LC-8A, equipped with an SPD-10A VP UV/Vis detector, and on a Hewlett Packard/Agilent 1100 series, equipped with a diode array detector, by using a Phenomenex Juppiter C18 300 Å (10 µm, 10×250 mm) column. Gradient elution was performed at 45 °C (monitoring at 260 nm) by building up a gradient starting with buffer A (0.1% TFA in water) and applying buffer B (0.1% TFA in acetonitrile) with a flow rate of 4 ml/min.
Samples containing PNAs (crude or purified), were lyophilized in a FD4 Freeze Dryer (Heto Lab Equipment) for 16 hours.
Circular dichroism (CD) spectra were obtained at 20 °C on a Jasco J-810 spectropolarimeter using 1-cm quartz cuvette (Hellma).
Ultraviolet (UV) spectra and UV melting experiments were recorded on a UV-Vis Jasco model V-550 spectrophotometer equipped with a Peltier ETC-505T temperature controller using 1-cm quartz cuvette (Hellma).

Synthesis of the (D, L) t-*dab*PNA monomer

N^{γ}-Fmoc-L-2,4-diaminobutyric acid, (**1** or **1'**) (Scheme 2). Commercial Fmoc/Boc-protected 2,4-diaminobutyric acid (L and D) 1 (200 mg, 0.45 mmol) was treated with a solution of TFA/DCM/H_2O 4.5:4.5:1 (8 ml) at 50 °C. After stirring for 1 h, the pH of the solution was adjusted to 5 by dropwise addition of 1 M aqueous KOH. The obtained white precipitate was filtered, washed with DCM and coevaporated three times with dry CH_3CN (138 mg of 2, 0.40 mmol, 90% yield). The crude precipitate contained prevalently one product, as evidenced by TLC, which showed only one spot at R_f= 0.14 (6:4 CH_2Cl_2/CH_3OH), and by LC-MS. ESI-MS *m/z*: 340.4 (found), 341.38 (expected for MH^+); δ_H (300 MHz, DMSO-d_6) 8.27 (3H, br s, NH_3^+), 7.29-7.89 (9H, aromatic CH Fmoc and Fmoc-N*H*), 4.32 (2H, m, FmocCH-CH_2), 4.22 (1H, m, FmocC*H*-CH_2), 3.90 (1H, m, CH_α), 3.14 (2H, m, CH_2NH), 1.92 (2 H, m, CH_2CH_α).

***N*$^{\gamma}$-Fmoc-*N*$^{\alpha}$-(thymin-1-ylacetyl)-2,4-diaminobutyric acid (L and D) 4,9** (Scheme **2**,**4**). Product **2** or **2'** (1 eq, 138 mg, 0.40 mmol) was dissolved in dry DMF (6 ml) and 0.6 eq of DIEA (41µL) and TMP (32.4 µL) reacted with TCH_2COOH (149 mg , 0.81 mmol, 2 eq), HATU (293 mg, 0.77 mmol, 1.9 eq), DIEA (137 µL, 0.8 mmol, 2 eq) and TMP (108 µL, 0.8 mmol, 2 eq,) which were previously preactivated for 2 min before adding to product **2** (or **2'**).

After 2 h the reaction was quenched by adding 60 ml of water, the crude was frozen to -80°C and lyophilized. The crude material obtained was purified by semipreparative HPLC on Shimadzu instrument using increasing amounts (15-70% in 25 min) of solution B in A, giving pure sample **4,9** (148 mg, 0.29 mmol, 72% yield) as a white powder; R_f= 0.50 (8:1:1 butanol:acetic acid:water); LCESI-MS (Figure 2) *m/z*: 507.00 (found), 507.52 (expected for MH^+); δ_H (600 MHz, DMSO-d_6) 11.35 (1H, br s, NH thymine), 8.54 (1H, br s, NH amide), 7.98 (2H, d, J=7.3, aromatic CH Fmoc), 7.77 (2H, d, J=7.3, aromatic CH Fmoc), 7.51 (2H, t, J=7.3, aromatic CH Fmoc), 7.49-7.51 (1H, m, Fmoc-N*H*), 7.42 (2H, t, J=7.3, aromatic CH Fmoc), 7.41 (1H, s, CH thymine), 4.43 (2H, s, CH_2 acetyl linker), 4.05-4.50 (4H, m, FmocC*H*-CH_2 and CH_α), 3.14 (2H, m, CH_2NH), 2.00 (1H, m, part of an AB system centred at 1.91, CH_2CH_α), 1.83 (1H, m, part of an AB system centred at 1.91, CH_2CH_α), 1.82 (3H, s, CH_3 thymine); δ_H (600 MHz, CD_3OD) 7.78 (2H, d, J=7.3, aromatic CH Fmoc), 7.64 (2H, d, J=7.3, aromatic CH Fmoc), 7.38 (2H, t, J=7.3, aromatic CH Fmoc), 7.36 (1H, s, CH thymine), 7.30 (2H, t, J=7.3, aromatic CH Fmoc), 4.47 (2H, s, CH_2 acetyl linker), 4.19-4.50 (4H, m, FmocC*H*-CH_2 and CH_α), 3.19 (1H, m, part of an AB system centred at 3.22, CH_2NH), 3.25 (1H, m, part of an AB system centred at 3.22, CH_2NH), 2.11 (1H, m, part of an AB system centred at 1.98, CH_2CH_α), 1.85 (1H, m, part of an AB system centred at 1.98, CH_2CH_α), 1.84 (3H, s, CH_3 thymine); δ_C (150 MHz, DMSO-d_6) 170.98 (COOH), 168.48 (CH_2*C*ONH), 160.10 (thymine C-4), 155.00 (OCONH), 147.96 (aromatic Fmoc 2C), 147.89 (thymine C-2), 146.36 (aromatic Fmoc 2C), 144.73 (thymine C-6), 131.65 (aromatic Fmoc 2CH), 131.11 (aromatic Fmoc 2CH), 129.18 (aromatic Fmoc 2CH), 124.15 (aromatic Fmoc 2CH), 111.96 (thymine C-5), 69.40 (Fmoc CH_2), 53.02 (CH_2 acetyl linker), 50.73 (CH_α), 44.1 (Fmoc CH), 41.30 (CH_2NH), 22.56 (*C*H_2CH_α), 15.91 (thymine CH_3).

$a_{L\text{-}dab}$ and $a_{L\text{-}dab}$ (13 and **13'**)

The monomers **13** and **13'** were synthesised starting from N6-(benzhydryloxycarbonyl)-adenine-9-yl-acetic acid and from Boc-(*S*)-DAB(Fmoc)-OH and Boc-(*D*)-DAB(Fmoc)-OH diaminoacids, the same synthetic strategy used in the case of products **4** and **9.** The monomers were purified by RP-HPLC and characterized by LC-ESIMS and NMR.

Solid phase synthesis of oligomers (5-15)

Solid support functionalization and manual solid-phase oligomerizations were carried out in short PP columns (4 ml) equipped with a PTFE filter, a stopcock and a cap. Solid support functionalization: Rink-amide resin (0.50 mmol NH_2/g, 128 mg) was functionalized with a lysine

(Fmoc-Lys(Boc)-OH, 0.5 eq, 14.8 mg, 32 μmol) using PyBOP (0.5 eq, 16.8 mg, 32 μmol) as activating agent and DIEA (1 eq, 12 μL, 64 μmol) as base for 30 min at room temperature. Capping of the unreacted amino groups was performed with Ac_2O (20%)/ DIEA (5%) in DMF. Loading of the resin was checked by measuring the absorbance of the released Fmoc group (ε_{301}=7800, quantitative yield) after treatment with a solution of piperidine (30%) in DMF (UV Fmoc test) and resulted reduced to 0.25 mmol/g respect to the initial functionalization. Automatic solid-phase assembly of the *aeg*PNAs was performed on an Expedite 8909 Nucleic Acid Synthesis System using a standard 2 μmol-scale protocol and Fmoc chemistry leaving the final Fmoc on in order to evaluate SPS yields by UV Fmoc test. Manual couplings of *dab*PNA monomers were monitored by UV Fmoc test in order to evaluate the incorporation yields of the new monomer. A glycine residue (3 eq) was attached to the N-terminus of all the oligomers by using PyBOP (3 eq)/DIEA (6 eq) as activating system in DMF. After removal and quantification of the Fmoc group, all oligomers were cleaved from the resin and deprotected under acidic conditions (TFA/m-cresol 4:1 v/v). The oligomers were isolated by precipitation with cold diethyl ether, centrifugation and lyophilization. Purified oligomers (semipreparative HPLC) were quantified and characterised by LC-ESIMS.

H-G-($t_{L\text{-}dab}$)$_{12}$-Lys-NH_2 (5) was assembled manually on Rink-amide-Lys-NH_2 resin (32 mg, 8 μmol 0.25 mmol/g,) using the following protocol: the monomer **4** Fmoc-$t_{L\text{-}dab}$-OH (120 μl, 24 μmol, 3 eq), and the coupling agent HATU (120 μl, 24 μmol, 3 eq), were dissolved in 100 μL of DMF and stored at rt for 5 min; then it was introduced into the reactor. Immediately 1/4 (30 μL) of the total amount of a base solution (120 μl, 24 μmol, 3 eq, TMP 0.2 M) was added to start the reaction, and the reaction mixture was stirred. The other three amount of the base (1/4) portions were added one every 15 minutes, and the coupling was left for 1h with shaking at room temperature.

Successively, unreacted amino groups were capped with PNA Cap solution for 5 min. Fmoc removal was accomplished with PNA Deblock solution (5 min) and was monitored for every step by UV measurements: average yield for the first six steps was 96% while for the last six steps a lowering of the yields from 96 to 70% was observed probably because of the enhanced aggregation tendency of the increasing homothymine chain (overall yield: 25%). Yield of the last coupling with glycine resulted to be of 97%. After cleavage and deprotection, the oligomer 5 was purified by semipreparative RP-HPLC using a linear gradient of 8% (for 5 min) to 25% B in A over 30 min: t_R=31.0 min; UV quantification of the purified product gave 100 nmol of 5; ESI-MS (Figure 3) *m/z*: 1134.8 (found), 1133.4 (expected for $[M+3H]^{3+}$).

H-G-t_{12}-K-NH_2 (6) Standard t_{12} *aeg*PNA was assembled on Rink-amide-Lys-NH_2 resin (32 mg ,0.25 mmol/g) on automatic synthesizer. After the synthesis was complete the final Fmoc was left on and removed manually to perform Fmoc UV test. The overall yield of t_{12} was of only 18% probably because the *flow through* synthesis of automatic synthesizer enhances the aggregation problems of the homothymine sequence. Glycine was incorporated manually as last residue with high efficiency (98% yield). The cleaved and deprotected oligomer was purified by semipreparative HP HPLC using a linear gradient of 8% (for 5 min) to 20% B in A over 30 min: t_R=27.9 min; UV quantification of the purified product gave 60 nmol of **6**; ESI-MS *m/z*: 1132.0 (found), 1697.1 (found), 1133.4 (expected for $[M+3H]^{3+}$), 1699.7 (expected for $[M+2H]^{2+}$).

H-G-$t_{dab}t_{11}$-K-NH_2 (7) The *aeg*PNA part of **8** was assembled on Rink-amide-Lys-NH_2 resin (0.25 mmol/g, 32 mg) by automatic synthesizer leaving the final Fmoc on (yield: 20%), while the $t_{L\text{-}dab}$ monomer was attached manually as last residue following the protocol described for 5 (yield: 95%). After last coupling with glycine, an overall yield of 18 % was obtained. After cleavage and deprotection, the oligomer was purified by semipreparative HP HPLC using a linear gradient of 8% (for 5 min) to 17% B in A over 35 min: t_R=29.8 min; UV quantification of the purified product gave 70 nmol of 7; ESI-MS *m/z*: 1133.0 (found), 1133.4 (expected for $[M+3H]^{3+}$), 1699.8 (found), 1699.7 (expected for $[M+2H]^{2+}$).

H-G-$t_6t_{dab}t_5$-K-NH_2 (8) The synthesis of the *aeg*PNA part of **8** was performed on Rink-amide-Lys-NH_2 resin (0.25 mmol/g, 32 mg) by automatic synthesizer except for the *dab*PNA monomer which was attached manually in the middle of the *aeg*PNA sequence (overall yield: 20%). Glycine was incorporated manually as last residue with a 95% yield. The cleaved and deprotected oligomer was purified by semipreparative HP HPLC using a linear gradient of 7% (for 5 min) to 19% B in A over 40 min: t_R=30.1 min; UV quantification of the purified product gave 80 nmol of **8**; ESI-MS *m/z*: 1132.8 (found), 1133.4 (expected for $[M+3H]^{3+}$), 1698.5 (found), 1699.7 (expected for $[M+2H]^{2+}$).

Oligomers **10**, **11**, **12**, **14, 15** were assembled manually on Rink-amide-K-NH_2 resin (8 mg, 2 µmol, 0.25 mmol/g) using the same synthetic procedure as described for oligomer **5**.

H-G-$(t_{D\text{-}dab})_6$K-NH_2 (10) Purified by HP HPLC using a linear gradient of 5% (for 5 min) to 22 % B in A over 25 min: t_R=25 min; UV quantification of the purified product gave 120 nmol; ESI-MS *m/z*: 900.07 (found), 900.8 (expected for $[M+2H]^{2+}$).

H-G-($t_{L\text{-}dab}$)$_6$K-NH$_2$ (11) Purified by HP HPLC using a linear gradient of 5% (for 5 min) to 22 % B in A over 25 min: t_R=25 min; UV quantification of the purified product gave 110 nmol; ESI-MS *m/z*: 900.08 (found), 900.8 (expected for $[M+2H]^{2+}$).

H-G-($t_{L\text{-}dab}$-$t_{D\text{-}dab}$)$_3$K-NH$_2$ (12) Purified by HP HPLC using a linear gradient of 5% (for 5 min) to 25 % B in A over 25 min: t_R=23 min; UV quantification of the purified product gave 95 nmol; ESI-MS *m/z*: 900.3 (found), 900.8 (expected for $[M+2H]^{2+}$).

H-G-($a_{L\text{-}dab}$)$_6$K-NH$_2$ (14) Purified by HP HPLC using a linear gradient of 4% (for 5 min) to 25 % B in A over 25 min: t_R=18.4 min; UV quantification of the purified product gave 101 nmol; ESI-MS *m/z*: 927.9 (found), 927.08 (expected for $[M+2H]^{2+}$).

H-G-($a_{L\text{-}dab}$-$a_{D\text{-}dab}$)$_3$K-NH$_2$ (15) Purified by HP HPLC using a linear gradient of 5% (for 5 min) to 25 % B in A over 25 min: t_R=22 min; UV quantification of the purified product gave 130 nmol; ESI-MS *m/z*: 900.07 (found), 927.08 (expected for $[M+2H]^{2+}$).

UV and CD studies

Purified oligomers were dissolved in a known amount of milliQ water and quantified by UV measurements (T=85 °C, absorbance value at λ=260 nm). The epsilon used for the quantification of the oligomers t_{12}(103.2 mM^{-1}), t_6 (51.6 mM^{-1}), a_6 (82.2 mM^{-1}) were calculated using the molar extinction coefficient of thymine (8.6 mM^{-1}) and adenine (13.7 mM^{-1}) of *aeg*PNA monomers.

Annealing of all PNA oligomers with complementary strands was performed by mixing equimolar amounts of the two components in 10 mM phosphate buffer at pH 7.5 to achieve duplex concentration of 4 μM. The solution was heated at 85 °C (5 min) and then allowed to cool slowly to room temperature.

Thermal melting curves (Figure 4) were obtained by recording the UV absorbance at 260 nm while the temperature was ramped from 20 to 97 °C at a rate of 0.5°C/min. T_m values, calculated by the first derivative method, were reported in Table 1.

CD spectra were recorded from 320 to 200 nm at 20°C: scan speed 50 nm/min, data pitch 2 nm, band width 2 nm, response 4 sec, 3 accumulations.

PART 3: Non enzymatic method for SNP (single nucleotide polymorphism) analysis.

This project was carried out during a period of the third year of Phd at University of Edinburgh (School of Chemistry) in the laboratory of Prof. M. Bradley and involved a project entitled "Non enzymathic method for SNP (single nucleotide polymorphism) analysis ". Single Nucleotide Polymorphism (SNP) refers to single base alterations which occur within the human genome giving rise to structure and functional protein modifications. SNPs, it is thought to be responsible of various diseases and its finding would help to predict hereditary diseases and the possibility of prophylactic treatments. Therefore high-throughput methods which were cost-efficient are highly required. Recently, The International HapMap Consortium genotyped more than 1 million in 269 individuals of SNPs[62] which can give an idea of the importance of the issue. Current methods for realizing SNPs analysis are enzymatic-based relying in the recognition by enzymes of allele differences. Examples of these methods are the restriction fragment length polymorphism (SNP-RFLP) [63] which use restriction enzymes and extension reactions with the use of polymerases and fluorescence modified nucleotides. If an allele contains a recognition site for a restriction enzyme and another not, digestion of the two alleles generate two fragments of different sizes. Other methods involve the use of microarrays with include specific markers for SNPs.

In reality today SNPs are designed primarily through microarrays, which allow the simultaneous analysis of hundreds of different SNPs and a quick analysis prepared by a computer, but in both cases it requires the use of specific marker enzyme.

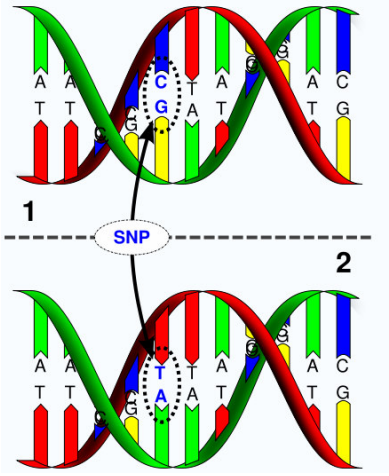

Figure 1 Example of polymorphism C/T = bp C/G substituted by bp T/A

3.1 Labelling method for molecules and nucleobases.

The aim of this project was to synthesize and characterize new fluorescently labelled nucleosides, to use as building blocks and primers for non enzymatic SNP analysis, chemically based.
Each nucleoside would be labelled with different fluorophores (FAM, TAMRA, Texas Red, Cy5) as shown as example in the following scheme.

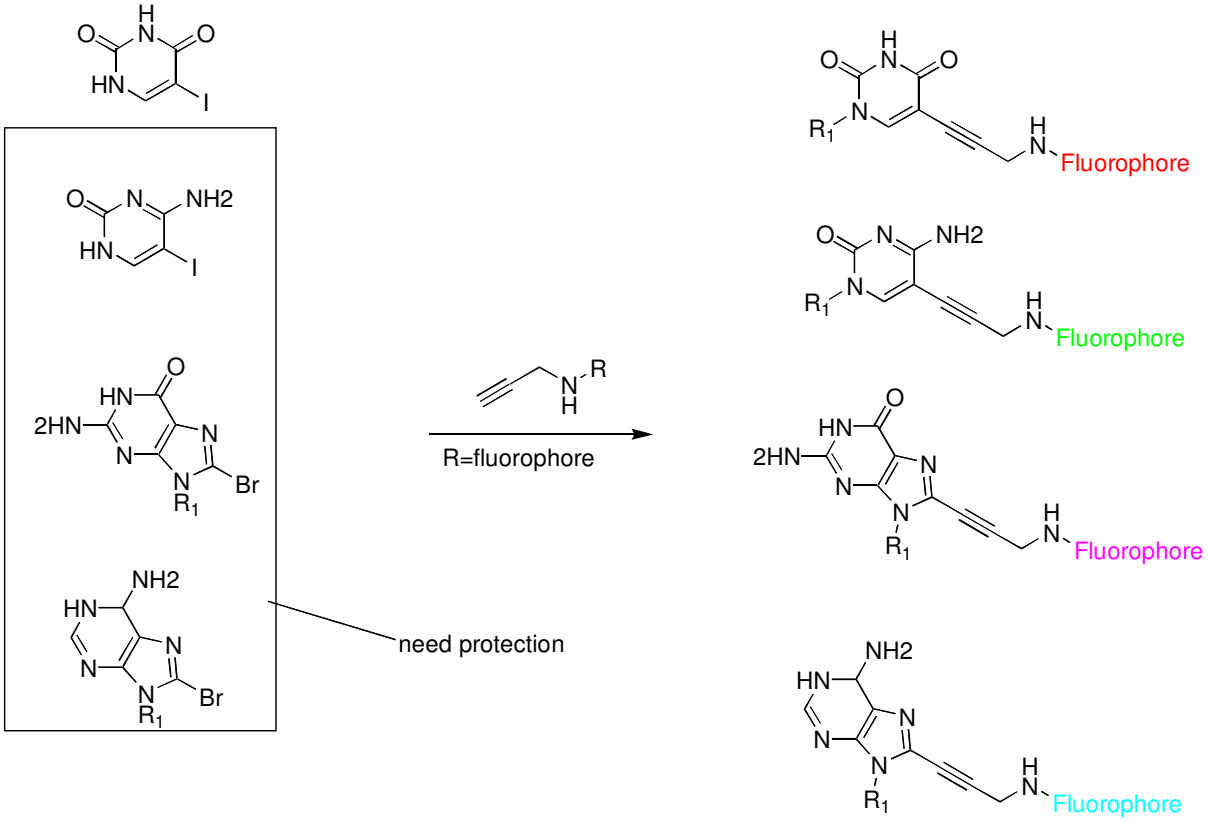

Scheme 1 Synthesis of novel fluorescently labelled nucleosides.

Fluorescence labelling of biologically active compounds is a technique for preparing biochemical probes for *in vivo* and *in vitro* studies. Conventional labelling methods rely upon reaction of amine or thiol with activated dyes, conditions under which side products may form.
In most cases, it is necessary to isolate the desired product from unreacted reagents and side products. The preparation of activated dye, moreover, can be difficult given their sensitivity to moisture and various nucleophiles. Thus, a procedure that allows facile preparation of the activated dye and labelling of biologically interesting compounds without chromatographic steps would be a useful tool. A versatile labelling method employing support bound nitrophenol active ester is

described. The method developed allowed the synthesis of pure fluorescently molecules using supported dyes on solid phase, and furthermore, allowing the solid support to be recycled several times.

Nitrophenol resin (**3**) was synthesized by standard coupling of amino methyl polystyrene resin with 3-hydroxi-4-nitrobenzoic acid (**2**). The nitrophenol resin (**3**) was then coupled to the carboxyl groups respectively of 5(6)-carboxirhodamine (Scheme 2) and of 5(6)-carboxifluorescein (Scheme 3), with the use of DIC as coupling reagents in presence of catalytic amount of 4-dimethylaminopyridine (DMAP), resulting in the activated ester resins (**4** and **7**). Upon reaction with amine nucleophiles in 2 different solvents, DMF and DCM, amide products (**5, 9** and **10**) were formed, and collected by simple filtration, and after rinsing of the resin and evaporation of the solvents, the dyes were obtained

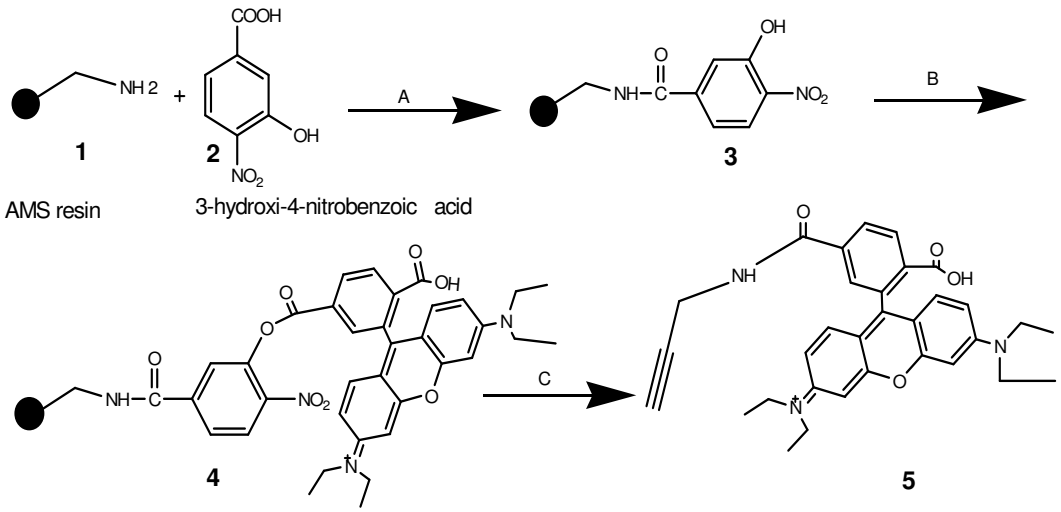

Schema 2 A) DIC, HOBt (3 eq) , 3-hydroxy-4-nitrobenzoic acid (3 eq) in DMF **B**) resin, DIC (1 eq) (3eq) DIEA, 5(6)-carboxirhodamine (6eq) (3 eq), DMAP catalytic amount in DMF **C**) propargylamine (0.9 eq) in DMF.

The purity and identity of the products were characterized by LC/MS equipped with a diode array detector and an ESI mass spectrometer. In figure 2 is showed the ESI-MS (positive mode) of the propargylammine labelled with 5(6) carboxyrhodamine.

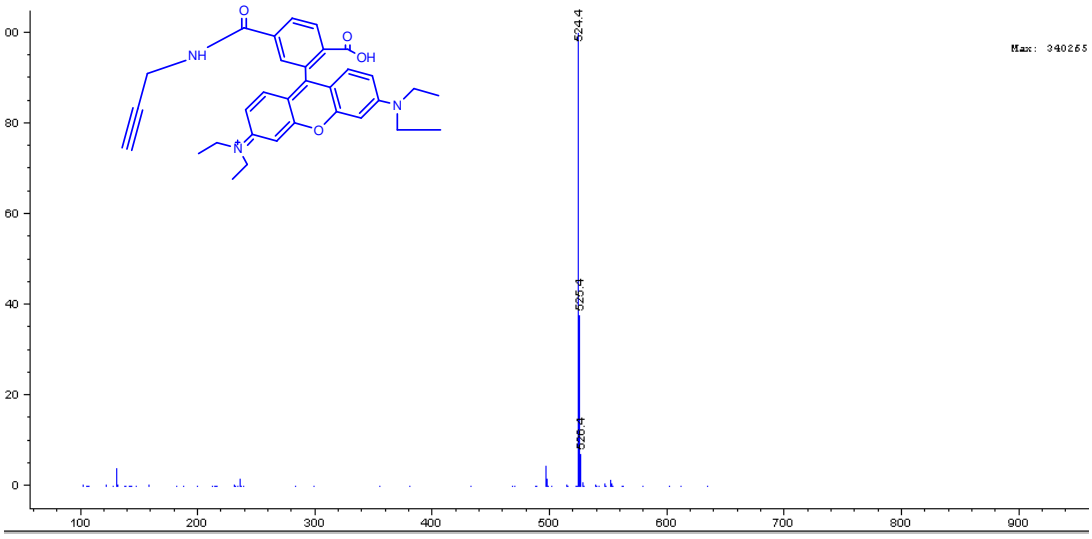

Figure 2 ESI-MS of 5(6)-carboxyrhodamine propargylamine.

Activated esters (**3**, **4**) were reacted with propargylamine (Scheme 1), 2-aminoethanethiol (Scheme 3) and 2,2-dimetoxy ethylamine (Scheme 4), respectively. The products obtained, were pure and did not require further purification (90-99% pure).

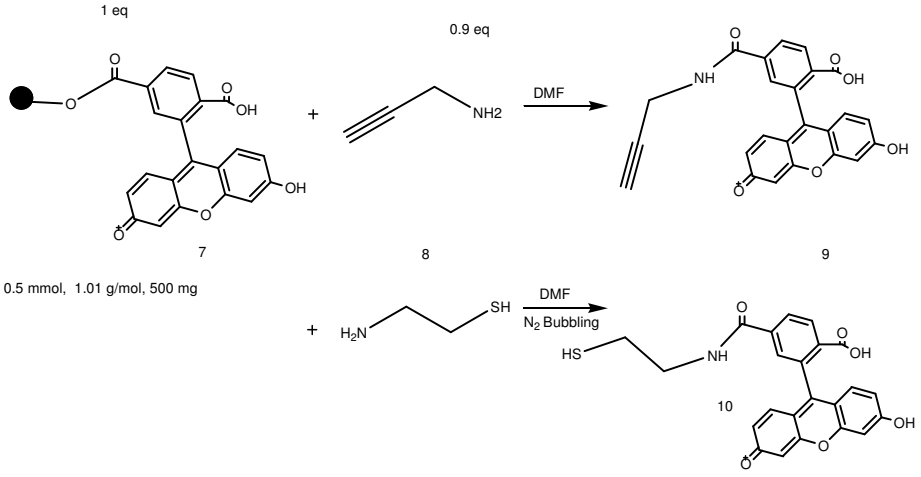

Scheme 3 of 5(6)-carboxyfluorescein cleavage from solid support by propargylamine and 2-aminoethanethiol.

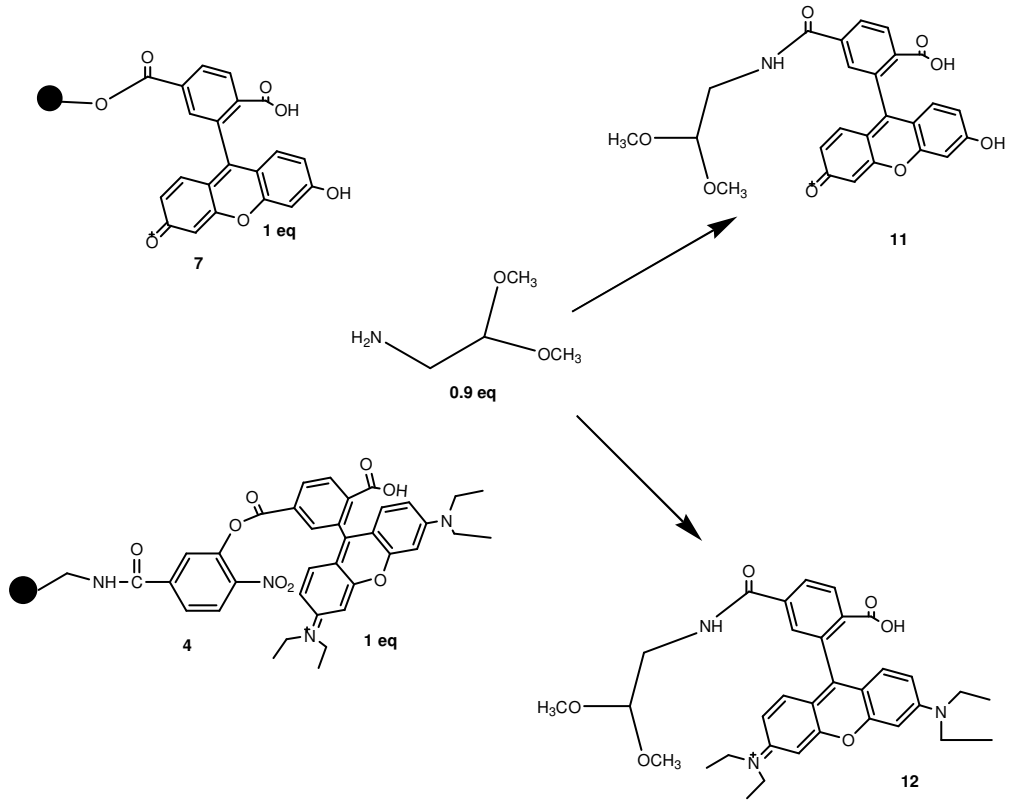

Scheme 4 5(6)-carboxyfluorescein and 5(6)-carboxyrhodamine cleavage from solid support by 2,2-dimethoxy ethylamine (0.9 eq).

In figure 3 are showed the ESI-MS (positive mode) respectively of 5(6)-carboxyrhodamine and of 5(6)-carboxyfluorescein 2,2-dimethoxy ethylamine complex, as we can notice only one peak of ionization was found for these compounds.

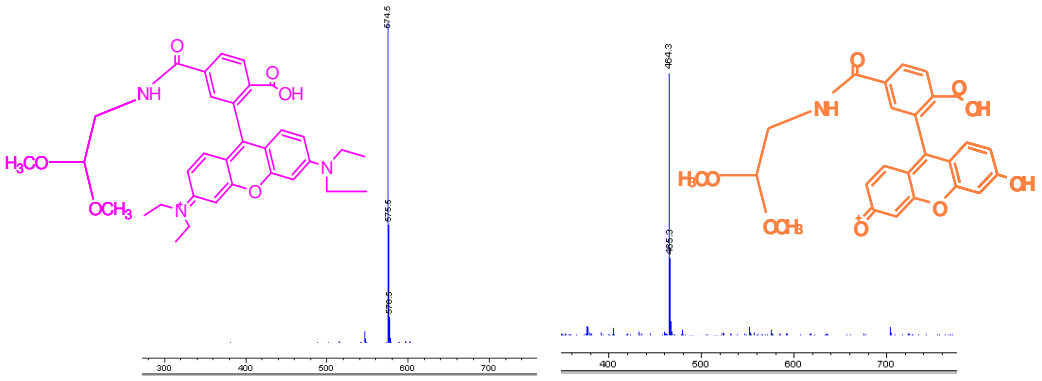

Figure 3 ESI-MS of products **11** and **12**.

Once the labelling method was optimized, a propagylamine linker was synthesized. Amino functionality of propagylamine was protected with trifluoacetic anhydride as described in Scheme 5.

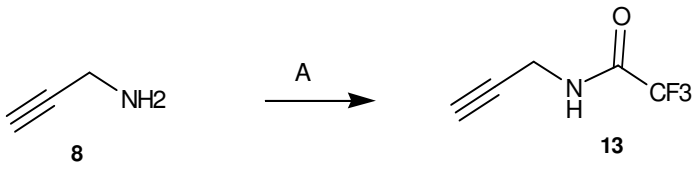

Scheme 5 A 1.12 eq TFAA, 2 eq TEA, CH_2Cl_2, 0 to rt, 1.1 M, 14 h, 74%

Chromatography column on silica gel, eluted with DCM, readily furnished the desired product **13** in good yield (74 %), which was fully characterized by LC-ESI MS and $^{1}H/^{13}C$ NMR.

The obtained product 2,2,2-trifluoro-N-prop-2ynyl-acetamide (**13)** was used to react, via classical Sonagashira coupling, performed with a palladium catalyst, and a copper (I) co catalyst (mechanism shown in Figure 4, with the 5-iodo-cytosine and 5-iodo-thymine derivatives to obtain products **15** and **17** in good overall yield (78% and 75%). (Scheme 6).

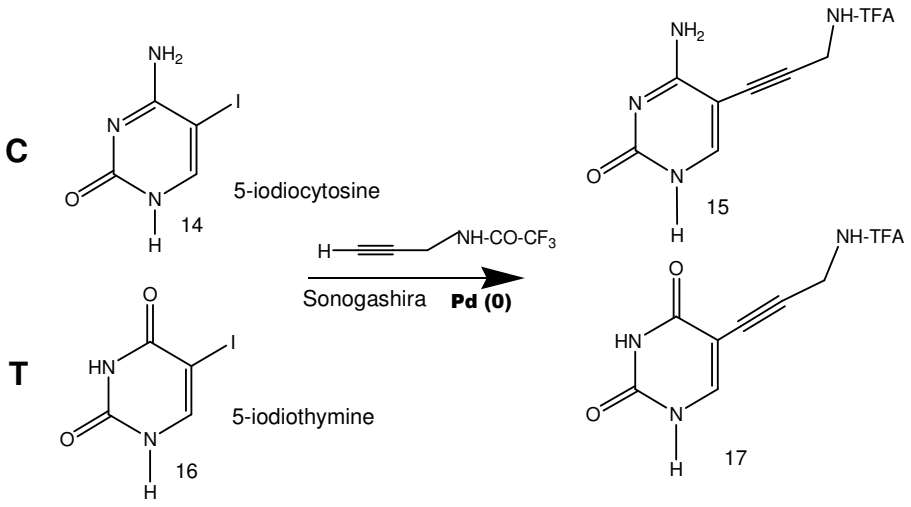

Scheme 6 Cytosine/thymine 1eq, $Pd[(C_6H_5)_3P]_4$ 10% in weight, CuI 20% mol, 5 eq Amberlite Ira-67, 0.2 M DMF.

Sonogashira coupling of aryl or vinyl halides with terminal alkynes is a transition metal-mediated cross coupling reactions, emerged as a powerful methods for the formation of carbon-carbon bonds.

The palladium complex activates the organic halides by oxidative addition into the carbon-halogen bond. In contrast, copper(I) halides react with the terminal alkyne and producecopper (I) acetylide, which acts as an activated species for the coupling reactions (Figure 4).

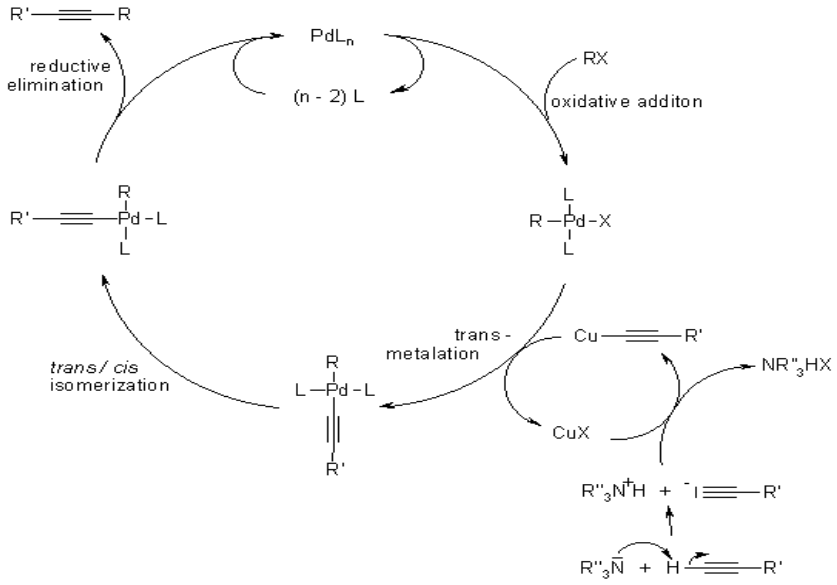

Figure 4 Sonogashira reaction mechanism.

Products **15** and **17** were deprotected (Scheme 7) in basic conditions (6 M NH_3 in H_2O/MeOH), giving the corresponding free amine. Coupling with supported dyes (**4**, **7**), quickly formed the desired labelled bases which were released to the reaction media and collected by filtration. The purity and identity of the products **20** and **21** was revealed by ESI-MS and NMR.

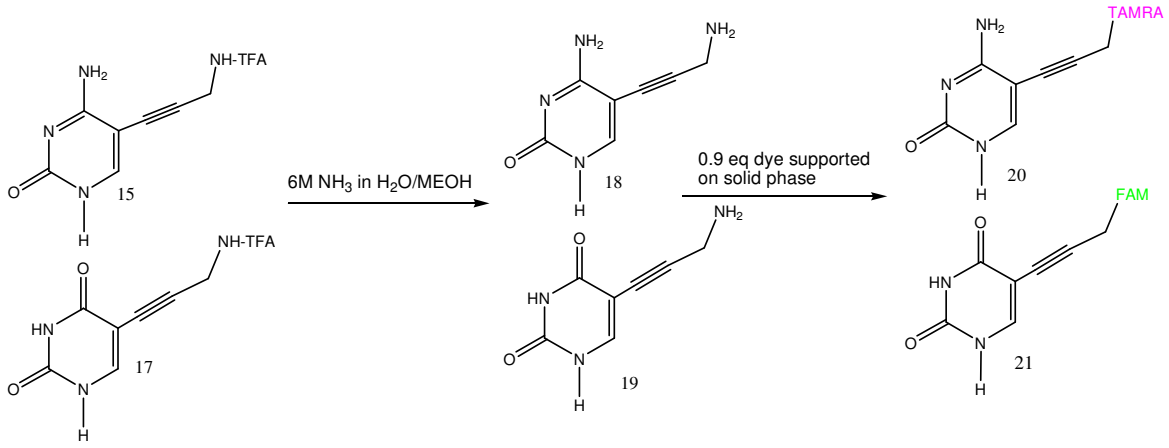

Scheme 7 Synthesis of novel fluorescently labelled nucleosides

3.2 Conclusion

A versatile labelling method employing supported nitrophenol activated ester was developed. This strategy can be adopted to label biologically active amines for use as molecular probes or nucleosides. The method allowed the synthesis of pure labelled molecules, without further chromatographic purification. Furthermore, and not less important, the solid support is recyclable, reducing in this way the cost for the syntheses. Two active esters, (**3**, **4**) and 3 different amines were tested. The obtained products were pure and did not require further purification (90-99% yield).The same strategy was used for nucleosides labelling allowing the synthesis of TAMRA-cytosine and FAM-thymine.

Once all fluorescently labelled nucleosides will be synthesized a new non-enzymatic SNPs detection could be carried out using high-throughput capability of microarray technology.

3.3 Materials and methods

Chemicals

All commercially available reagents were used as received. Amberlite IRA-67, 10% palladium on charcoal, and CuI were obtained from Aldrich Chemical Company, Inc. DMF (DriSolv) was purchased from EMD Chemicals, Inc. Nucleoside substrates were obtained from Berry & Associates or Sigma. Propargylamine, 2-aminoethanethiol, 2,2-dimetoxy ethylamine and 5(6)-carboxyfluorescein were purchased from Sigma Aldrich. Rhodamine WT was purchased from Abbey color. Thin-layer chromatography (TLC) was conducted with E. Merck silica gel 60 F254 pre-coated plates, (0.25 mm) and visualized using a combination of UV, anisaldehyde, ceric ammonium molybdate, and potassium permanganate staining. ICN silica gel (particle size 0.032-0.063 mm) was used for flash column chromatography.

Apparatus

^{1}H NMR and ^{13}C NMR spectra were recorded on Bruker 250 MHz with automatic sample changers at 25 °C on Chemical shifts (δ) are given in parts per million (ppm) and all coupling constants (J) in Hz. Proton chemical shifts were referenced to residual CHD_2SOCD_3 (δ=2.49, quin) and CHD_2OD (δ=3.30, quin) signals. ^{13}C NMR chemical shifts were referenced to the solvent (CD_3SOCD_3: δ=39.5, sept; CD_3OD: δ=49.0, sept). Analytical HPLCs HPAgilent1100 withauto-sampler, LC/MS HP Agilent 1100 with ES and APCI mass detector auto-sampler

Preparation of Nitrophenol Resin (3). In a 50-mL solid-phase extraction (SPE) e cartridge containing amino methyl polystyrene resin (1g ,1.01 mmol, 1 eq) pre-swelled in DMF (15 mL) were added 4-hydroxy-3-nitrobenzoic acid (**2**, 3.03 mmol, 555 mg, 3 eq), previously preactiveted with DIC (3 eq, 3.03 mmol, 382.39 mg, 469 μL), HOBT (3.30 mmol, 464 mg, 3 eq,) 30 minutes. After overnight shaking, the reaction mixture was washed with DMF (20 mL, 5 times), DCM, and methanol (20 mL, 5 times alternatively). To remove any undesirable side product, mainly esters, DMF (5 mL) and piperidine (0.5 mL) were added to the cartridge and allowed to shake for 1.5 h. The resin was filtered and washed with DMF (20 mL, 5 times). The resulting piperidine salt was removed via the addition of a 10% HCl solution (in DMF, 20 mL) and was allowed to shake for 1.5 h. The resin was then filtered; washed with DMF, methanol, and DMC (20 mL, 5 times each); and dried by nitrogen gas flow.

Solid phase supported dyes

5(6)-carboxyfluorescein (1.53 mmol, 564.5 mg, 3 eq,), DIC (1.53 mmol, 190.6 mg, 234 µL, 3 eq,) (1 eq, 0.505 mmol, 500mg,) in DMF (20ml) were shaked for 30 minutes. The mixture 5(6)-carboxyfluorescein/HOBt/DIC was then added to nitro phenol aminomethyl polystyrene resin (0.505 mmol , 505 mg, 1 eq,). A little amount of DMAP was added before shaking overnight. The same procedure was followed to couple to the mixture 5(6)-tetraethylcarboxyrhodamine (1.53 mmol, 732 mg, 3 eq,), DIC (1.53 mmol, 190.6 mg, 234 µL,3 eq,), in DMF. After overnight shaking, the resin was washed with DMF (20 mL, 5 times), DCM, methanol (20 mL, 5 times) and Et_2O (20 ml, 5 times). The resulting resin was then dried in a vacuum oven, overnight at 40°C.

Cleavage of dye from solid support.

General protocol

In a 50-mL SPE cartridge 5(6)-carboxyfluorescein or 5(6)- tetraethylcarboxyrodamine polystyrene loaded resin (1 eq, 505, mg 0.5 mmol/g), were added 0.9 eq of nucleofilic molecules:

propargylamine (0.45mmol, 24.8 mg, 31µL), 2,2-dimethoxy ethylamine (0.45mmol, 47.3, 49 µL) in 3 ml of deareated DMF. On addition of nucleofile the DMF solution turned colour indicating release of the desired labelled product. The reaction mixture was stirred for 30 minutes at room temperature. The resin was washed with the DMF collecting all in a flask , the solvent was evaporated under reduced pressure leaving purple oil (molecules labelled with 5(6)-tetraethylcarboxyrodamine and orange one (molecules labelled with 5(6)-carboxyfluorescein).

Esi-Ms positive mode eluted 95% MEOH 0.1% TFA

5 ESI-MS *m/z*: 524.4 (found), 524.6 (expected for $[M+H]^+$); **9** ESI-MS *m/z*: 414.4 (found), 414.3 (expected for $[M+H]^+$); **10** ESI-MS *m/z*: 436.3 (found), 436.4 (expected for $[M+H]^+$); **11** ESI-MS *m/z*: 464.3 (found), 464.4 (expected for $[M+H]^+$); **12** ESI-MS *m/z*: 574.5 (found), 574.6 (expected for $[M+H]^+$)

Thiolated 5(6)-carboxyfluorescein

5(6)-carboxyfluorescein polystyrene loaded resin (0.2 mmol, 200 mg, 1eq) was treated with N_2 purged DMF (3ml). 2-aminoethanethiol (cysteamine) (0.18 mmol, 15.4 mg, 0.9 eq) in 1ml of deareated DMF was added and the mixture maintained under a blanket of nitrogen. On addition of Cysteamine the DMF solution turned reddish indicating release of the desired thiolated 5(6)-carboxyfluorescein. The reaction mixture was stirred for 30 minutes under N_2 before filtering by SPE cartridge. The resin was further washed with N_2 purged DMF and the solvent evaporated under reduced pressure leaving an orange solid which was identified as thiolated 5(6)-carboxyfluorescein.

The thiolated compound tends to oxidize to disulfide if in presence of oxygen and must be stored as a solid at - 20°C. Thiolated dyes can also be stored in solution if in presence of 0.1 M TCEP reducing agent.

Synthesis of 2,2,2-Trifluoro-N-prop-2ynyl-acetamide (13)

Propargylamine (8.8 4 g, 160 mmol) and TEA (45 ml, 320 mmol, 2eq were dissolved in CH_2Cl_2 (50 ml) at 0°C . Trifluoacetic anhydride (25 ml, 180 mmol, 1.13 eq) was added dropwise over 30 min. the reaction mixture was warmed to r.t. stirred for 14 h and evaporated in vacuo to a brown oil. Et_2O (200ml) and 1M NH_4OAc (300 mL) were added. The organic layer was separated and washed with H_2O (100 mL), dried (Na_2SO4) and purified by column chromatography eluted with CH_2Cl_2 to yield a yellow oil (17.9 g, 118 mmol, 74 % yield).

Product **13** (17.9 mg, 118 mmol) were dissolved in 6 ml obtaining a solution of 2.98 g/ml density.

2,2,2-Trifluoro-N-prop-2ynyl-acetamide **^{1}H NMR** (250 MHz, $CDCl_3$) δH 7.19 (1H, br signal, NH), 4.26 (2H, ddd, J= 5.5, 2.6, 0.4 Hz, CH2), 2.4 (1H, t, J= 2.6 Hz, CH), **^{13}C NMR** (62.5 MHz, $CDCl_3$), δC 157.2 (q, J=37.9 Hz, *C*OCF_3), 115.5 (q, J=287.2 Hz, CF_3), 73.4 (CH), 77.4 (C), 30.1 (CH_2), **ES** m/z (%) 150.2 (m-H, 100).

5-iodocytosine (**14)**

^{1}H NMR (250 MHz, d6-DMSO), δH 7.9 (H, s, C6*H*), 7.5 (H, br, N*H*), 6.2 (2H, br signal, NH_2) **^{13}C NMR** (62.5 MHz, DMSO), δC 164.8 (*C*4), 156.0 (*C*=O), 153.2 (*C* 6), 55.4 (*C*5, *C*-I)

TFA-alkynylmethylamino cytosine (**15)**

5-iodo-cytosine **14** (300 mg 1.25mmol) were dissolved in DMF (Vol 6.2mL , 0.2M), before addition of 2,2,2-Trifluoro-N-prop-2ynyl-acetamide (2 eq, 2.5mmol, 377.55 mg, 126.5 µL), CuI 20% molar ratio [0.25 mmol, 47.6 mg], $Pd[(C_6H_5)_3P]_4$ 10% in weight [35 mg], Amberlite Ira-67 (1.25 g, 6.25 mmol, 5mol/eq).The reaction mixture was stirred or 14 h at 40°C and monitored by TLC (95:5 DCM/MEOH) comparing the Rf of starting material Rf=0.3 and of Sonogshira product Rf=0.5. The reaction mixture was filtered over a plug of SiO_2 (5:1 $CH2Cl_2$: MEOH eluent), the solvents were removed at reduced pressure with gentle heating (approx 35 C), giving a crude product which was purified by flash chromatography on silica gel (95:5 DCM/MEOH) to afford sonogashira product (254mg, 0.97 mmol, 78 % yield).

^{1}H NMR (250 MHz, d6-DMSO) δ_H 7.9 (H, s, C6*H*), 7.5 (H, br, N*H*), 7.19 (1H, br signal, NH), 6.2 (2H, br signal, NH_2) 4.26 (2H, ddd, J= 5.5, 2.6, 0.4 Hz, CH2), **^{13}C NMR** (62.5 MHz, DMSO), δC

δC 164.8 (*C*4), 157.2 (q, J=37.9 Hz, *C*OCF3), 156.0 (*C*=O), 153.2 (*C* 6), 115.5 (q, J=287.2 Hz, CF3), 99.5 (*C*5) 73.4 (CH), 77.4 (C), 30.1 (CH_2).

Alkynylmethylamino cytosine (18)

254 mg 0.97 mmol of product **15**, were deprotected with 6 M NH_3 in H_2O/MeOH. After 2 hours the reaction was complete and ethylacetate (100ml) was added. The organic layer was separated dried with Na_2SO_4, filtrated and evaporated in vacuo. The pure product was obtained 0.87 mmol, 144 mg. **^{1}H NMR** (250 MHz, d6-DMSO) δH 7.9 (H, s, C6*H*), 7.5 (H, br, N*H*), 6.2 (2H, br signal, NH_2) 4.26 (2H, ddd, J= 5.5, 2.6, 0.4 Hz, CH2), 2.4 (1H, t, J= 2.6 Hz, CH), **^{13}C NMR** (62.5 MHz, DMSO), δC 164.8 (*C*4), 156.0 (*C*=O), 153.2 (*C* 6), 99.5 (*C*5) 73.9 (C alchin), 77.9 (C alchin), 30.1 (CH_2).

Tamra-cytosine (20)

In a SPE cartridge, to nitro phenol amino polystyrene resin (1 eq, 500 mg, 0.5 mmol/g) functionalized with 5(6) carboxy rhodamine, were added 0.9 eq (0.45 mmol, 74 mg) of **15** and were shaked at room temperature. The nucleoside **20** labelled with 5(6)carboxyrhodamine was furnished in 30 minutes pure with an overall yield of 30%.

5-iodo thymine (16)

^{1}H NMR (250 MHz, d6-DMSO) δH 11.8 (s, 1H, 3-H), 11.3 (s, 1H, N-H), 8.09 (s, 1H, 6-H), **^{13}C NMR** (62.5 MHz, DMSO), δC 161.8 (*C*4), 151.5 (*C* 2, *C*=O), 147.3 (*C* 6), 67.8 (*C*5).

TFA-alkynylmethylamino thymine (17)

5-iodo thymine **16** (300 mg 1.26 mmol) were dissolved in DMF (Vol 6.2mL , 0.2M) solution, before addition of 2,2,2-Trifluoro-N-prop-2ynyl-acetamide (377.55 mg, 126.5 µL, 2.5mmol, 2 eq) CuI 20% molar ratio [47.6 mg, 0.25 mmol,], $Pd[(C_6H_5)_3P]_4$ 10% in weight [35 mg], Amberlite Ira-67 (1.25 g, 6.25 mmol , 5 mol/ eq) and heated to 40°C. The reaction mixture was stirred or 14 h at 40°C and monitored by TLC (6:4 Hexane/AcOEt) comparing the Rf of starting material Rf=0.1 and of Sonogshira product Rf=0.3.The reaction mixture was filtered over a plug of SiO_2 (5:1 CH_2Cl_2 : MEeOH eluent), the solvents were removed at reduced pressure with gentle heating (approx 35 C), giving a crude product which was purified by flash chromatography (6:4 Hexane/AcOEt) to afford sonogashira product. (247 mg , 0.94 mmol, 75 % yield).

^{1}H NMR (250 MHz, d6-DMSO) δH 11.8 (s, 1H, 3-H), 11.3 (s, 1H, N-H), 8.09 (s, 1H, 6-H), 7.5 (H, br, N*H*), 4.26 (2H, ddd, J= 5.5, 2.6, 0.4 Hz, CH_2),**^{13}C NMR** (62.5 MHz, DMSO), δC 161.8 (*C*4),

157.2 (q, J=37.9 Hz, *C*OCF3), 151.5 (*C* 2, *C*=O), 147.3 (*C* 6), 115.5 (q, J=287.2 Hz, CF3), 99.4 (*C*5) 73.4 (C alchin), 77.4 (C alchin), 30.1 (CH_2).

Alkynylmethylamino thymine (**19)**

247 mg, 0.94 mmol of product **17**, were deprotected with 6 M NH_3 in H_2O/MeOH. After 2 hours the reaction was complete and ethylacetate (100ml) was added. The organic layer was separated, dried with Na_2SO_4, filtrated and evaporated in vacuo. The pure product (0.84 mmol, 140 mg) was obtained. **^{1}H NMR** (250 MHz, d6-DMSO) δH 11.8 (s, 1H, 3-H), 11.3 (s, 1H, N-H), 8.09 (s, 1H, 6-H), 7.5 (H, br, N*H*), 4.26 (2H, ddd, J= 5.5, 2.6, 0.4 Hz, CH_2),**^{13}C NMR** (62.5 MHz, DMSO), δC 161.8 (*C*4), 151.5 (*C* 2, *C*=O), 147.3 (*C* 6), 99.4 (*C*5) 73.4 (C alchin), 77.4 (C alchin), 30.1 (CH_2).

Fam-thymine (**21**)

In a polystyrene cartridge, to nitro phenol amino polystyrene resin (1 eq, 500 mg, 0.5 mmol/g) functionalized with 5(6) carboxy fluorescein, were added 0.9 eq (0.45 mmol, 74 mg) of **16** and were shaked at room temperature. The nucleoside **21** labelled with 5 (6) carboxy fluorescein was furnished in 30 minutes pure with an overall yield of 30%.

1H NMR (250 MHz, (d6-DMSO): 11.8 (s, 1H, 3-H thy), 11.3 (s, 1H, N-H1 thy), 9.26 (1H, t, J=5.3 Hz, NH, isomer a), 9.15 (1H, t, J=5.3 Hz, NH, isomer b), 8.44 (1H, d, J=0.7 Hz, HC(4) of isomer a), 8.27 (1H, dd, J1=7.9, J2=1.5 Hz, HC, isomer b), 8.15 (1H, dd, J1=7.9 Hz, J2=1.2 Hz, HC(5) of isomer 2), 8.12 (s, 1H, 6-H thy),8.09 (1H, d, J=8.0 Hz, HC(4) of isomer 6), 7.71 (1H, s, HC(7), isomer a), 7.39 (1H, d, J=8.0 Hz, HC(7) of isomer 5), 6.73-6.74 (2H, m, CH of isomer 5 and 6), 6.53-6.64 (4H, m, CH, isomer 5 and 6), 4.11 (2H, dd, J1=5.4 Hz, J2=2.4 Hz, HCCCH2- of isomer A), 3.99 (2H, dd, J1=5.2 Hz, J2=2.6 Hz, CH2- of isomer B), 3.17 (1H, t, J=2.4 Hz, HCCCH2- of isomer A), 3.10 (1H, t, J=2.4 Hz, HCCCH2 of isomer B).

Part III of my Phd thesis has been difficult to describe because the data have been covered by a British Patent Application n. 0718255.3, “Nucleobase Characterisation" of 19th September 2007, The University Court of the University of Edinburgh.

REFERENCES

1. Watson, J. D. and Crick F. H.C *Nature*, **1953**, *171*, 737-738.
2. Zamechnik, P. C.; Stephenson, M. L.; *Proc. Natl. Acad. Sci. USA* ,**1978**, *75*, 280.
3. Gewirtz, A.M. ; Sokol, D.L.; Ratajczak, M.Z.; *Blood*, **1998**, 92-712.
4. Crooke, S. T., Therapeutic Applications of oligonucleotides **1995,** Springer-Verlag:Heidolbery.
5. Hoogsteen, K.; *Acta. Crystal.*, **1963**, *16***,** 907.
6. Demidov V. V.; *Expert Rev. Mol. Diagn.*, **2003,** *3(2)*, 121-124.
7. Vet, J .A. M.; Van der Rijt, B. J. M.; Blom H. J.; *Expert Rev. Mol. Diagn*., **2002**, *2*, 77–86.
8. Mao, C.; Sun, W.; Shen, Z.; Seeman, N. C.; *Nature,* **1999**, *397*, 144.
9. Stanca, S. E; Eritja, R.; Fitzmaurice, D.; *Faraday Discuss.***, 2006**, *131*, 155 – 165.
10. Kwok, S.; Kellog, D. E.; Mickinney, N.; Spasic, D.; Goda, L.; Levenson, L.; Sninsky, J.J.; *Nucleic Acids Res.,* **1990**, *18(4)*, 999-1005.
11. Juliano, R. L.; Akhtar, S.; *Antisense Res. Dev*, **1992**, *2*, 165–176.
12. Meyer, O.; Kirpotin, D.; Hong, K.; Sternberg, B.; Park, J. W.; Woodlei, M. C.; Papahadjopoulos, D.; *J. Biol. Chem.*, **1998**, *25*, 15621– 15627.
13. Kim, J. S.; Kim, B. I.; Maruyama, A.; Akaike, T. ; Kim, S.W.; *J. Control. Release*, **1998**, *53*, 175–182.
14. Agrawal, S.; Goodchild, J.; Civeira, M. P. ; Thornton, A. H.; Sarin, P. S.; Zamecnik, P. C.; *Proc. Natl. Acad. Sci. U. S. A*., **1988**, *85,* 7079– 7083.
15. Egholm, M.; Buchardt, O.; Christensen, L.; Behrens, C.; Frier, S.M.; Driver, D.A.; Berg, R. H. ; Kim, S. K.; Norden, B.; Nielsen, P.E.; *Nature*, **1993**, *365*, 566–568.
16. (a) Strivchak, E. P.; Summerton, J. E.; Weller, D. D.; *Nucleic Acids Res*., **1989**, *17*, 6129. (b) Nielsen, P. E.; *Annu. Rev. Biophys. Biomol. Struct*, **1995**, *24*, 167.
17. Chen, X.; Dudgeon, N. ; Shen, L.; Wang, J. H.; *Drug Discovery today*, **2005**, *10*, 8, 587-593.
18. a) Milligan, J.; Matteucci, M. D.; Martin, J. C.; *J. Med. Chem.*, **1993**, *36*, 1921-37. b) Gryaznov, S. & Chen, J. K.; *J. Am. Chem. Soc*., **1994**, *116*, 3143-44.
19. Anderson, K. P; Fox, M. C; Brown-Driver, V; *et al*. *Antimicrob Agents Chemother*, **1996,** *40*, 2004-11.
20. Kurreck, J.; *Eur. J. Biochem.*, **2003,** *270*, 1628–1644.
21. Fluiter, K. et al.; *Nucleic Acids Res*, **2003,** *31*, 953–962.
22. Nielsen, P. E.; Egholm, M.; Berg, R. H.; Buchardt, O.; *Science*, **1991**, *254*, 1497 – 1500.

23. Uhlman E.; Peymann, A.; *Chem. Rev.*, **1990**, *90*, 543.
24. Demidov, V. V.; Potaman, V. N.; Kamenetskii, M. D. F.; Egholm, M.; Buchart O.; Sonnischsen, S. H. ; Nielsen, P. E.; *Biochem Pharmacol.*,**1994**, *48*, 1310–1313.
25. Egholm, M.; Buchardt, 0.; Christensen, L.; Behrens, C.; Freier, S. M.; Driver, D. A.; Berg, R. H.; Kim, S. K.; Norden, B.; Nielsen, P. E.; *Nature*, **1993**, *365*, 566.
26. Casale, R.; Jensen, I. S.; Egholm, M.; **1999** *In: Peptide nucleic acids: protocols and applications.* (Eds: P. E. Nielsen, M. Egholm) Horizon Scientific Press, Wymondham, United Kingdom, 39-50.
27. Uhlmann, E.; Peyman, A.; Breipohl, G.; Will, D. W.; *Angew Chem. Int. Ed*. **1998**, *37*, 2796-2823.
28. Uhlamann, E.; Will, D. W.; Breiphol, G.; Langer, D.; Ryte, A.; *Angew Chem*. **1996**, *108*, 2793-2797.
29. Egholm, M.; Buchardt, 0.; Christensen, L.; Behrens, C.; Freier, S. M.; Driver, D. A.; Berg, R. H.; Kim, S. K.; Norden, B.; Nielsen, P. E. *Nature* **1993**, *365*, 566.
30. Tomac, S.; Sarkar, M.; Ratilainen, T.; Wittung ,P.; Nielsen, P. E.; Nordén, B.; Gräslund, A.; *J. Am. Chem. Soc.*, **1996,** *118*, 5544-5552.
31. Brown, S. C.; Thomson, S. A.; Veal, J. M.; Davis, D. G. *Science*, **1994**, *265*, 777.
32. Leijon, M.; Graslund, A.; Nielsen, P. E.; Buchardt, O.; Norden, B.; Kristensen, S. M.; Eriksson, M.; *Biochemistry*, **1994,** *33*, 9820-9825.
33. Betts, L.; Josey, J. A.; Veal J. M.; Jordan, S. R.; *Science*, **1995**, *270*, 1838.
34. Rasmussen, H.;. Kastrup, J. S.; Nielsen, J. N.; Nielsen. J. M.; Nielsen, P. E. *Nature Struct. Biol.,* **1997**, *4*, 98.
35. Shabih, S; Sajjad, K; Arif, A.; *J Chem Technol Biotechnol*, **2006**, *81*, 892-899.
36. Knudsen, H.; Nielsen, P. E.; *Nucleic Acids Res.*, **1996**, *24*, 494-500.
37. Lohse, T.; Dahl, O.; Nielsen, P. E.; *Proc. Natl. Acad. Sci.*, **1999**, *96*, 11804-11808.
38. Demidov, V. V.; Yavnilllovich, M. V.; Belotserkovskii, B. P.; Frank-Kamenetskii, Nielsen, P. *Proc. Natl. Acad. Sci.*, USA. **1995**, *92*, 2637-41.
39. Igloi, G.L.; *Expert Rev Mol Diagn*, **2003**, *3*, 17–26.
40. Xi, C.; Balberg, M.; Boppart, S. A.; Raskin, L.; *Appl Environ Microbiol.*, ***2003***, *69(9)*, 5673-5678.
41. Petersena, K.; Vogelb, U.; Rockenbauerc, E.; Vang Nielsena, K.; Kølvraac, S.; Bolundc, L; Nexø, B.; *Molecular and Cellular Probes*, **2004**, *18*, 117–122.
42. Arlinghaus, H. F., Schröder, M., Feldner, J. C.; Brandt, O.; Hoheisel, J. D.; Lipinsky, D.**;** *Appplied Surface Science*, **2004**, *231-232*, 392-396.

43. Svenson, S.; Tomalia, D. A.; *Advanced Drug Delivery Reviews*, **2005**, *57*, 2106-2129.
44. Li, Y.; Tseng, Y. D.; Kwon, S. Y., D'Espaux L.; Bunch, J. S.; Mceuen, P. L.; and Luo, D; *Nat. Mater.*, **2004**, *3*, 38-42.
45. Shchepinov, M. S.; Mir, K. U.; Elder, J. K.; Frank-Kamenetskii, M. D.; Southern, E. M. *Nucleic Acids Res.*, **1999** *27(15)*, 3035–3041.
46. Gardel, M. L.; Valentine, M.T.; Weitz, D.A.; In: Brues KS (ed.), Microscale diagnostic techniques 2005 Springer New York.
47. Mukhopadhyay, A; Granick, S; *Curr Opin Colloid Interface Sci*, **2001**, *6*, 423.
48. Ray, A; Norden, B.; *FASEB J.*, **2000**, *14*, 1041-1060.
49. Kumar V. A. *Eur. J. Org. Chem.*, **2002**, *13*, 2021-32.
50. Haaima, G., Lohse, A.; Buchardt, O.; Nielsen P.E; *Angew. Chem., Int. Ed.*, **1996**, *35*, 1939-1941.
51. Gangamani, B. P.; Kumar, V. A.; Ganesh K. N.; *Tetrahedron*, **1996**, 52, 15017-15030.
52. Gangamani, B. P.; Kumar, V. A.; Ganesh K. N.; *Tetrahedron*, **1999**, *55*, 177-192.
53. Gangamani, B. P.; Kumar, V. A.; Ganesh K. N.; *Nucleosides Nucleotides*, **1999**, *18*, 1409-1411.
54. Jordan, S.; Schwemler, C.; Kosch, W.; Kretschmer, A.; Schwenner, E.; Milke, B.; *Bioorg. Med. Chem. Lett.*, **1997**,*7* , 687-692.
55. Sforza, S.; Galaverna, G.; Dossena, A.; Corradini, R.; Marchelli, R.; *Chirality*, **2002**, *14*, 591-598.
56. Hyrup, B.; Egholm, M.; Nielsen, P.E.; Wittung, P.; Norden, B.; Buchardt, O.; *J. Am. Chem. Soc.*, **1994**, *116*, 7964-7970.
57. Meienhenrich, U. J.; Munoz Caro, M.;. Bredhoft; Jessberger K.; Thiemann H.P.; *PNAS*, **2004**, *101 (25)*, 9182-9186.
58. Glavin, D. P. ; Bada, J. L.; *Lunar and Planetary Science* XXXV (**2004**).
59. Petersen, K. H.; Buchardt, O.; Nielsen, P. E.; *Bioorg. Med. Chem. Lett.*, **1996**, *6(7)*, 793-796.
60. Slaitas, A; Yeheskiely, E; *J. Peptide Res.*, **2002**; *60(5)*, 283-91.
61. Corradini, R; Sforza, S; Dossena, A; Palla, G; Rocchi, R; Filira, F; Nastri, F; Marchelli, R.; *J. Chem. Soc. Perkin Trans.*, **2001**, *1*, 2690-2696.
62. Kruglyak, L; *Nature Genetics*, **2005**, 37, 1299-1300.
63. Zhang, R.; Zhu, R.; Zhu, H.; Nguyent, T; Yao, F.; Xia, K; Liang, D; Liu, C.; *Nucleic Acids Res.*, **2005**, *33*, 489-492.

ABSTRACT

Nell'ambito di questo lavoro di tesi la candidata si è occupata dello studio di nuovi sistemi molecolari basati su acidi nucleici e analoghi (ODN) per la realizzazione di sistemi utilizzabili nel *drug delivery* o in diagnostica.

La prima parte di questo lavoro di tesi ha riguardato la costruzione di sistemi dendrimerici utilizzando molecole di ODN ed analoghi, lineari e ramificate, come *building blocks* autoassemblanti, sfruttando la caratteristica che hanno filamenti complementari di acidi nucleici (ed analoghi) di legarsi l'uno all'altro in maniera specifica. Sono stati realizzati 2 tipi di sistemi dendrimerici: un sistema monomolecolare autoassemblante (**A**), formato esclusivamente da molecole di PNA *tridendron* e un sistema bimolecolare (**B**) costituito da un *tridendron* di PNA a sequenza mista non auto-complementare, e un *crosslinker* di DNA. Entrambi i sistemi hanno la capacità di formare una rete tridimensionale mediante la formazione di ibridazioni specifiche W-C.

I componenti dei due sistemi sono stati realizzati in fase solida utilizzando una chimica di tipo Fmoc per il PNA, e quella del fosforoammidito per il DNA. Tutti gli oligomeri, deprotetti e distaccati dal supporto solido, sono stati purificati via HPLC e caratterizzati da MALDI-TOF e ESI -MS. Un dettagliato studio spettroscopico, è stato quindi effettuato su entrambi i sistemi per verificare la formazione di una rete oligonucleotidica, consentendo quindi di chiarire le proprietà cinetiche e termodinamiche dei sistemi realizzati. Infine, la candidata ha effettuato esperimenti di microreologia "Multiple Particle Tracking" (MPT) in collaborazione con il Prof. P. Netti e il dottor S. Fusco del Dip. di ingegneria dei materiali dell'Università "Federico II", per testare la capacità dei sistemi in esame di realizzare idrogels in grado incapsulare eventualmente farmaci per applicazioni in *drug delivery*.

Nella seconda parte del lavoro della sua tesi di dottorato, la dott.ssa M. Moccia si è occupata della sintesi, caratterizzazione e studi di *binding* di nuovi analoghi oligonucleotidici, allo scopo di esplorare loro nuove possibili applicazioni terapeutiche o diagnostiche. Questo progetto è stato realizzato in collaborazione con i dottori G. Roviello e D. Musumeci dell'IBB-CNR di Napoli.

I nuovi γ-nucleopeptidi ideati (*dab*PNA) sono basati su un *backbone* formato da unità di acido 2,4-diamminobutirrico (DABA) connesse alle nucleobasi attraverso un legame ammidico mediante un ponte metilencarbonilico. Dapprima Nielsen, nel 1993, e poi Meierhenrich, in seguito al rinvenimento del diamminoacido DABA e delle nucleobasi nel suolo meteorico, hanno proposto i *dab*PNA come probabile materiale genetico primordiale.

Per realizzare gli oligomeri di dabPNA, oggetto del presente studio, sono stati sintetizzati innanzitutto i nuovi monomeri $t_{L\text{-}dab}$, $t_{D\text{-}dab}$, $a_{L\text{-}dab}$ e $a_{D\text{-}dab}$, a partire da *building blocks*

opportunamente protetti, ottenendo in buona resa i nuovi nucleoamminoacidi chirali opportunamente purificati e caratterizzati via NMR ed ESI-MS.

Inizialmente sono stati sintetizzati gli oligomeri $(t_{L\text{-}dab})_{12}$ e $(t_{D\text{-}dab})_6$ adottando strategie sintetiche che preservino le proprietà ottiche del prodotto, e sono stati effettuati studi di ibridazione con acidi nucleici naturali. Dagli esperimenti CD e UV sia con il DNA (dA_{12}) e RNA (A_{12}) non si è rivelata nessuna significativa evidenza di legame. Inoltre l'introduzione di un monomero di *dab*PNA nella parte centrale o all'N terminale di un filamento t_{12} di *aeg*PNA ha portato ad oligomeri caratterizzati da una minor affinità di legame verso il DNA complementare rispetto ad un filamento interamente costituito da *aeg*PNA, denotando che la presenza di monomeri di *dab*PNA disturba la struttura della duplex PNA/DNA. Siccome entrambi gli enantiomeri del *dab*PNAs basati su L- o D-DABA non legano acidi nucleici naturali abbiamo esplorato la possibilità che nucleopeptidi complementari basati su D o L-DABA formare complessi. Questa proprietà è interessante per lo sviluppo di nuovi sistemi dendrimerici basati sul DABA, come nuovi materiali, ed anche per la realizzazione di nuovi sistemi diagnostici come per esempio molecular beacon. Per verificare questa possibilità i monomeri $a_{L\text{-}dab}$ e $a_{D\text{-}dab}$ sono stati oligomerizzati in fase solida per ottenere gli esameri :$(a_{L\text{-}dab})_6$, $(a_{L\text{-}dab}\text{-}\ a_{D\text{-}dab})_3$ e $(t_{L\text{-}dab}\text{-}t_{D\text{-}dab})_3$. Dagli esperimenti di CD e UV, abbiamo riscontrato evidenza di legame solo nel caso degli oligomeri complementari con chiralità alternata $(a_{L\text{-}dab}\text{-}a_{D\text{-}dab})_3$ e $(t_{L\text{-}dab}\text{-}t_{D\text{-}dab})_3$, eanche se la stabilità del complesso formato non è molto elevata (T_m= 11°C). Ulteriori esperimenti saranno effettuati per stabilire meglio la stabilità e la stechiometria dei complessi nucleopeptidici.

La terza parte del presente lavoro di tesi di dottorato è stata svolta presso il laboratorio del prof M. Bradley presso la School of Chemistry di Edimburgo ed ha riguardato un progetto dal titolo "Metodo non enzimatico per analisi SNP (single nucleotide polymorphism)". I polimorfismi da singolo nucleotide (SNP) si riferiscono ad alterazioni di singole basi che si verificano nel genoma umano e che danno luogo pertanto a modifiche della struttura e della funzionalità delle proteine, relative ai geni modificati . Risulta quindi importante occuparsi delle malattie originate da tali polimorfismi. Lo scopo di questo progetto è stato quello di sintetizzare e caratterizzare nuovi nucleosidi marcati ciascuno con 4 differenti fluorofori da usare per sviluppare un nuovo metodo di rivelazione degli SNP di tipo non enzimatico, utilizzando sia la tecnologia del microarray che quella del PNA. In primo luogo è stato messa a punto una nuova metodica di marcatura con fluorofori, ottimizzata inizialmente con l'uso di piccole molecole organiche nucleofile, il colorante supportato in fase solida viene così facilmente e velocemente rilasciato; successivamente tale metodo è stato usato per marcare le basi azotate opportunamente modificate in precedenza. Tale procedura è stata utilizzata per ottenere i nucleosidi modificati della citosina e della timina marcati rispettivamente con 5(6)-carbossi rodamina e 5(6)-carbossi fluoresceina. Una volta ottenuta tutti e quattro i

nucleosidi modificati marcati si potrà procedere alla messa a punto del metodo non enzimatico basato sul microarray per la rivelazione degli SNP.